RENSIT:
RadioElectronics. NanoSystems. Information Technologies

Journal "Radioelectronics. Nanosystems. Information Technologies" (abbr. RENSIT)
publishes original articles, reviews and brief reports, not previously published, on topical problems in **radioelectronics (including biomedical) and fundamentals of information, nano- and biotechnologies and adjacent areas of physics and mathematics.**

Designed for **researchers, graduate students, physics students of senior courses and teachers**.
It turns out **2 times a year** (that includes 2 issues)

Authors of journal are academicians, corresponding members and foreign members of Russian Academy of Natural Sciences (RANS) and their colleagues,
as well as other russian and foreign authors on presentation of their manuscripts by the members of RANS, which can be obtained by authors before sending articles to editors.
And also after its receiving - on recommendation of a member of editorial board of journal, or another member of Academy of Natural Sciences, that gave her opinion on article at request of editor.
The editors will accept articles in both **Russian and English** languages.

Articles are internally peer reviewed (**double-blind peer review**) by members of the Editorial Board.
Some articles undergo external review, if necessary.

Journal RENSIT is included in the **DB SCOPUS, EBSCO Publishing,** in the international abstracts database - **Ulrich's International Periodicals Directory**,(USA, New York, http://www.ulrichsweb.com), in the **AJ and DB VINITI RAS** (http://www.viniti.ru), and DB **Russian Science Citation Index (RSCI** http://elibrary.ru/project_risc.asp).
Full-text content is posted in the DB of the **Russian Scientific Electronic Library**
- information resource on the Internet http://elibrary.ru and is available for registered users.
And also - in Open Access **CyberLeninka NEB** of Russian Federation http://cyberleninka.ru.
On journal's website http://www.rensit.ru posted metadata publications
and **RENSIT: Radioelectronics. Nanosystems. Infomation Technologies - english version** (cover-to-cover translation) of journal, which is a party to **CrossRef.**

The founder - the **Russian Academy of Natural Sciences**
Publisher - Publishing Center of the Russian Academy of Natural Sciences
Publisher Address: 119002 Moscow, per. Sivtsev Vrazhek 29/16

CONTENTS

SPINTRONICS

CHRONICLE

RUSSIAN ACADEMY OF NATURAL SCIENCES

DEPARTMENT OF RADIOELECTRONICS, NANOPHYSICS AND INFORMATION TECHNOLOGIES PROBLEMS

RENSIT:

RADIOELECTRONICS. NANOSYSTEMS. INFORMATION TECHNOLOGIES.
2018, VOL. 10, № 3

FOUNDED IN 2009
2 ISSUES PER YEAR
MOSCOW

ISSN 2414-1267 online

The journal is registered by the Ministry of Telecom and Mass Communications of the Russian Federation. Certificate El. no. FS77-60275 on 19.12.2014

EDITORIAL BOARD ADDRESS
218-219 of., 7 b., 11, Mokhovaya str.,
125009 MOSCOW, RUSSIAN FEDERATION
TEL. +7 495 629 3368
FAX +7 495 629 3678 FOR VLADIMIR I. GRACHEV

From the Editors

This issue of RENSIT journal, 2018, 10 (3) is devoted to spintronics, one of the most rapidly developing areas of science and technology. And although it was not possible to organize a selection of works on the most acute problems of spintronics within a single issue, the editors of the journal believe that a certain slice, reflecting the level and variety of research developed primarily in Russia, is nevertheless marked. The editors hope that further work on the most pressing problems of the development of spintronics will be reflected in the pages of our journal.

SPINTRONICS: PHYSICAL FOUNDATIONS AND DEVICES

Yuri K. Fetisov, Alexander S. Sigov

MIREA-Russian Technological University, https://www.mirea.ru
Moscow 119454, Russian Federation

fetisov@mirea.ru, sigov@mirea.ru

Abstract. **"Spintronics" is one of the most rapidly developing branches of science and technology, which is currently considered as the most promising technology for the further development of the elemental base for information technology. Spintronics includes physical effects caused by the spins of individual electrons and spin-polarized currents flowing in thin magnetic and semiconductor films and heterostructures, and information processing devices based on them. The review provides qualitative estimates demonstrating potential advantages of spintronics in comparison with semiconductor micro- and nanoelectronics. Physical phenomena that form the scientific basis of spintronics, such as domain microstructures, skyrmions, spin waves, spin-polarized current, giant and tunnel magnetoresistance, spin transfer of angular momentum are considered. Prospective spintronics materials, including ferromagnetic metals and semiconductors, semimetal ferromagnetic oxides, Heusler alloys are listed. The possibilities of controlling spin currents using magnetic fields, mechanical deformations in multiferroic structures, and ultrashort optical pulses are shown. The spintronic devices that are under development or already made are described, such as high-sensitivity magnetic field sensors, random access magnetic memory elements, ultra-high frequency nanogenerators, spin diodes and spin transistors, and a spin holographic processor. The final part lists the main research centers for spintronics abroad and in Russia, and provides a list of overview publications on the topic.**

Keywords: **spintronics, magnetic heterostructures, spin-polarized current, spin waves, skyrmion, magnetoresistance, tunnel effect, magnetic field sensors, spin transistor, spin generator, spin processor**

PACS: 67.57.Lm, 72.25.Ba, 75.70.-i, 75.76.+j

Bibliography - 23 references *Received 19 March 2018; accepted 21 May 2018*

RENSIT, 2018, 10(3):343-356 **DOI: 10.17725/rensit.2018.10.343**

Contents

1. INTRODUCTION

The term "spintronics" represents one of the fastest growing direction of science and technology, which, apparently, will make a significant contribution to the development of electronics and information technology in the 21st century. Almost all currently existing electronics is based on the process of electron's charge transfer – electric current. An attempt to use the second fundamental characteristic of an electron, its own magnetic moment – "spin", opens new possibilities to improve performance of existing elecronic devices and create new devices, including the development of high-sensitivity magnetic field sensors, data storage elements with higher recording density and higher operation speed, microwave and terahertz nano-oscillators, new methods of information processing using quantum coherent effects, etc. As many specialists believe, the traditional semiconductor electronics approaches its physical limits in terms of miniaturization and operation speed. This will result in violation of the Moore's law in the near future, which predicts an increase of the computers power by a factor of two every 18 months. Since significant part of the modern economy is based on information technology, the solution of this problem is of specific importance. Currently, the spintronics is considered as the most promising base for further development of the information technology.

In the broad sense, the term "spintronics" include physical effects of magnetic nature, which arise because of magnetic properties of substances and are associated with their own spin and orbital magnetic moments of electrons, as well as their applications in micro- and nano-sizes information processing devices [1-3]. Such phenomena (domains in magnetic films, magnetic resonances, spin waves, magnetoresistance, etc.) are investigated and successfully used in practice for more than 100 years. In a narrow sense, the term "spintronics" includes physical effects which arise due to the spins of individual electrons and spin-polarized currents. Such effects as the spin-dependent transport, tunnel magnetoresistance, excitation of ferromagnetic resonance by a spin- polarized current, etc were discovered in the 1980s. Some of these effects have already found practical application and had a revolutionary impact to the development of information technologies [4-6].

This review provides qualitative estimates which demonstrate potential advantages of spintronics in comparison with traditional electronics, enumerates basic physical phenomena and materials, forming a scientific basis of spintronics, and presents some spintronic devices that have already been fabricated or will be created in the near future.

2. ELECTRONICS AND SPINTRONICS

According to the ideas of modern physics, the behavior of elementary particle "electron" is described by the quantum mechanics. The electron has a mass $m = 9.1 \cdot 10^{-31}$ kg, carries an elementary charge $e = 1.6 \cdot 10^{-19}$ C, has its own mechanical moment $J = h/4\pi$ (where $h = 6.62 \cdot 10^{-34}$ J·is the Planck's constant) and associated magnetic moment $M = \mu_B = 9.27 \cdot 10^{-24}$ J/T (where μ_B is the Bohr's magneton). Besides that, being in a bound state in atom, the electron also has a mechanical and magnetic moments caused by its rotation around the nucleus of the atom. Motion of the electron is described by the quantum mechanics laws, but for qualitative evaluations it can be regarded as a classical particle and the laws of classical nonrelativistic mechanics can be used.

An electron in a quasi-free state, i.e. moving, for example in a semiconductor, possesses a kinetic energy $W_k \sim mv^2/2 \sim kT$, where v is the electron's velocity, $k = 1.38 \cdot 10^{-23}$ J/K is the Boltzmann's constant, T is the temperature in Kelvin. The electron energy at room temperature can be estimated using the approach of the molecular-kinetic theory, as $W_k \sim 1.38 \cdot 10^{-23} \cdot 300 \sim 4 \cdot 10^{-21}$ J. The speed of the electron of this energy is $v = (2kT/m)^{1/2} \approx 10^5$ m/s, which is

much less than the speed of light. The electron covers the distance L ~ 100 nm (the characteristic size of elements in microelectronics) during the time $\tau \sim L/v \sim 10^{-7}/10^{5} \sim 10^{-12}$ seconds.

In digital microelectronics, an electron is used as the carrier of information, i.e. the presence of an electron in a limited region of space corresponds to "1", and its absence corresponds to "0". Therefore on the basis of the above calculation, one can make an optimistic estimate for the minimum energy required for recording one bit of information $W_{min} \approx W_k \sim 10^{-21}$ J. The minimum time which is required for recording or reading this bit of information is $\sim 10^{-12}$ seconds. Modern computers have achieved operation frequency about of 10 GHz, which corresponds to minimum switching time for one element $\sim 10^{-10}$ sec, that is two orders of magnitude higher, than the estimate gave.

In spintronics, a physical parameter used to record an information, is the magnetic moment of electron μ_B. According to quantum mechanics, an electron placed in external magnetic field B can have a projection of magnetic moment on the magnetic field direction $+\mu_B$ or $-\mu_B$. The positive projection corresponds, for example, to "1", and negative projection corresponds to "0". For estimates let us use classical expression for magnetic moment energy in an external magnetic field $W = -\mu_B B$. By substituting in the formula value of B ~1 T, which is achievable in real conditions, we obtain the energy which is required for recording/reading of one bit of information $W \sim 9.27 \cdot 10^{-24} \cdot 1 \sim 10^{-23}$ J. The time which is required to change projections of magnetic moment of an electron can be estimated using classical approach and considering the motion of magnetic moment in an external magnetic field. This motion is described by the Landau-Lifshitz equation and represents a rotation of magnetic moment around the field direction with the frequency $f = \gamma B$, where $\gamma \approx 3 \cdot 10^{10}$ Hz/T is the gyromagnetic ratio. The period of this rotation at B = 1 T is $1/f \sim 3 \cdot 10^{-11}$ s. Respectively, the rotation of magnetic moment by π must occur in an instant (switching time) of the order of $\tau \sim 10^{-11}$ sec.

It follows from the above estimates, that when magnetic moment (spin) of the electron is used for writing the information, instead of the electron charge, the energy of writing of one bit of information can be reduced from $\sim 4 \cdot 10^{-21}$ J to 10^{-23} J, that is decreased by 2-3 orders of magnitude. The time for one bit recording using the spin memory element in comparable to the time for one bit recording using the charge element. Additional advantage of spintronics, in comparison with electronics, as will be shown shortly, is the possibility of non-volatile memory elements realizing and higher radiation stability of spintronic devices.

The results of experimental investigations carried out during recent years, let to hope that information processing and recording devices based on the spintronics technology will do significantly exceed characteristics of the devices using a charge of electron.

3. PHYSICAL FOUNDATIONS OF SPINTRONICS

3.1. Magnetic structures and spin waves

In many-electron atoms, the magnetic moments of electrons are added up with their orbital moments and form magnetic moment of the atom. In solid states consisting of such atoms, the exchange interaction between electrons leads to the ordering and appearance of spontaneous magnetization of a sample in the absence of external magnetic field. Depending on the nature of the interaction, the magnetic ordering is ferromagnetic or antiferromagnetic. In such magnetically ordered samples, placed in external constant or variable magnetic fields, there are various phenomena that can be used to create information recording and processing devices.

In the 1960s and 1980s, at home and abroad, domain structures in thin ferromagnetic films with different types of magnetic anisotropy were investigated. It was shown that in dielectric

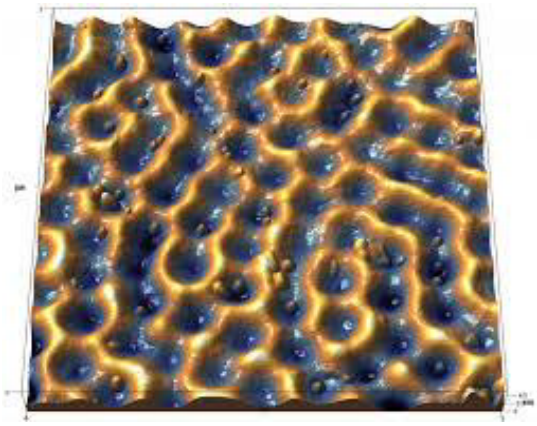

Fig. 1. *Bubble magnetic domains in ferromagnetic film.*

single-crystal films of yttrium iron garnet $Y_3Fe_5O_{12}$ (YIG) substituted with Ga, La, Sr, Sc, and other ions of thickness 1-10 μm and "easy axis" anisotropy, grown by the liquid-phase epitaxy method on dielectric substrates, there can be stable "bubble magnetic domains" (BMD) of micron and submicron sizes (**Fig. 1**). Methods for the bubbles generation and control their motion using pulsed magnetic fields were developed and prototypes of magnetic memory elements were fabricated. However, due to technological difficulties and high cost of garnet films this direction of spintronics has not received further development.

In 1970-2000, much attention in the country and abroad was paid to investigations of spin waves (SW) in single-crystal films of pure YIG and Ga-substituted YIG grown by the liquid-phase epitaxy method on singlecrystal substrates of gallium-gadolinium garnet $Gd_3Ga_5O_{12}$ with different crystallographic orientation (**Fig. 2**). It was shown that YIG is a unique material with extremely low magnetic losses in the microwave range ~0.5-30 GHz.

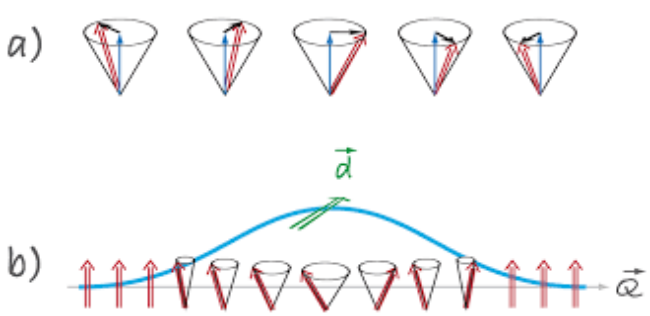

Fig. 2. *Schematic representation of a spin wave. The magnetization rotates around direction of magnetic field*

Spin waves in YIG films of thickness 1-20 μm arise due to the long-range dipole-dipole interaction, have the group velocity of v_g ~(1-10)·10^3 m/s, the wavelength of λ ~1-500 μm, the characteristic propagation lengths from hundreds of μm to several cm, and losses of electromagnetic signal to the SW conversion of ~1-10 dB, depending on the wave length. Characteristics of dipole SWs can be easily controlled by means of relatively weak external magnetic fields H ~100-3000 Oe, which gives them significant advantages over, for example, surface acoustic waves. A number of spin- wave devices for microwave signals processing, such as frequency-tunable filters and resonators, low-noise microwave generators signals, controlled phase shifters and microwave delay lines etc have been developed. Some of these spin-wave devices have found applications in special signal processing systems. However, due to high cost of epitaxial films these devices are still not used in commercial scale.

In recent years, interest to the spin-wave electronics again rose significantly because of achievements in the generation and detection of spin waves in metallic films (permalloy) of submicron and nanometer thickness, which are less expensive than epitaxial garnet films [7]. Spin waves in metal films have a purely exchange nature, their wavelength is a fraction of one microns, and propagation distances reaches units-hundreds of microns. The frequency, wavelength and velocity of exchange SW can be tuned approximately in the same range as for dipole SW, by changing external magnetic field. This opens up possibilities of creation of new controlled spin-wave microwave devices of micron sizes. We emphasize that spin-wave devices realize the basic principle of spintronics – transfer of magnetic moment (spin) without charge transfer. Therefore, characteristics of spin-wave devices may turned out to be better than characteristics of similar semiconductor devices.

Recently, new objects – "skyrmions" in thin ferromagnetic films were discovered, which may be promising for applications in spintronics devices [8]. Skyrmion is a stable two-dimensional topological structure with magnetization distribution in the form of ring with a diameter of ~10-30 nm. The skirmion is formed in a ferromagnetic or antiferromagnetic film 1-100 nm thick due to the competition between exchange interactions between the spins of neighboring atoms and the Dzyaloshinsky-Moriya interaction (**Fig. 3**). Methods for generating and detection of the skyrmions, control of their motion using external magnetic fields are under development now. Usage of skyrmions for information storage, are believed, will allow to increase data storage density and speed of information recording by 1-3 orders, in comparison with existing devices. Studies in this direction are at the stage of physical effects and demonstration of principal possibilities.

3.2. Spin-polarized current

Since the electron has both the "e" charge, its own spin, and its own magnetic moment μ_B, then the electric current ("motion of electrons") transfers not only the charge, but also the spin (i.e., the magnetic moment). For most materials (metals, semiconductors, etc.) the electric current contains a number of electrons with magnetic moment directed along definite direction (for example, the direction of magnetic field) which is equal to a number of electrons whose magnetic moment is directed in the opposite direction. As a result, the total "spin current", i.e. resultant magnetic moment transferred by the electrons is zero. One of the main tasks of spintronics is development of spin current generation methods (or "spin-polarized current") and methods for detection of spin current [9]. As a characteristic of the spin current, is used the "degree of spin polarization of the current" $P = (N_+ - N_-)/(N_+ + N_-)$, where N_+ is the number of electrons with a spin directed along, for example, the field, N_- is the number of electrons with spin directed against the magnetic field. The degree of polarization P = 0 for unpolarized current and P = 1 for completely polarized current.

The main way to obtain the spin-polarized current is the transmission of electric current through a ferromagnet placed in magnetic field (internal magnetic field of an anisotropic ferromagnet) with subsequent injection of this current into a conventional (non-ferromagnetic) metal or semiconductor through the interface (**Fig. 4**). Using such ferromagnetic materials as Fe, Co, Ni allowed to obtain spin currents with polarization of P ~0.1-0.4. When the spin-polarized current enters a conventional conductor, the degree of the current polarization rapidly decreases due to the scattering of electrons by phonons. To date, the relaxation times and the relaxation lengths of the spin-polarized current τ > 100 ns and l > units μm, respectively, are achieved.

For detection of the spin current (i.e., determination of degree of polarization) several methods have been developed.

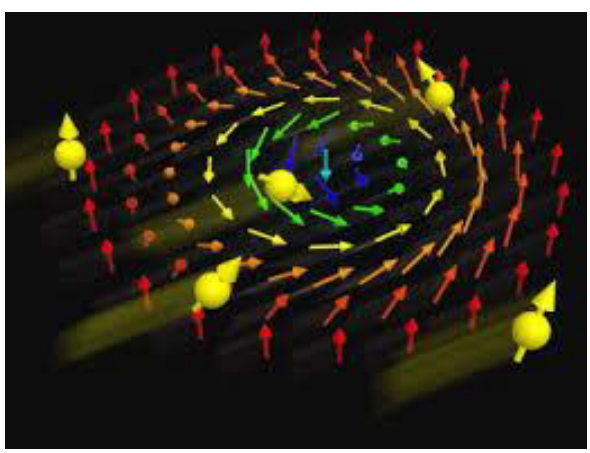

Fig. 3. *Schematic representation of magnetization distribution in skyrmion.*

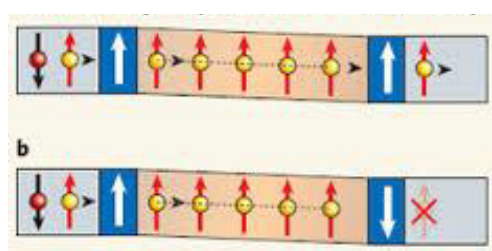

Fig. 4. *Schematic representation of a spin-polarized current in conductor: left - injector, in the center - conductor, right - detector.*

In the *spin-resolving photoemission method* the electrons are emitted from the surface of material and detected in a vacuum using the Moth analyzer which is sensitive to the spin direction. This is the most direct method, but it is limited on energy resolution and depth in within the upper 5-10 Å of the material, which makes the analysis sensitive only to surface states and impurities. *The magnetic tunnel transition method* uses two ferromagnetic layers separated by a thin insulating layer layer, usually Al_2O_3 or $SrTiO_3$, that form a planar tunnel junction. The polarization is obtained by measuring electrical resistance of such a sandwich MR $=2P^2/(1+P^2)$. The problem is the sensitivity of the MR to the surface state and material of the barrier, because the MR measured is not so much property of a ferromagnet, but property of the entire device. In the *point contact method* the polarization is calculated from the measured magnetoresistance.

Specific properties of the spin-polarized current exhibit in various effects observed in the structures with layers of nanometer thickness.

The first of these effects, known as anisotropic magnetoresistance (AMR), is the change in the resistance of ferromagnetic sample in an external magnetic field. Resistance of the sample depends on the mutual orientation of the current and the direction of the magnetic field. Relative change in resistance of ferromagnetic metals, for example Ni, does not exceed a fraction of a percent.

In 1988, the effect of a *giant magnetoresistance* (GMR) was discovered. The effect manifests in a structure consisting of two layers of ferromagnetic metal (for example, Co) separated by a thin layer of non-ferromagnetic conductor (for example, Cu) (**Fig. 5**). The electric current is passed through the conductor layer in the plane of the structure. Resistance of the structure depends on the mutual direction of magnetizations of ferromagnetic layers. The resistance is small for parallel orientation of

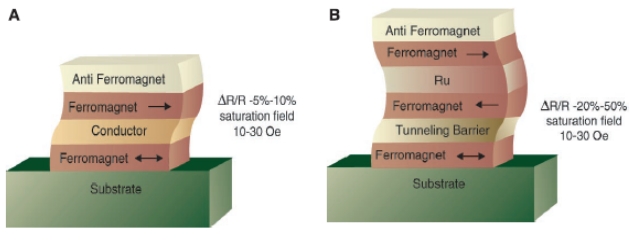

Fig. 5. *Schematic representation of structures: A - with giant magnetoresistance, B - with tunneling magnetoresistance.*

magnetizations of the layers, it increases for a counter orientation of the magnetizations. Magnitude of the relative change in resistance can reach ten of percent, which is much larger than the value of ordinary magnetoresistance and justifies the use of the term "giant". The effect arises due to dependence of the electrons scattering efficiency on the spin direction.

Even greater change in the resistance is observed for *tunnel magnetoresistance* (TMR) effect. The effect is observed in a structure containing two layers of ferromagnetic metal, separated by a dielectric layer with thickness of units of nanometers. The electric current is passed perpendicular to the plane of the structure. Due to the small thickness of the dielectric, the electrons can tunnel through the barrier, creating an electric current. The resistance of the structure is small if the magnetizations of the layers are directed in one direction and increases with the opposite orientation of the magnetizations. The relative change in the tunneling magnetoresistance of a structure can reach hundreds of percent.

The next effect is the *spin momentum transfer* (SMT) [10] reflects the property of polarized electrons to transfer the angular moment (**Fig. 6**). The effect is observed when a spin-polarized current of sufficiently high density is injected into a thin ferromagnetic layer perpendicular to the surface and manifests itself as a change in the magnetization direction of the ferromagnetic layer. This results in an excitation of oscillations of the ferromagnetic layer magnetization with frequencies close to the magnetic resonance frequencies. The phenomenon was first predicted

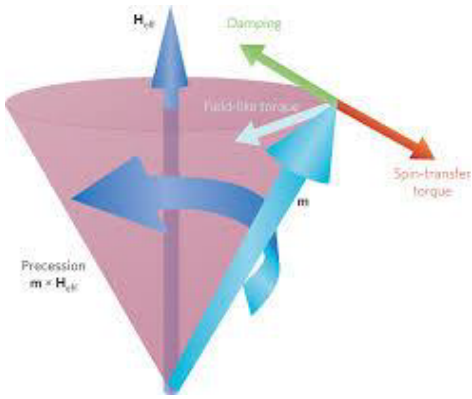

Fig. 6. *Geometry of excitation of magnetization precession when mechanical moment is transmitted by spin current.*

theoretically, and then found experimentally in Co films.

The *spin Hall effect* [11] is an analog of the usual Hall effect for the electron current. The spin Hall effect is observed in the propagation of the electron current in the film of a nonmagnetic conductor in the absence of an external magnetic field. The effect is manifested in the deflection of electrons with different spin directions to opposite sides of the film (**Fig. 7**). The effect arises from the spin-dependent scattering of electrons by impurities. An inverse spin Hall effect was also found in which the spin current leads to a spatial separation of electrons with different spin directions. As a result, an electric voltage is generated between the edges of the film. The effect can be used to detect spin waves.

3.3. Materials of spintronics

A great attention is being paid now to search of new materials that provide effective generation of spin-polarized currents at room temperatures and compatible with well-designed technologies of modern electronics [12-13]. In addition to the basic materials of spintronics - ferromagnetic metals Fe, Co and Ni, perspective are weakly doped ferromagnetic semiconductors, semi-metallic ferromagnetic oxides, Heusler alloys, and some organic materials. Among semiconductors the most interesting materials are groups of A3B5 and A2B6. For example, diluted magnetic semiconductors based on GaAs, in which the individual atoms are random are replaced by magnetic ions Mn^{2+} with a concentration up to 0.07, which have p-type conductivity at room temperatures as well as the semiconductors with a halcogenide structure of the type $Cd_{1-x}Mn_xGeP_2$. Using of semiconductors will significantly accelerate and facilitate the process of the spintronics integration with modern semiconductor technologies. The next materials, which are considered as the most promising for applications in spintronics, are the semimetals such as CrO_2 and oxides of some semiconductors, for example ZnO doped with Co. Semimetals are unusual ferromagnets that have electrons at the Fermi level in a single-spin state: all with spin along the magnetic field, or all with spin against the field. Electrons with opposite-directed spin have gap in the density of states at the Fermi level and therefore do not contribute to the conductivity. The charge carriers in such materials have degree of polarization P = 1. To candidates in semimetals are Fe_3O_4, LaSrMnO and SrFeMoO. Heusler's alloys are a big class of materials that are promising for spintronics. Heusler alloys include, for example, NiMnSb, PtMnSb, CoMnSi, CoMnGe, CoMnSn, and others. Most Heusler alloys are ferromagnets with a Curie temperature of 200 K to 10^3 K. They have a degree of electrons polarization at the Fermi level P ~ 1, which makes them semimetals [14-15].

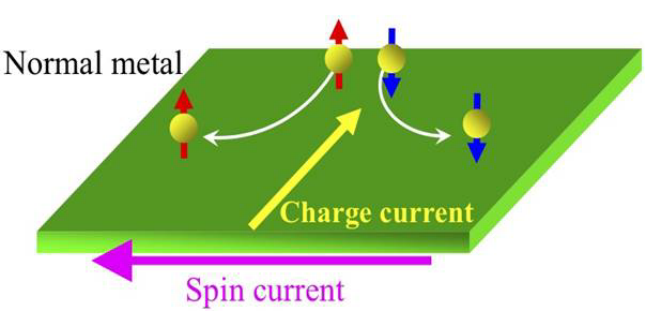

Fig. 7. *The spin Hall effect.*

3.4. Control of effects

There are several approaches to management spin currents and effects used in the spintronics.

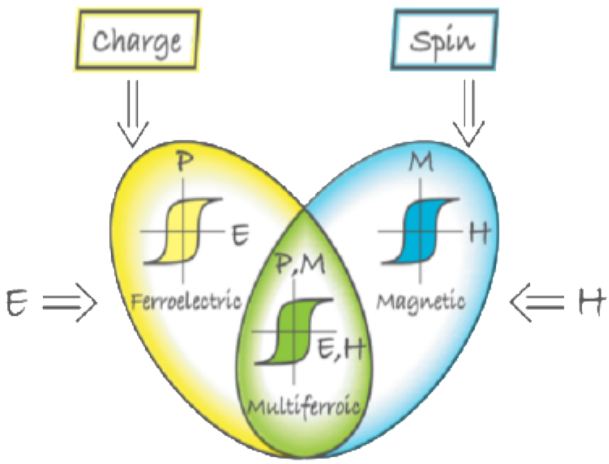

Fig. 8. *Multiferroics are the materials that posses simultaneously ferromagnetic, ferroelectric and ferroelastic properties.*

The main one is the control of the spin-polarized currents by means of a magnetic field, orientation and magnitude of which can easily be changed with external sources, for example, by passing a normal current through the conductors. Amplitude of magnetic fields should be from a fraction of mT to units of T. Such fields are sufficiently easy to implement in a small space using currents or ferromagnets.

The second way is to control the spin currents with the help of multiferroic materials that are simultaneously both ferromagnetic and ferroelectric, such as bismuth ferrite $FeBiO_3$ (**Fig. 8**) [16, 17]. An electric field applied to such material changes its magnetic parameters: saturation magnetization, orientation of the magnetization, magnetic anisotropy field and others. There are dozens of single crystal multiferroics, but only few of them exhibit sufficiently large effects at room temperatures.

Magnetic parameters of many ferromagnetics are strongly dependent on mechanical stresses that can be create artificially with the help of external strains, temperature changes etc. This opens up opportunities, for example, in composite film structures ferromagnet-piezoelectric, manage magnetization of the ferromagnetic layer, by applying an electric voltage to the piezoelectric layer (**Fig. 9**) [18]. Combination of piezoelectric effect and magnetostriction allows, as shown experimentally on structures containing Ni film of nanometer thickness and a piezoelectric with a large piezoelectric modulus (lead zirconate ceramic titanate, crystalline magnesium niobate-titanate lead, lithium niobate, etc.) allows much stronger change the orientation of the magnetization, than in single-phase multiferroic crystals. Interlayer of multiferroics or ferroelectrics are also used as an insulating layer to enhance tunneling magnetoresistance.

Finally, in recent years management of spintronic effects has been demonstrated by using ultrashort optical pulses due to inverse Faraday effect (**Fig. 10**) [19]. The effect is as follows: a light pulse with circular polarization of femtosecond duration (~10^{-13} - 10^{-14} s) falls on the surface of a ferromagnetic film and creates a pulsed magnetic field B of up to units of T. This field during the pulse can change the orientation of the ferromagnet magnetization, excite spin waves of microwave or terahertz

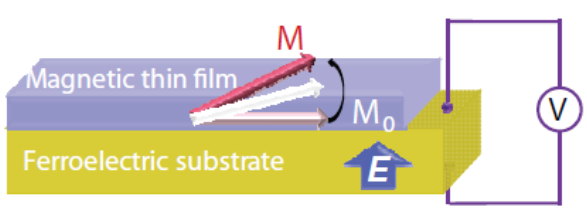

Fig. 9. *Composite ferromagnet- piezoelectric structure in which direction of magnetization is switched by an electric field.*

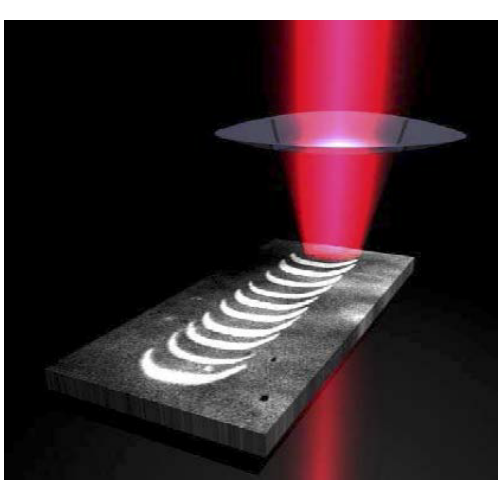

Fig. 10. *Magnetization reversal of a ferromagnetic film with optical pulses.*

frequency bands, change the parameters of the spin-polarized current. It is expected, that control with optical pulses will reduce the switching time of spintronics devices up to ~ 10^{-14} s, which is orders of magnitude shorter than switching times of microelectronic devices.

4. SPINTRONIC DEVICES

By now, several different information processing devices based on the spintronics principles were realized and even more are under development.

The first of them are the magnetic fields sensors [20]. Design of the sensor is shown in Fig. 5. It contains two ferromagnetic layers separated by a layer of non-ferromagnetic metal, most often Cu. A magnetically rigid layer with large anisotropy (as a rule – antiferromagnet) is deposited to one of the ferromagnetic layers. Because of the exchange interface interaction the magnetization of this layer is fixed, while orientation of the second ferromagnetic layer can be changed with the help of a weak external magnetic field H. Change of the layer magnetization orientation due to the GMR effect leads to a change in the resistance of the sensor for a direct current flowing through an average layer. Such sensors allows to register magnetic fields in the range of ~10^{-8}–10^{-2} T for units of nanoseconds. GMR sensors are widely are used to read information recorded on magnetic disks, which led to increase the information capacity and speed of the disks for several orders for the last 20 years. In addition, GMR sensors are widely used in automotive and aviation industry, in security systems, in magnetic defectoscopy, etc. (**Fig. 11**). In 2007, A. Fert and P. Grünberg were awarded the Nobel Prize in physics for these developments.

Almost all leading electronic companies in the world are working on the creation of the STT-MRAM (Spin-Transfer Torque Magnetic Random Excess Memory), the random access memory based on structures with a spin-tunnel

Fig. 11. *Field sensors based on giant magnetoresistance and their application.*

effect, which in the coming years can replace both semiconductor memory and normal MRAM memory. The design of the STT-MRAM memory element is shown schematically in **Fig. 12**. Each cell contains a structure with a magnetic tunnel junction that is responsible for storing information, and a transistor, through which addressing is organized. The logical "1" corresponds to the parallel orientation of the magnetizations of the fixed and free magnetic layers, and the logical "0" corresponds to the antiparallel orientation of the magnetizations of the layers.. The recording is carried out by passing a spin-polarized current through the tunnel junction, which changes the orientation of the magnetization of the free magnetic layer. For reading, a weak current is passed through the cell and the state of the cell is determined by its resistance. Using the STT effect, instead of external magnetic fields, to change the state of the cell, made it possible to reduce significantly the recording energy. Advantages of the STT-MRAM memory are higher density

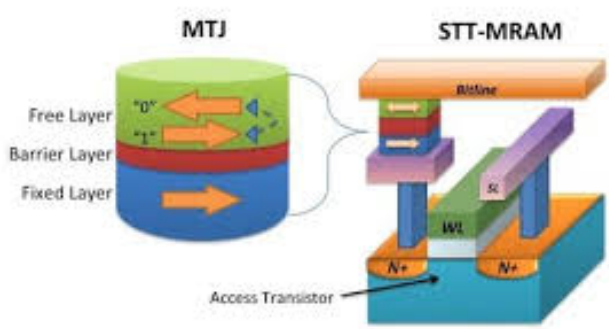

Fig. 12. *Schematic view of the Magnetic Random Access Memory element.*

of information recording and higher speed. It is significant that MRAM is a non-volatile memory, the data in which are stored for unlimited time period without power supply, in contrast to dynamic (DRAM) semiconductor memory.This means that the long process of downloading programs from disks to the computer's memory is excluded, which greatly improves the speed and reduces the power consumption of information systems. According to preliminary estimates, memory based on spintronic technology should also have increased radiation resistance. In 2016, the company Everspin began commercial production of a 40-nanometer STT-MRAM memory with a capacity of 256 Mbit. In Russia, the company "Crocus NanoElectronica" plans to start production of the STT-MRAM memory chips.

A promising area is development of spin nano-generators of microwave range, using effect of ferromagnetic resonance excitation with spin current (**Fig. 13**) [21]. Such generators have dimensions of the order of ~100 nm, consumption power at the level of microwatt, frequency of radiation is in the range from units to tens of GHz, and generate power of tens of *nW*. Research is currently under way on optimization of structures, increase of output power, formation of frequency characteristics of generators. A possibility of creating phased antenna arrays based on such generators has been demonstrated, that will allow to increase their power is 2-3 orders of magnitude. It is proposed to use nano-generators for transmission of information on short distances, for example, inside microprocessors.

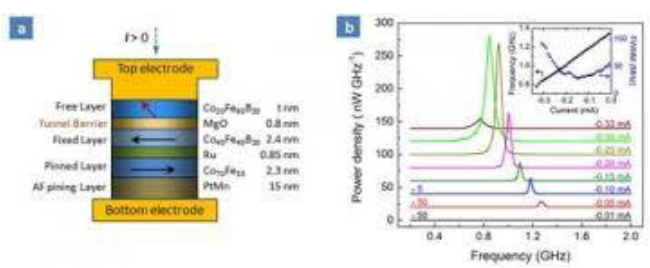

Fig. 13. *Design and frequency spectrum of spin-current microwave oscillator.*

The first step towards creating computers using principles of spintronics, is the development of elements, which are functional analogues of diodes and transistors used in traditional electronics. Respectively, dozens prototypes of spin diodes and spin transistors were proposed and implemented, such as Johnson spin transistor (named for the inventor), a hybrid spin transistor, SPICE-transistor, spin-field-effect transistor and others [2, 22].

As an example, **Fig. 14** shows a schematic view of the spin-field effect transistor. Like the usual transistor, it has source and drain contacts (ferromagnets) and a gate (semiconductor). Spin-polarized carriers leave the source with spins parallel to the magnetization of the ferromagnet and process in motion due to the Rashba effect. In this case, the electrons must move at a rate of 1% of the light speed in vacuum. For sufficient strength of magnetic field (the velocity of electrons in a given case is very important), the spins of the electrons reverse their orientation. As a result, the resistance of the channel increases and the current decreases. By varying potential on the shutter one can change conductivity of the device. This device behaves like a conventional field-effect transistor with the feature that the magnetization of its contacts (and, consequently, its electrical characteristics) is sensitive to external magnetic field.

In addition to traditional approaches, new approaches can be used in spintronics for

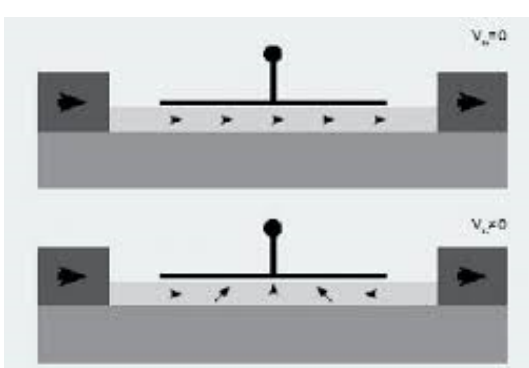

Fig. 14. *Schematic view of the spin-field transistor.*

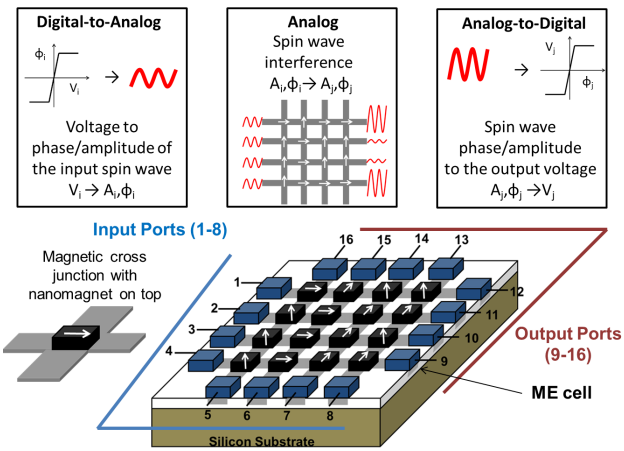

Fig. 15. *Principle of operation and design of the spin holographic processor.*

processing of signals, taking into account specific properties of spin waves [23]. **Fig. 15** shows, as an example, the structure of a spin holographic processor. it uses coherence of spin waves propagating in a thin ferromagnetic film. Input converters (4 + 4) excite in structured film spin waves. Phase and amplitudes of these waves depend on the voltage at the input converter. In the places where the wave beams overlap, the spin current generates a voltage, whose amplitude depends on the phases of the interfering waves. As result, the signals corresponding to certain transformations of the input signals are formed at the outputs. We emphasize that in this device all processing of information occurs on spin waves, in analogy with optical processors. The development of technology is likely to allow processing of big data sets.

Finally, spintronics can become the main base for creating quantum computers working on new principles radically different from currently used. Electron Is a quantum particle with spin which obey the quantum mechanics laws (along with the optical photon). It is the most suitable object for implementation so-called "q-bit". It is believed that the first samples of real quantum computers will appear already within the next ten years.

5. RESEARCH CENTERS ON SPINTRONICS

Fundamental and applied research in the field of spintronics and its applications are currently engaged in dozens of universities and research centers of large electronic firms. Leading role in terms of scientific achievements and volumes of research play organization of the USA [24]. The main customers and sponsors in this area in the US are the Defense agency of perspective research projects (DARPA), the US Department of Defense (DOD), the Naval Research Laboratory (NRL), the National Science Foundation (NSF), such firms as IBM, Honeywell, Motorola, Infineon, Cypress Semiconductor, NEC, Toshiba, Federal Products Inc., Nonvolatile Electronics, and others. Research are conducted, as a rule, in the frames of national programs, such as "Technology Reinvestments Project", "Magnetic Materials and Devices Project", "Spintronics", "SPns IN Semiconductor Project", "Quantum Information Science and Technology" and others.

Below are some of the leading research centers in the field of research and applications of spintronics:

C-SPIN (**Minnesota, USA**) is the Center for spintronics of materials, interfaces and new architecture. Multi-discipline university and industrial research Centre. They develop technologies of spintronic computing devices and memory chips. Located at the State University of Minnesota. The Center is funded by a five-year grant of $28 million from Semiconductor Research Corporation and DARPA.

CSEQuIN is the Center for spin effects and quantum information in nanostructures. It is at the University of Buffalo. Its laboratory of spintronics and semiconductors is financed by DAPRA.

CSQC (**California, USA**) is the Center for spintronics and quantum computers. It is a part

of the California Institute of nanosystems at the University of Santa Barbara, USA.

NANOSPIN is the project of the European Commission. It unites 8 academic and industrial partners from 6 EU countries on the basis of interest in spintronic materials and devices.

Spintec is a research laboratory, where they try to transfer the bridge from fundamental research to promising technologies for production of spintronic devices. It is located in Grenoble, under the leadership of the Commissariat for Atomic Energy (CEA) and the National Center of scientific research (CNRS) of France. Main subjects: memory devices, memory chips, MRAM, transfer of spin, semiconductor devices.

In **France**, the universities "Paris-Sud", "Paris-Saclay", "Paris-13", and "Université de Lorraine" deal with both fundamental problems of spintronics and the development of new devices. The research is funded by CNRS and the Commission of Atomic Energy of France.

Oakland University in the United States, where focus on theoretical research into the creation of spintronic generators of microwaves and development of devices. Works are financed by National Science Foundation of the United States, DARPA, and electronic companies.

In Germany, more than 20 scientific groups from various universities are involved in spintronics research. Research is carried out within the framework of two Priority Programs and 9 Special Research Programs

In Japan and China, similar researches in the field of spintronics are conducted in universities and research centers of leading electronic companies.

In Russia, researches on spintronics are carried out by individual scientific groups in institutes of the Russian Academy of Sciences and universities. In particular, in the Institute of Radioengineering and Electronics of RAS, Institute of General Physics of RAS, Institute of General and Inorganic Chemistry of RAS, Institute of Physics of Microstructures

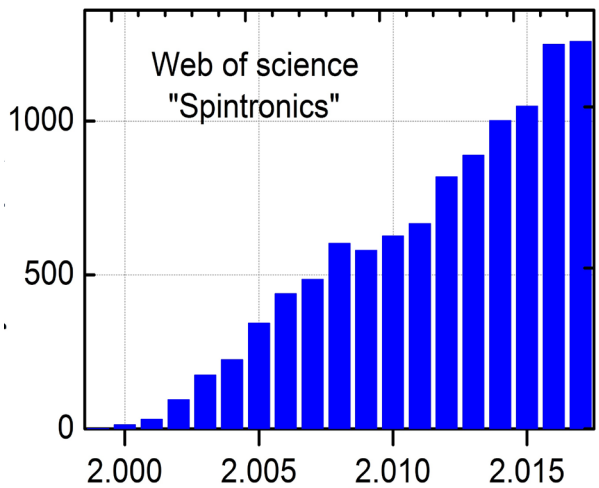

Fig. 16. *Publications on spintronics: on the Y-axis - the number of publications, on the X-axis - the year.*

of RAS, Institute of Metal Physics of UB RAS, Institute of Physics of SB RAS, in the Russian Technological University, the Sain-Peterburg Electrotechnical University "LETI", Saratov State University, Far Eastern Federal University, Russian Quantum Center, Russian company "Crocus-Nanoelectronics", and a number of other organizations. Unfortunately, the contribution of Russian researchers and developers in the research in this area is still insignificant. It's connected with organizational problems (absence of State programs) and with the absence of a target financing. However, the qualification, experience and existing international contacts allow Russian scientists join to research in the field of spintronics and cut backlog.

First publications on spintronics appeared in 1999, now the number of publications is more than 6 thousand and continues to grow. In **Fig. 16** is a graph of annual growth in the number of publications in the leading international journals, built on database Web of Science using keyword "spintronics". According to Web of Science, number of articles count on "spintronics" reaches 9709 and is growing steadily. Annual number of references to articles on the topic "spintronics" in 2016 exceeded 28 thousand, which indicates extraordinary popularity and importance of this direction.

6. CONCLUSION

Brief summary of research and development in the field of spintronics allows us to make the following conclusion:

- Spintronics is the most promising platform for element base of systems for processing and storage of information.
- Spintronics devices allow realize a higher density data storage, will have higher speed of information processing, reduced energy consumption, and higher radiation resistance than existing electronic devices on semiconductors.
- To date, the prototypes of such spintronics devices as highly sensitive magnetic field sensors; non-volatile magnetic random access memory elements; spin-field diodes and transistors; tuned microwave nano-generators, and so on. New principles of information processing based on spintronic technology are under development.
- Leading countries are carrying out intensive research in the area of spintronics in universities and research departments of companies. In the US, investigations are financed by military departments, National Science Foundation, companies IBM, Honeywell, Motorola, Infineon, NEC, Toshiba and others.
- In the US, Europe and Asia (Japan, China) spintronic studies are held as a part of a specially organized programs, executors of which are scientific groups from universities, public and private research organizations.
- In Russia there are several scientific groups in the institutes of the Academy of Sciences and leading universities involved in fundamental research in the area of spintronics. To reduce lag of domestic researchers from Western competitors it is necessary to organize state programs on this direction and increase funding.

ACKNOWLEDGMENTS

The work is supported by the Ministry of Education and Science of the Russian Federation (project 8.1183.2017) and the Russian Foundation for Basic Research (grant 16-29-14017).

REFERENCES

1. Wolf SA, Awschalom DD, Buhrman RA, Daughton JM, von Molnár S, Roukes ML, Chtchelkanova AY, Treger DM. Spintronics: A spin-based electronics vision for the future. *Science*, 2001, 294(5546):1488-1495.
2. Zutic I, Fabian J, Das Sarma S. Spintronics: Fundamental and application. *Reviews of modern physics,* 2004, 76(2):323-410.
3. Bader SD, Parkin SSP. Spintronics. In: *Annual Review of condensed matter physics,* 2010, 1:71-88.
4. Wolf SA, Chtchelkanova AY, Treger DM. Spintronics – A retrospective and perspective. *IBM Journal of Research and Development,* 2006, 50(1)101-110.
5. Fert A. Nobel Lecture: Origin, development and future of spintronics. *Reviews of Modern Physics*, 2008, 80(4):1517-1530.
6. Ohno H. A window on the future of spintronics. *Nature Materials*, 2010, 9(12):952-954.
7. Nikitov SA, Kalyabin DV, Lisenkov IV, Slavin AN, Barabanenkov YuN, Osokin SA, Sadovnikov AV, Beginin EN, Morozova MA, Sharaevsky YuP, Filimonov YuA, Khivintsev YuV, Vysotsky SL, Sakharov VK, Pavlov ES. Magnonics: a new research area in spintronics and spin wave electronics. *Phys. Usp.*, 2015, 58:1002–1028; DOI: 10.3367/UFNe.0185.201510m.1099.
8. Fert A, Cros V, Sampaio J. Skyrmions on the track. *Nature Nanotechnology,* 2013, 8:152-156.
9. Ohno Y, Young DK, Beschoten B, Matsukura F, Ohno H, Awschalom DD. Electrical Spin Injection in a Ferromagnetic Semiconductor Heterostructure. *Nature,* 1999, 402:790-792; DOI: 10.1038/45509.

10. Ralph DC, Stibes MD. Spin transfer Torque. *J. Magn. Magn. Mater.*, 2008, 320:1190-1216.
11. Wunderlich J, Byong-Guk Park, Irvine AC, Zârbo LP, Rozkotová E, Nemec P, Novák V, Sinova J, Jungwirth T. Spin hall effect transistor. *Science*, 2010, 330(6012):1801-1804.
12. Felser C, Fecher GH, Balke B. Spintronics: A challenge for solid-state chemistry. *Angewandte Chemie International Edition,* 2007, 46(5):668-699.
13. Awschalom DD, Flatte ME. Challenges for semiconducter spintronics. *Nature Physics,* 2007, 3(3):153-159.
14. Han W, Kawakami RK, Gmitra M, Fabian Ya. Graphene spintronics. *Nature nanotechnology,* 2014, 9(10):794- 807.
15. Drogeler M, Franzen C, Volmer F, Pohlmann T, Banszerus L, Wolter M, Watanabe K, Taniguchi T, Stampfer C, Beschoten B. Spin lifetimes exceeding 12 ns in graphene nonlocal spin valve devices. *Nano Lett.*, 2016, 16(6):3533-9; http://arxiv.org/pdf/1602.02725.pdf.
16. Bea H, Gajek M, Bibes M, Barthélémy A. Spintronics with multiferroics. *Journal of Physics Condensed Matter,* 2008, 20(43):434221.
17. Pyatakov AP, Zvezdin AK. Magnetoelectric and multiferroic media. *Phys. Usp.*, 2012, 55:557–581; DOI: 10.3367/UFNe.0182.201206b.0593.
18. Bukharaev AA, Zvezdin AK, Pyatakov AP, Fetisov YuK. Straintronics: a new trend in micro-, nanoelectronics, and material science. *Phys. Usp.*, accepted; DOI: 10.3367/UFNe.2018.01.038279.
19. Kirilyuk A, Kimel A, Rasing T. Ultrafast optical manipulation of magnetic order. *Rev Mod Phys* 2010, 82(3):2731-2784.
20. Parkin S, Jiang X, Kaiser C, Panchula A., Roche K., Samant M. Magnetically engineered spintronics sensors and memory. *Proceedings of IEEE*, 2003, 91(5):661-680.
21. Demidov VE, Urazhdin S, Ulrichs H, Tiberkevich V, Slavin A, Baither D, Schmitz G, Demokritov SO. Magnetic nano-oscillator driven by pure spin current. *Nature Mater.*, 2012, 11:1028.
22. Ognev AV, Samardak AS. Spintronics: physical principles, devices, future. *Vestnik Dal'nevostochn. Otdel. Ross. Akad. Nauk,* 2006, 4:70-80 (in Russ.).
23. Khitun A. Multi-frequency magnonic logic circuits for parallel data processing. *J. Appl. Phys.*, 2012, 111:054307.
24. Hellman F, Hoffmann A, Tserkovnyak Y, Beach GSD, Fullerton EE, Leighton C, MacDonald AH, Ralph DC, Arena DA, Dürr HA, Fischer P, Grollier J, Heremans JP, Jungwirth T, Kimel AV, Koopmans B, Krivorotov IN, May SJ, Petford-Long AK, Rondinelli JM, Samarth N, Schuller IK, Slavin AN, Stiles MD, Tchernyshyov O, Thiaville A, Zink BL. Interface-Induced Phenomena in Magnetism. *Rev Mod Phys.*, 2017, 89(2):025006.

EFFECTIVE SPIN-ORBIT INTERACTION IN NARROW QUANTUM WELLS

Zhanna A. Devizorova, Vladimir A. Volkov

Kotelnikov Institute of Radioengineering and Electronics of the Russian Academy of Sciences, http://cplire.ru
11/7, Mokhovaya Str., Moscow 125009, Russian Federation

devizorovazhanna@gmail.com, VoVA@cplire.ru

Abstract. **Rashba and linear Dresselhaus interactions are believed to yield dominant contribution to the spin splitting of two-dimensional electrons in the quantum wells based on A_3B_5 compounds. We show that the interfacial spin-orbit interaction significantly renormalizes the value of the corresponding Rashba (α_{SIA}) and Dresselhaus (α_{BIA}) parameters. For this purpose, we solve the effective mass equation in a quantum well supplemented by the original boundary conditions on the atomically sharp interfaces and calculate the interfacial contributions to α_{SIA} and α_{BIA}. Our results explain a considerable spread in the experimental data on spin-orbit parameters in GaAs/AlGaAs quantum wells. We also demonstrated that the non-equivalence of the interfaces leads to the anisotropy of the spin splitting even in quantum wells with zero average electric field.**

Keywords: **quantum wells, spin splitting of two-dimensional electrons, spin-orbit interactions, interfacial terms**

PACS: 71.22.+i, 71.70.Ej, 73.21.Fg, 73.20.-r, 73.21.-b

Bibliography - 17 references *Received 08 October 2018; accepted 28 November 2018*

RENSIT, 2018, 10(3):357-362 **DOI: 10.17725/rensit.2018.10.357**

Contents

I. INTRODUCTION

The conservation of the spin polarization is crucial for spintronic device applications. Due to the spin-orbit interaction (SOI), electrons in quantum wells (QWs) experience spin relaxation and dephasing by Dyakonov-Perel mechanism [3]. In the QWs based on A_3B_5 compounds there are two types of the SOI: Dresselhaus [1] and Rashba [2]. The Dresselhaus-type SOI is believed to originate from the lack of inversion symmetry in the bulk crystal and is proportional to the Dresselhaus parameter α_{BIA}. The Rashba-type SOI is due to the structural asymmetry and is proportional to the parameter α_{SIA}. If α_{BIA} and α_{SIA} are equal, the spin polarization of a helical spin state is conserved [4]. To achieve this regime, one should know and control the values of both parameters. In the envelope functions approximation they are determined by the following expressions $\alpha_{BIA}^{(0)} = \gamma_c \left\langle \hat{p}_z^2 \right\rangle / \hbar^3, \alpha_{SIA}^{(0)} = a_{so} \left\langle \partial_z V(z) \right\rangle$, where γ_c и a_{so} are bulk constants [18]. Thus, it is believed that the parameter α_{SIA} can be tuned by using the gate electrodes or by choosing the ratio between the dopant concentration on the two sides of QW, while the parameter α_{BIA} is determined by choosing the material and the width of QW. However, the experimental determination of the bulk constants γ_c and a_{SO} is still challenging. In spite of many experimental investigations in a wide range GaAs-based QWs, the precise value of γ_c is still being discussed controversially in the literature.

The parameter γ_c was measured by Marushchak with collaborators for bulk GaAs [5[and the value γ_c = 24 eV·Å^3 was obtained which is in the good agreement with kp-theory and has not been revised yet. But since 1990th γ_c bas been measured not in bulk GaAs, but in QWs with the interfaces [4, 6-15]. There is a considerable spread in the data obtained (see **Fig. 1**), moreover, they are inconsistent with the theoretical results. As it was pointed out in Ref. [17], the possible reason of the spread is an incomplete account of the interfacial spin-orbit interaction (ISOI). Thus, not bulk values, but some effective quantities containing the information about the microscopic structure of the interfaces are obtained in the experiments. The theory of ISOI in the

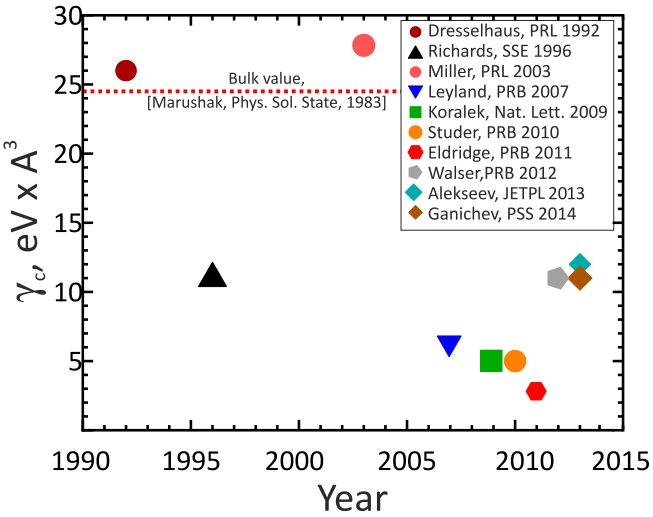

Fig. 1. *The values of the bulk spin-orbit constant γ_c extracted from the experimental data obtained by different groups in GaAs/AlGaAs quantum wells. There is a considerable spread in the data and inconsistency with the result of bulk measurements.*

wide unilaterally doped GaAs quantum well, where the electrons are pushed toward the (001) GaAs/AlGaAs heterointerface by the built-in electric field was developed in Refs. [16 and 17]. The interfacial contributions to the α_{BIA} and α_{SIA} were shown to be of the same order as bulk ones. However, in a more general situation the electrons interact with atomically sharp interfacial potentials of two heterointerfaces, and ISOI at both of them contribute to α_{BIA} and α_{SIA}. To take it into account, we develop the theory of the ISOI in the QWs with an arbitrary thickness and potential profile in the present paper.

2. GENERAL THEORY OF SPIN-ORBIT INTERACTION IN NARROW QUANTUM WELLS

In the QWs grown in $z||[001]$ direction, the spin splitting of the 2*D* electron spectrum has the general form

$$E_{SS} = 2p\sqrt{\alpha_{BIA}^2 + \alpha_{SIA}^2 + 2\alpha_{BIA}\alpha_{SIA}\sin 2\phi}, \quad (1)$$

where $p_x = p\cos\phi$, $p_y = p\sin\phi$ are the components of 2D momentum.

To derive the interfacial contributions to α_{BIA} and α_{SIA} we begin with 3*D* problem in which an effective wave function ϕ of the conduction electron obeys the effective mass equation inside the QW of the thickness *d*. The corresponding Hamiltonian $\hat{H}$ contains the terms $\hat{H}_{BIA}$ and $\hat{H}_{SIA}$ describing the spin splitting of the spectrum arising due to the lack of inversion symmetry in the bulk crystal and asymmetry of the structure, respectively:

$$\hat{H} = \frac{\hat{p}^2}{2m^*} + V(z) + \hat{H}_{BIA} + \hat{H}_{SIA}, \quad (2)$$

$$\hat{H}_{BIA} = \frac{\gamma_c}{\hbar^3}\left[\sigma_x p_x(p_y^2 - \hat{p}_z^2) + \sigma_y p_y(\hat{p}_z^2 - p_x^2) + \sigma_z \hat{p}_z(p_x^2 - p_y^2)\right], \quad (3)$$

$$\hat{H}_{SIA} = a_{so}(\sigma_x p_y - \sigma_y p_x)\partial_z V(z), \quad (4)$$

where σ_x, σ_y and σ_z are the Pauli matrices.

Aiming to take into account the microscopic structure of the interfaces, we introduce appropriate boundary conditions (BCs) for the effective wave function. The phenomenological BC for a single (001) GaAs/AlGaAs heterointeface with C_{2v} symmetry taking into account the spin-orbit interaction with atomically sharp interfacial potential was derived in Refs. [16 and 17] from the general physical requirements. Since the interfaces are, in general, non-equivalent we describe them by such BCs with different phenomenological parameters

$$\hat{\Gamma}_1\phi(z)|_{z=d/2} = 0, \quad \hat{\Gamma}_2\phi(z)|_{z=-d/2} = 0, \quad (5)$$

$$\hat{\Gamma}_{1(2)} = \left[\begin{array}{l} \hat{1} - i\frac{R_{1(2)}}{\hbar}\hat{\mathbf{p}}\mathbf{n} - i\frac{2m^*\gamma_c R_{1(2)}}{\hbar^4}(\sigma_y p_y - \sigma_x p_x)\hat{\mathbf{p}}\mathbf{n} + \\ + \frac{(\chi + \chi^{\text{int}}_{1(2)})R_{1(2)}}{\hbar}\boldsymbol{\sigma}(\hat{\mathbf{p}}\times\mathbf{n}) - \frac{2m^*\gamma^{\text{int}}_{c_{1(2)}}}{\hbar^3}(\sigma_y p_y - \sigma_x p_x) \end{array}\right]. \quad (6)$$

Here $\mathbf{n}$ is the unit vector directed along the external normal to the corresponding interface; R_1 (R_2) is a real quantity describing the spectrum of the Tamm's states near the right (left) boundary if they exist (for this sake the condition $R > 0$ must be fulfilled); χ is the bulk spin-orbit parameter (χ = 0.082 for GaAs); $\gamma^{\text{int}}_{c_1}$, χ^{int}_1 and $\gamma^{\text{int}}_{c_2}$, χ^{int}_2 characterizes the spin-orbit interaction at the right and left heterointerfaces, respectively.

In the lowest order over the scalar contributions of the interfaces and the ISOI parameters, the operators $\hat{\Gamma}_{1(2)}$ in the BCs (5) can be transformed to the unitary form

$$\begin{array}{l} \hat{\tilde{\Gamma}}_{1(2)} = \exp(i\hat{g}_{1(2)}\hat{p}_z/\hbar) \text{ with } \hat{g}_{1(2)} \text{ satisfying} \\ \hat{g}_{1(2)} = -R_{1(2)}n_z - \frac{2m^*\gamma_c R_{1(2)}}{\hbar^3}(\sigma_y p_y - \sigma_x p_x)n_z - \\ -\frac{(\chi + \chi^{\text{int}}_{1(2)})R^2_{1(2)}}{\hbar}(\sigma_x p_y - \sigma_y p_x) - \\ -\frac{2m^*\gamma^{\text{int}}_{c_{1(2)}}R_{1(2)}}{\hbar^3}(\sigma_y p_y - \sigma_x p_x)n_z, \end{array} \quad (7)$$

where $n_z = 1$ for the right interface and $n_z = -1$ for the left one. To obtain $\hat{\tilde{\Gamma}}_{1(2)}$ we multiply $\hat{\Gamma}_{1(2)}$ by

the operator $\left\{1+\left[\left(\chi+\chi_{1(2)}^{\text{int}}\right)R_{1(2)}/\hbar\right]\boldsymbol{\sigma}(\hat{\mathbf{p}}\times\mathbf{n})-\right.$ $\left.-\left[2m^*\gamma_{c_{1(2)}}^{\text{int}}/\hbar^3\right](\sigma_y p_y-\sigma_x p_x)\right\}^{-1}$ from the left and neglect the terms nonlinear over the SOI parameters.

If the system allows to perform spin diagonalization, the operators $\hat{g}_1$ and $\hat{g}_2$ transform into scalar quantities $\angle d_1$ and $\angle d_2$, respectively, having the dimensionality of length. In this case the operator $\hat{\Gamma}_{1(2)}$ just shifts the right (left) boundary to the new position $z_r = d/2 + \angle d_1$ ($z_l = -d/2 + \angle d_2$ which depends on the spin projection $\sigma = \pm 1$ and the corresponding interfacial parameters. Such spin diagonalization is possible in the systems with only one type of SOI (Rashba or Dresselhaus).

We begin with the case when only Rashba SOI is present. The resulting problem reads as

$$\left(\frac{\hat{p}_z^2}{2m^*}+V(z)+a_{so}p\sigma\partial_z V\right)\psi_\sigma(z)=E_\sigma\psi_\sigma(z), \quad (8)$$

$$\psi_\sigma(z)|_{z=d/2+\Delta d_1}=0, \quad \psi_\sigma(z)|_{z=-d/2+\Delta d_2}=0, \quad (9)$$

$$\Delta d_{1(2)}=-R_{1(2)}n_z+\frac{\tilde{\chi}_{1(2)}R_{1(2)}^2}{\hbar}p\sigma, \quad (10)$$

where $\tilde{\chi}_{1(2)}=\chi+\chi_{1(2)}^{\text{int}}$, p is the absolute value of $2D$ momentum.

The further analysis is organized as follows. At first we consider the simple problem

$$\left(\frac{\hat{p}_z^2}{2m^*}+V(z)\right)\psi^{(0)}=E^{(0)}\psi^{(0)}, \quad (11)$$

$$\psi^{(0)}(z)|_{z=z_r}=0, \quad \psi^{(0)}(z)|_{z=z_l}=0, \quad (12)$$

which allows an exact numerical solution for an arbitrary potential profile $V(z)$. Next we assume $\angle d_1$ and $\angle d_2$ to be much smaller than d and obtain the energy spectrum of the problem (8)-(10). In the lowest order over the SOI parameters it reads as

$$E_\sigma=E^{(0)}+a_{so}\left\langle\psi^{(0)}|\partial_z V|\psi^{(0)}\right\rangle p\sigma+ +\left.\frac{\partial E^{(0)}}{\partial z_r}\right|_{-\frac{d}{2},\frac{d}{2}}\Delta d_1+\left.\frac{\partial E^{(0)}}{\partial z_l}\right|_{-\frac{d}{2},\frac{d}{2}}\Delta d_2. \quad (13)$$

Finally, we calculate the spin splitting $E_{SS} = (E_{+1} - E_{-1})$ and, comparing it with (1), obtain α_{SIA}

$$\alpha_{SIA}=\alpha_{SIA}^{(0)}+\frac{\tilde{\chi}_1R_1^2}{\hbar}\left.\frac{\partial E^{(0)}}{\partial z_r}\right|_{-\frac{d}{2},\frac{d}{2}}+\frac{\tilde{\chi}_2R_2^2}{\hbar}\left.\frac{\partial E^{(0)}}{\partial z_l}\right|_{-\frac{d}{2},\frac{d}{2}}. \quad (14)$$

Here the last two terms are the desired interfacial contributions. In the system with only Dresselhaus-type SOI we have

$$\Delta d_{1(2)}=-R_{1(2)}n_z-\frac{2m^*\tilde{\gamma}_{c_{1(2)}}R_{1(2)}}{\hbar^3}n_z p\sigma, \quad (15)$$

where $\tilde{\gamma}_{\tilde{n}_{1(2)}}=\gamma_{\tilde{n}}+\gamma_{\tilde{n}_{1(2)}}^{\text{int}}$. Performing the similar analysis as before we obtain interfacial contributions to α_{BIA}

$$\alpha_{BIA}=\alpha_{BIA}^{(0)}-\frac{2m^*(\gamma_c+\tilde{\gamma}_{c_1})R_1}{\hbar^3}\left.\frac{\partial E^{(0)}}{\partial z_r}\right|_{-\frac{d}{2},\frac{d}{2}}- -\frac{2m^*\tilde{\gamma}_{c_1}R_1}{\hbar^3}\left.\frac{\partial E_2^{(0)}}{\partial z_r}\right|_{-\frac{d}{2},\frac{d}{2}}+\frac{2m^*(\gamma_c+\tilde{\gamma}_{c_2})R_2}{\hbar^3}\left.\frac{\partial E_1^{(0)}}{\partial z_l}\right|_{-\frac{d}{2},\frac{d}{2}}+ +\frac{2m^*\tilde{\gamma}_{c_2}R_2}{\hbar^3}\left.\frac{\partial E_2^{(0)}}{\partial z_l}\right|_{-\frac{d}{2},\frac{d}{2}}, \quad (16)$$

where $E_1^{(0)}=\left\langle\psi^{(0)}(z)|\hat{p}_z^2/2m^*|\psi^{(0)}(z)\right\rangle$,
$E_2^{(0)}=\left\langle\psi^{(0)}(z)|V(z)|\psi^{(0)}(z)\right\rangle$.

One can expect that since all spin-orbit constants are small in general case when both Rashba and Dresselhaus type terms are allowed in the effective spin Hamiltonian, the corresponding spin splitting has the form (1), where in the lowest order over SOI parameters, α_{SIA} and α_{BIA} are still determined by Eqs. (14) and (16), respectively. This assumption will be verified below on a simple example.

It is important to note that the interfacial contributions to α_{SIA} and α_{BIA} can be calculated in a QW with arbitrary doping level and potential distribution since one is always able to find $E^{(0)}$ and $\psi^{(0)}$ numerically. However, in some cases transparent analytical results can be obtained. As an example we now consider the "narrow" QW in which the size quantization energy much exceeds the energy of the electron interaction with the smooth (in the atomic scale) potential $V(z)$. Treating the potential $V(z)$ as a perturbation, we obtain from Eqs. (14) and (16) for the ground subband

$$\alpha_{SIA}=\alpha_{SIA}^{(0)}-\frac{2\tilde{E}_0}{\hbar}\frac{(\tilde{\chi}_1R_1^2-\tilde{\chi}_2R_2^2)}{d}+ +\frac{eFd}{2E_0}\frac{E_0}{\hbar}\frac{(\tilde{\chi}_1R_1^2+\tilde{\chi}_2R_2^2)}{d}, \quad (17)$$

$$\alpha_{BIA}=\alpha_{BIA}^{(0)}-\frac{2k_0^2}{\hbar}\left[\frac{\gamma_c(R_1+R_2)}{d}+ +\frac{\tilde{E}_0}{E_0}\frac{(\tilde{\gamma}_{c1}R_1+\tilde{\gamma}_{c2}R_2)}{d}+\frac{eFd}{4E_0}\frac{(\tilde{\gamma}_{c2}R_2-\tilde{\gamma}_{c1}R_1)}{d}\right], \quad (18)$$

where

$$k_0 = \pi / d, \;\; eF = \langle \psi_0(z) | V'(z) | \psi_0(z) \rangle,$$
$$\psi_0(z) = \sqrt{2/d} \cos k_0 z, \;\; E_0 = \frac{\hbar^2 k_0^2}{2m^*}, \qquad (19)$$
$$\tilde{E}_0 = E_0 - \frac{1}{2} \langle \psi_0(z) | z V'(z) | \psi_0(z) \rangle.$$

It follows from Eqs. (17) and (18) that the ISOI not only renormalizes the values of α_{BIA} and α_{SIA}, but also affect the qualitative behaviour of the spin splitting. The spin splitting is anisotropic in the structures where both Dresselhaus- and Rashba-type SOIs are present. In the framework of the envelope functions approximation, α_{SIA} is commonly assumed to be nonzero only in the structures with built-in or external electric field. However, it is seen from the Eq. (17) that if the interfaces are non-equivalent, i.e. $\tilde{\chi}_1 R_1^2 \neq \tilde{\chi}_2 R_2^2$, the α_{SIA} is finite even in the QWs with zero average electric field. This effect gives rise to anisotropy of the spin splitting in such structures. Our theory naturally explains the results of Ref. [4] where significantly nonzero α_{SIA} was observed in the nominally symmetric QW with equally doped sides and zero average electric field. At the same time, the interfacial contribution to α_{BIA} is nonzero even for structures with identical boundaries, i.e. $\gamma_{c_1}^{int} = \gamma_{c_2}^{int}$ and $R_1 = R_2$.

Now we check if the above assumption regarding the additivity of the Rashba and Dresselhaus contributions in the lowest order over SOI constants is fulfilled in the "narrow" QW. For this purpose, we calculate the spin splitting starting from the 3D problem (2)-(5) with both types of SOI and compare obtained α_{SIA} and α_{BIA} with ones satisfying (17) and (18).

Aiming to analyse the effect of ISOI on the spin splitting, we take into account the interaction with the interfacial potential exactly. At the same time, bulk SOI $\hat{H}_{BIA} + \hat{H}_{SIA}$ and the smooth potential $V(z)$ which average value is assumed to be small in comparison with the size quantization energy are treated perturbatively. At first, we consider the following problem

$$\frac{\hat{p}_z^2}{2m^*} \phi^{(0)}(z) = \in^{(0)} \phi^{(0)}(z), \qquad (20)$$

$$\hat{\Gamma}_1 \phi^{(0)}(z)|_{z=d/2} = 0, \;\; \hat{\Gamma}_2 \phi^{(0)}(z)|_{z=-d/2} = 0. \qquad (21)$$

Introducing the values

$$\alpha_{1(2)} = 2m^* \tilde{\gamma}_{c_{1(2)}} R_{1(2)} p / \hbar^3,$$
$$\beta_{1(2)} = \tilde{\chi}_{1(2)} R_{1(2)}^2 p / \hbar,$$
$$\Delta = (\alpha_1 + \alpha_2) e^{-i\phi} - i(\beta_1 - \beta_2) e^{i\phi},$$
$$\tilde{\Delta} = (\alpha_1 - \alpha_2) e^{-i\phi} + i(\beta_1 - \beta_2) e^{i\phi}$$

we obtain the eigenvalues and eigenfunctions of the problem (20)-(21) in the lowest order over the scalar contributions of the interfaces and the ISOI parameters $\in_{\pm}^{(0)} = E_0 [1 + 2(R_1 + R_2)/d \pm 2|\Delta|/d]$,

$$\phi_{\pm}^{(0)}(z) = \begin{pmatrix} C_1^{\pm} e^{-ik_{\pm}z} + C_3^{\pm} e^{ik_{\pm}z} \\ C_2^{\pm} e^{-ik_{\pm}z} + C_4^{\pm} e^{ik_{\pm}z} \end{pmatrix}, \qquad (22)$$

where

$$k_{\pm} = k_0 [1 + (R_1 + R_2)/d \pm |\Delta|/d],$$
$$C_2^{\pm} = \mp \frac{\Delta^*}{|\Delta|} C_1^{\pm}, \;\; C_3^{\pm} = \left[1 + ik_0 (R_1 - R_2) \pm \frac{\tilde{\Delta}}{\Delta} |\Delta| \right] C_1^{\pm}, \qquad (23)$$

$$C_4^{\pm} = \left[\mp \frac{\Delta^*}{|\Delta|} - ik_0 \tilde{\Delta}^* \right] C_1^{\pm}, \qquad (24)$$

and $|C_1| = (1/4d)[1 - (R_1 + R_2)/d \mp |\Delta|/d]^{-2}$.

Next we find the spectrum of the problem (2)-(5) using the eigenfunctions (22) as a basis $\phi(z) = A\phi_+^{(0)} + B\phi_-^{(0)}$ and considering $\hat{\delta}H = \hat{H}_{BIA} + \hat{H}_{SIA} + V(z)$ as a perturbation

$$\begin{pmatrix} \in_+^{(0)} + \langle \phi_+^{(0)} | \delta\hat{H} | \phi_+^{(0)} \rangle & \langle \phi_+^{(0)} | \delta\hat{H} | \phi_-^{(0)} \rangle \\ \langle \phi_-^{(0)} | \delta\hat{H} | \phi_+^{(0)} \rangle & \in_-^{(0)} + \langle \phi_-^{(0)} | \delta\hat{H} | \phi_-^{(0)} \rangle \end{pmatrix} \begin{pmatrix} A \\ B \end{pmatrix} = E \begin{pmatrix} A \\ B \end{pmatrix}. \qquad (25)$$

As it was expected, we obtain that the resulting spin splitting of the spectrum has the form (1) with α_{SIA} and α_{BIA} satisfying Eqs. (17) and (18), respectively.

The values of the interfacial parameters can be extracted from comparison with the experiment, as it was done for the wide one-side doped quantum well GaAs/AlGaAs in Ref.[17]. Let us, for example, evaluate the values $\tilde{\chi}_1 R_1^2$ and $\tilde{\chi}_2 R_2^2$ comparing Eq. (17) with the experimental data from Ref. [4]. Due to the fact that all quantum wells were grown under the same conditions we assume the interfacial parameters to be equal for all structures. However, in each quantum well the left interface is not equivalent to the right one. We also suppose $\tilde{E}_0 \approx E_0$. For the symmetrical sample with $F = 0$ and $d = 12$ nm the parameter $\alpha_{SIA} = (0.4 \cdot 10^{-3}) v_F$ ($v_F = 4.11 \cdot 10^7$ sm/s is the Fermi velocity) is determined

from the difference between $\tilde{\chi}_1 R_1^2$ and $\tilde{\chi}_2 R_2^2$. Thus, we can estimate this difference as $\tilde{\chi}_1 R_1^2 - \tilde{\chi}_2 R_2^2 = 1.4\text{Å}^2$. Next we consider the sample with the same thickness and asymmetrical doping for which [4] $\alpha_{SIA} = (1.3 \cdot 10^{-3})\ v_F$. Performing the self-consistent solution of the Shrödinger and Poisson equations, we obtain $F = 2.085 \cdot 10^5\ V/sm$. Thus, we evaluate $\tilde{\chi}_1 R_1^2 + \tilde{\chi}_2 R_2^2 = 7.7$ 2. Finally, we find $\tilde{\chi}_1 R_1^2 = 4.6\text{Å}^2$, $\tilde{\chi}_2 R_2^2 = 3.1\text{Å}^2$. The experimental data presented in Ref. [4] is not enough to calculate $\tilde{\chi}_1$, $\tilde{\chi}_2$, R_1 and R_2 separately. However, some estimates can be obtained. The typical value of R is in the order of ~20Å [17]. Thus, we evaluate $\tilde{\chi}_1 \sim 0.012$ and $\tilde{\chi}_2 \sim 0.008$. The corresponding values $\tilde{\chi}_1^{int} \sim -0.07$ and $\tilde{\chi}_2^{int} \sim -0.74$ are the same order as bulk value $\chi = 0.082$.

3. CONCLUSION

In conclusion we developed the theory of ISOI in the narrow QWs. We have obtained the renormalization of the Dresselhaus and Rashba parameters arising from the SOI at two heterointerfaces. The considerable spread in the experimentally determined values of spin-orbit constants can originate from the dependence of α_{BIA} and α_{SIA} on the interfacial parameters and, thus, on the growth conditions. We also have demonstrated that the microscopic dissimilarity of the interfaces leads to the finite Rashba parameters even in the QWs with zero average electric field. This result explains the experimental data of Ref. [4] where nonzero α_{SIA} was obtained in the symmetric structure.

REFERENCES

1. Dresselhaus G. Spin-Orbit Coupling Effects in Zinc Blende Structures. *Phys. Rev.*, 1955, 100(2):580-586.
2. BychkovYuA, Rashba EI. Properties of a 2*D* electron gas with lifted spectral degeneracy. *JETP Lett.*, 1984, 39(2):78-81.
3. Dyakonov MI, Perel VI. Spin relaxation of conduction electrons in noncentrosymmetric semiconductors. *Sov. Phys. Solid State,* 1972, 13(12):3023-3026.
4. Koralek JD, Weber CP, Orenstein J, Bernevig BA, Zhang Sh-Ch, Mack S, Awschalom DD. Emergence of the persistent spin helix in semiconductor quantum wells. *Nature,* 2009, 458(7238):610-613.
5. Marushchak VA, Stepanova MN, Titkov AN. Spin relaxation of conduction electrons in moderately doped gallium arsenide crystals. *Sov. Phys. Solid State*, 1983, 25:2035.
6. Dresselhaus PD, Papavassiliou CMA, Wheeler RG, Sacks RN. Observation of spin precession in GaAs inversion layers using antilocalization. *Phys. Rev. Lett.*, 1992, 68:106.
7. Richards D, Jusserand B, Allan G, Priester C, Etienne B. Electron spin-flip Raman scattering in asymmetric quantum wells: spin orientation. *Solid-State Electronics*, 1996, 40(1-8):127-131.
8. Miller JB, Zumbuhl, DM Marcus CM, Lyanda-Geller YB, Goldhaber-Gordon D, Campman K, Gossard AC. Gate-Controlled Spin-Orbit Quantum Interference Effects in Lateral Transport. *Phys. Rev. Lett.*, 2003, 90:076807.
9. Krich JJ, Halperin BI. Cubic Dresselhaus spin-orbit coupling in 2*D* electron quantum dots. *Phys. Rev. Lett.,* 2007, 98(22):226802.
10. Leyland WJH, Harley RT, Henini M, Shields AJ, Farrer I, Ritchie DA. *Phys. Rev. B*, 2007, 76:195305; Studer M, Walser MP, Baer S, Rusterholz H, Schon S, Schuh D, Wegscheider W, Ensslin K, Salis G. *Phys. Rev. B*, 2010, 83:235320.
11. Eldridge PS, Hubner J, Oertel S, Harley RT, Henini M, Oestreich M. Spin-Orbit Fields In Asymmetric (001)-Oriented GaAs/$Al_xGa_{1-x}As$ Quantum Wells. *Phys. Rev. B*, 2011, 83(4):041301.
12. Walser MP, Siegenthaler U, Lechner V, Schuh D, Ganichev SD, Wegscheider W, Salis G. Dependence of the Dresselhaus spin-orbit interaction on the quantum well width. *Phys. Rev. B,* 2012, 86:195309.
13. Alekseev PS. Anisotropic interface contribution to the spin-orbit interaction in quantum wells. *JETP Lett.*, 2013, 98(2):84-87.
14. Ganichev SD, Golub LE. Interplay of Rashba/Dresselhaus spin splittings probed by photogalvanic spectroscopy. *Phys. Status Solidi B,* 2014, 251(9):1801-1823.
15. Devizorova ZhA, Volkov VA. Spin splitting of two-dimensional states in the conduction band of asymmetric heterostructures: Contribution from the atomically sharp interface. *JETP Lett.,* 2013, 98(2):101-106.

16. Devizorova ZhA, Shchepetilnikov AV, Nefyodov YuA, Volkov VA, Kukushkin IV. Interface contributions to the spin-orbit interaction parameters of electrons at the (001) GaAs/AlGaAs interface. *JETP Lett.,* 2014, 100(2):102-109.
17. Winkler R. *Spin-orbit coupling effects in two-dimensional electron and hole systems.* Berlin, Springer, 2003, p. 194.

SPIN INTERACTIONS AT THE INTERFACES FERROMAGNETIC OXIDE/FERROMAGNETIC INTERMETALLIC SUPERLATTICE

Alexey A. Klimov
MIREA- Russian Technological University, http://mirea.ru
Moscow 119454, Russian Federation

Viktor V. Demidov, Timur A. Shaykhulov, Gennady A. Ovsyannikov, Karen Y. Constantinian, Sergey A. Nikitov
Kotelnikov Institute of Radioengineering and Electronics of RAS, http://cplire.ru/
Moscow 125009, Russian Federation

Vladimir L. Preobrazhensky
Prokhorov General Physics Institute of RAS, http://igp.ras.ru/
Moscow 119991, Russian Federation

Nicolas Tiercelin, Philippe Pernod
Institut d'Electronique, de Microélectronique et de Nanotechnologie, Université de Lille, https://www.iemn.fr/
Centrale Lille, ISEN, Univ Valencienes UMR 8520-IEMN, LIA LICS/LEMAC, F- 59652, Villeneuve d'Ascq Cedex, France

aleks-klimov@yandex.ru, demidov@cplire.ru, shaihulov@hitech.cplire.ru, gena@hitech.cplire.ru, karen@hitech.cplire.ru, vladimir.preobrajenski@univ-lille.fr, nicolas.tiercelin@univ-lille.fr, philippe.pernod@univ-lille.fr, nikitov@cplire.ru

Abstract. **The magnetic properties of the heterostructures consisting of platinum Pt, epitaxially grown manganite optimally doped by strontium $La_{0.7}Sr_{0.3}MnO_3$ (LSMO), rare earth intermetallic superlattices consisting of exchange-coupled layers $TbCo_2$/FeCo (TCFC), and the epitaxial film of yttrium iron garnet $Y_3Fe_5O1_2$ (YIG) were investigated. The TCFC material provides giant magnetostriction, large magnitude of the magnetomechanical coupling coefficient, and controlled induced magnetic anisotropy. In addition TCFC, as well as Pt, has strong spin-orbit interaction. Experimental studies have shown that the magnetic interaction of the heterostructure ($TeCo_2$/FeCo)n/LSMO has an antiferromagnetic character. An increase of linewidth of the ferromagnetic resonance in the Pt/LSMO structure was observed and explained by the spin current flow induced in Pt film by the LSMO film at ferromagnetic resonance. In the TCFC/YIG heterostructure, an electric voltage induced in the TCFC film was observed and explained by the inverse spin-Hall effect under conditions of ferromagnetic resonance.**

Keywords: **heterostructure, manganite, intermetallic superlattice, yttrium iron garnet, ferromagnetic resonance, spin current, inverse spin-Hall effect**

PACS: 75.47.Lx, 75.25.-j, 75.70.Cn, 71.20.Lp

Bibliography - 34 references *Received 12 November 2018; accepted 10 December 2018*

RENSIT, 2018, 10(3):363-372 **DOI: 10.17725/rensit.2018.10.363**

Contents

1. INTRODUCTION

The development of spintronic devices based on magnetoactive materials with the nanoscale interfaces is an important task, which requires the study of the physics of structural and phase transformations in thin films and at the interfaces. Spintronics is based on phenomena associated with the transfer of the spin moment. A "pure" spin current can be created by several

mechanisms, among which the most effective are the spin-Hall effect [1] and the spin pumping in ferromagnetic resonance mode [2]. The magnetic heterostructure as a rule consists of magnetic and nonmagnetic layers. Materials with a strong spin-orbit interaction play an important role in the detection of the spin current. A pure spin current (J_S) can be detected using the inverse spin-Hall effect (ISHE) in a material with strong spin-orbit interaction by converting into conduction current $J_c = \theta_{SH}(\hbar/2e)(J_S \cdot \sigma)$, where θ_{SH} is the angle of spin-Hall effect, σ - carrier polarization.

However, not only non-magnetic normal metals can be used as ISHE spin current detectors. In a number of works, it was shown that magnetic metals, such as permalloy Py (NiFe), as well as Fe, Co, Ni can be used as spin current detectors [3-5]. $TbCo_2$/FeCo structures containing Tb element with a strong spin-orbit interaction (high atomic weight *Z*) are distinguished by giant magnetostriction, a large value of the magnetomechanical coupling coefficient, controlled induced magnetic anisotropy and the ability to induce spin-orientation transitions by a magnetic field or elastic stresses [6, 7]. In turn, rare earth manganite perovskites with the structure $Re_{1-x}A_xMnO_3$ (Re are rare earth materials such as La or Nd), and A - alkaline earth metals such as Sr, Ca, Ba) exhibit a wide range of unusual electrical and magnetic properties, including high (up to 100 %) magnetic polarization, the effect of colossal magnetoresistance, etc (see review [8]). Manganite films for which the Curie temperature T_C is close to room temperature is especially attractive for practical use. A number of studies on the excitation of the spin current by ferromagnetic resonance in LSMO/N structures (N is a normal metal, usually platinum) were made in [9, 10]. However, there are no data on the temperature dependences of the width of the ferromagnetic resonance (FMR) line during the generation of spin current in ferromagnets and on the magnitude of the spin conductivity of the LSMO/Pt boundary. We have investigated the magnetic properties of heterostructures consisting of platinum Pt, epitaxially grown manganite $La_{0.7}Sr_{0.3}MnO_3$ (LSMO), rare earth intermetallic superlattices consisting of exchange-coupled layers $TbCo_2$/FeCo (TCFC), and the epitaxial film of yttrium iron garnet $Y_3Fe_5O_{12}$ (YIG). Our studies are focused on the effects associated with the excitation and generation of spin current in the structures.

2.FERROMAGNETIC RESONANCE IN MANGANITE EPITAXIAL FILMS

The Hilbert damping parameter α is a measure of the spin precession relaxation in homogeneous ferromagnets caused by spin-orbit interaction [11]. The width of the homogeneous FMR line induced by Hilbert damping is proportional to the FMR frequency ω, $\Delta H_G = \alpha\omega/\gamma$ ($\gamma = g\mu_B/\hbar$ is the gyromagnetic ratio) and describes the situation for the homogeneous case. In the ferromagnetic structure of a ferromagnet and a normal metal, the FMR line is additionally broadened due to the generation of the spin current, inhomogeneity of the magnetization of the ferromagnet, interaction with another material, two-magnon scattering and the appearance of eddy current in the ferromagnet. As a result, the FMR linewidth can be represented as a sum

$$\Delta H_{PP} = \Delta H_G + \Delta H_I + \Delta H_{2M} + \Delta H_E, \quad (1)$$

where ΔH_I, ΔH_{2M}, ΔH_E are the widths of the lines for damping caused by the inhomogeneous state of a ferromagnet, two-magnon scattering and damping caused by eddy current, respectively [12, 13]. A change in the magnetic properties of materials such as its anisotropy or magnetization affects the inhomogeneous broadening of the FMR line (ΔH_I) which is independent of frequency [12, 13]. The magnetic field of an alternating current caused by FMR induces eddy currents in a thin conductive film. These currents produce an additional change in the amplitude of the alternating current magnetic fields of the heterostructure. The influence of eddy currents on ferromagnetic resonance in a conducting ferromagnetic system can lead to

broadening of the FMR linewidth (ΔH_E) and to the change in the shape of the FMR spectrum at non-uniform microwave field [14-16]. The mechanism of two-magnon scattering leads to the connection of homogeneous precession (k = 0) with degenerate finite spin-wave modes [17, 18]. In a ferromagnet/normal metal heterostructure the precession of magnetization in a ferromagnet causes a spin current to flow through the boundary into the normal metal, which broadens the FMR line. The theory [19] predicts the spin current to flow through the boundary of the ferromagnetic and nonmagnetic layers perpendicular to the interface.

The linewidth of ferromagnetic resonance ΔH_{pp}, measured by scanning the external magnetic field H, is defined as the difference in the field positions between the extremes H_{p+}, H_{p-} of the first derivative of the dP/dH microwave absorption signal (see **Fig. 1**). At this value, the resonance field H_0, defined as the point of transition of the signal dP/dH through zero is always in the range $H_{p+} < H_0 < H_{p-}$. Note, that the determination of the linewidth by approximating the FMR spectrum by several Lorentz lines gives an approximate 10% correction in the value of ΔH_{pp}.

Experimental studies were performed on $La_{0.7}Sr_{0.3}MnO_3$ (LSMO) epitaxial films, which were deposited by magnetron sputtering onto (110) $NdGaO_3$ (NGO) single crystal substrates at T = 820°C and oxygen pressure of 0.15-1 mbar. Pt films 10-20 nm thick were deposited ex situ immediately after cooling of the manganite film. Magnetic characteristics were measured by FMR using a Bruker spectrometer (frequency 9.51 GHz). The experimental samples were located in the microwave cavity of the spectrometer so that the sample plane was always parallel to the direction of the constant external magnetic field and the magnetic component of the microwave field (parallel orientation). The method of sample preparation and FMR measurements are described in [20]. Obtained films were investigated immediately after the deposition and cooling to room temperature (d-LSMO), and were annealed after the growth at T = 820°C for one hour (h-LSMO). For h-LSMO films, 40 nm thick, we determined the attenuation α_0 of the spin precession at room temperature from linewidth ΔH_{PP} = 28 Oe which corresponds to $\alpha_0 = \Delta H_{PP} \cdot \gamma/\omega = 8 \cdot 10^{-3}$. The increase in attenuation $\alpha = \alpha_0 + \alpha'$ during the deposition of Pt on the LSMO can occur due to the flow of the spin current through the Pt/LSMO boundary. For Pt deposited on the h-LSMO film with thickness of 10 nm the parameter α increases by 10%. Using [21, 22], one can calculate the spin conductivity in the Pt/LSMO heterostructure:

$$g^{\uparrow\downarrow} = \frac{4\pi M_s t_{LSMO}}{g\mu_B}\alpha', \qquad (2)$$

where $\gamma = 17.605 \cdot 10^6$ is gyromagnetic ratio for an electron, $\omega = 2\pi \cdot 9.51 \cdot 10^9 s^{-1}$ is microwave angular frequency, M_s = 300 Oe is LSMO film magnetization, t_{LSMO} = 40 nm is LSMO film thickness, $\mu_B = 9.274 \cdot 10^{-21}$ erg/G is the Bohr magneton, g = 2 is the Lande factor. At room temperature, an increase in the FMR linewidth after deposition of Pt $\Delta H_{Pt/LSMO} - \Delta H_{LSMO} = 4$ Oe and, therefore, $g^{\uparrow\downarrow} = 0.4 \cdot 10^{19}$ m^{-2} was obtained. This value of the spin conduction of the boundary slightly exceeds $g^{\uparrow\downarrow} \sim 10^{18}$ m^{-2}, obtained from measurements of the spin current on the same Pt/LSMO structures using the inverse spin-Hall effect [23]. For comparison, $g^{\uparrow\downarrow} = 2.1 \cdot 10^{19}$ m^{-2}

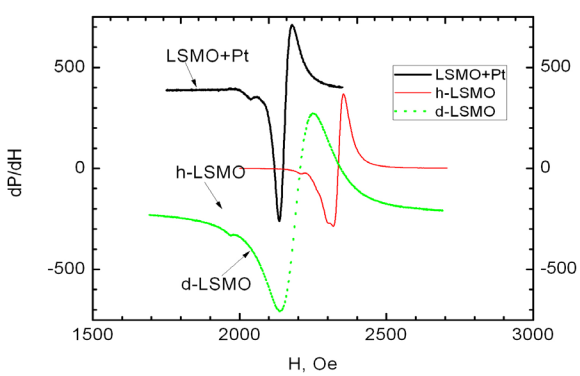

Fig. 1. *FMR spectra for d-LSMO and h-LSMO films and Pt/h-LSMO heterostructures. Spectra for d-LSMO and Pt/h-LSMO are shifted along the dP/dH axis.*

[24] was obtained for Py/Pt boundaries, and $g^{\uparrow\downarrow} = 4.8 \cdot 10^{20}$ m^{-2} [25] for YIG/Pt.

When estimating the spin conductivity, using (2), other mechanisms of spin precession damping were not been taken into account. The effective one-dimensional spin conductivity of a normal metal layer connected in series with the spin conductivity of the gext interface contributes to the effective spin conductivity of the structure [26, 27].

$$g_{eff} = (1/g^{\uparrow\downarrow} + 1/g_{ext}). \quad (3)$$

The expression for g_{ext} is obtained by solving the spin diffusion equation with the corresponding boundary conditions. In the case of the ferromagnet/normal metal structure, the following spin conductivity expression was obtained [22]

$$g_{ext} = \tanh(d_{Pt}/\lambda_d)/(2\lambda_d \rho_{Pt}), \quad (4)$$

where ρ_{Pt}, d_{Pt} and λ_d are the specific resistance, thickness and diffusion length for the Pt film, respectively. For a thickness of d_{Pt} = 10 nm, exceeding λ_d = 3 nm [22], $\tanh(d_{Pt}/\lambda_d) \approx 1$, and the contribution to the line width from the spin conductivity in the Pt film is equal at room temperature:

$$\Delta H_{ext} = (\omega/\gamma) g \cdot \mu_B \cdot h/(2\pi 4 e^2 M_s d_F \rho_{Pt} \lambda_d) \approx 6\ Oe, \quad (5)$$

where g = 2, M_s = 300 *Oe*, $d_F = 4 \cdot 10^{-6}$ cm, $\rho_{Pt} = 3 \cdot 10^{-5}$ Ω cm, $\lambda_d = 3 \cdot 10^{-7}$ cm, $h/e^2 = 2.6 \cdot 10^4$ Ω. The broadening of the FMR line due to the effective spin conductivity of the normal metal layer is equal to the contribution from the spin current. The large value of this broadening is probably caused by an error in determining the spin relaxation length λ_d. The temperature dependences of the linewidth for the *b*-LSMO manganite film and for the Pt/*b*-LSMO heterostructure are presented in **Fig. 2**. With a decrease in the temperature the ΔH_{pp} markedly increased. Increasing M_s with decreasing T may cause an increase in the linewidth (see expression (5)). But below T = 200 K, the magnetization M_s is saturated, and the width of the FMR line continues to grow.

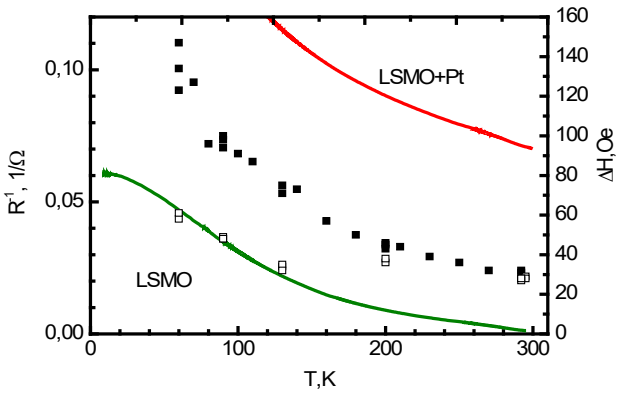

Fig. 2. *Temperature dependences of the width of the FMR lines of the b-LSMO film (open squares) and Pt/b-LSMO heterostructures (filled squares). The temperature dependences of the resistance of LSMO manganite films (green line) and Pt/b-LSMO heterostructures (red line) are presented.*

When a Pt film is deposited on top of an LSMO film, the overall conductivity of the structure increases (see Fig. 2). The increase in ΔH_{pp}, which is observed in the experiment after the deposition of Pt at low temperatures, can be fully explained by the generation of the spin current in the Pt/LSMO heterostructure. With decreasing temperature, the resistivity of the Pt film decreases in proportion to T, and the resistance of the LSMO film changes by more than one order of magnitude. The contribution of all layers to the resistivity of the heterostructure is explained by the fact that the LSMO film together with the Pt film acts as parallel resistors [28]. An increase in ΔH_{pp} with decreasing temperature can be caused by damping caused by eddy current, which is proportional to the conductivity of the structure.

3. FMR FOR TCFC/LSMO HETEROSTRUCTURE

The FMR spectrum of the TCFC/LSMO heterostructure presented in **Fig. 3**a, was measured at the frequency $\omega/2\pi$ = 9.74 GHz at T = 300 K with a constant field lying in the plane of the heterostructure and directed along the axis of easy magnetization of the heterostructure. Three areas of ferromagnetic order are visible in the structure. The temperature dependences of the resonance fields H_0 for three lines of the FMR spectrum are shown in Fig. 3b. The line in the

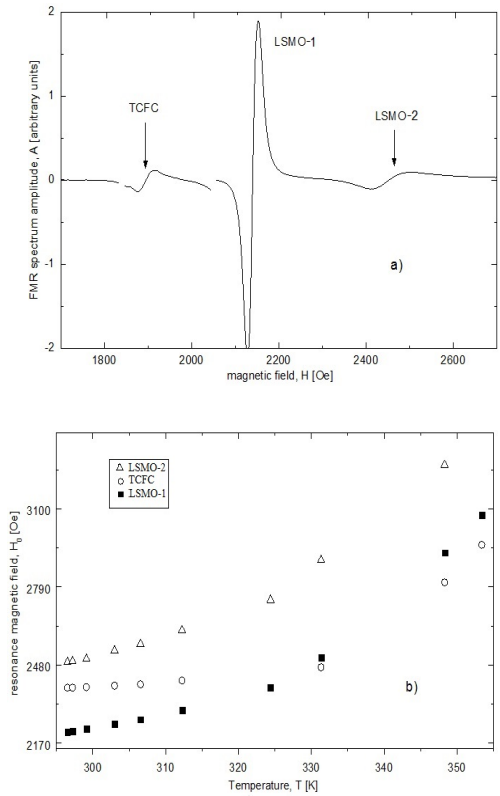

Fig. 3. *(a) FMR spectrum of the TCFC/LSMO heterostructure. The constant magnetic field is directed along the easy axis of magnetization, T = 300K. The scale of the TCFC superlattice line has been increased 10 times. (b) Temperature dependences of the resonant magnetic field for three lines of FMR. Triangles, filled rectangles and circles refer to LSMO-2, LSMO-1 and TCFC film correspondingly*

1900 Oe area in Fig. 3a is caused by the presence of a TCFC superlattice in the structure. It is seen that at $T \leq 300$ K, the field $H_0(T)$ of this line slowly decreases with decreasing temperature, which indicates a high Curie temperature of the film (above 360 K). Two other lines refer to the LSMO film: LSMO-2 corresponds to the part of the LSMO film that lies under the TCFC superstructure, while LSMO-1 refers to the part of the LSMO film that is not covered by the TCFC film. The number of electron spins for the LSMO-1 and LSMO-2 peaks is determined by the topology of the sample (the area covered by the TCFC and the non-covered parts of the chip). Estimation of the number of spins was carried out by calculating the area of the absorption line of the FMR spectrum. The widths of the FMR spectra (ΔH) of these two lines of the LSMO film differ by 40–50 Oe.

Since both parts of LSMO-1 and LSMO-2 are located on the same substrate and have the same crystal structure, the observed difference of ΔH in peaks is most likely caused by the interaction of the TCFC superlattice and LSMO film. A similar broadening of the FMR line for structures with ferromagnet/normal metal interfaces was observed previously (see the part 2 of the article) and is explained theoretically [19] by the spin current leaving the ferromagnet in a normal metal during FMR.

Solving the Landau-Lifshitz-Gilbert equation gives two resonance relations $\omega(H_0)$, describing the FMR in TCFC and LSMO-2 films. With allowance for uniaxial and biaxial anisotropies, these relations are similar to those obtained in [29] for an autonomous LSMO film deposited on an (011) $NdGaO_3$ orthorhombic substrate, which causes the uniaxial magnetic anisotropy [20]. Taking into account the magnetic interaction in the expressions for the resonant frequency $\omega(H_0)$[20], the value of H_0 should be replaced by the sum of two terms $H_{01} + H_{J1}$ and $H_{02} + H_{J2}$ for the LSMO-2 film and TCFC superlattices, respectively. Here, $H_{J1} = J/(M_1 d_1)$ and $H_{J2} = J/(M_2 d_2)$ (d_1 and d_2 of the thickness of the LSMO and TCFC layers, respectively) give an effective interlayer exchange interaction for the LSMO-2 and TCFC films.

To determine the structure parameters, we first calculate the angular dependence of the FMR response of an autonomous LSMO film (LSMO-1). Then, using the magnitude of the magnetization obtained by fitting the dependence of the resonant field on the angle, we calculate the angular dependence of H_0 for the LSMO-2 film. Then, the exchange interaction constant J is determined. Finally, the obtained value J is used to calculate the angular dependence of H_0 for the TCFC film and for calculating the value M_2. As a result, the data obtained allow us to conclude that the TCFC/LSMO interface can be characterized by antiferromagnetic interlayer interaction with a constant J = -0.24 erg/cm.

4. RARE-EARTH INTERMETALLIC SUPERLATTICES

The structure in the form of a 'sandwich' (FeCo/$TbCo_2$/FeCo)/MgO/(FeCo/$TbCo_2$/FeCo) (TCFCM), which is promising for creating the magnetically controlled switches, was investigated [30]. The two films (in brackets) are three-layer polycrystalline films of intermetallic compounds with a thickness of 2 nm (FeCo) and 6 nm ($TbCo_2$), which are separated by a thin layer of MgO with a thickness of 3 nm. This structure was deposited on a silicon substrate with dimensions of 5×5×0.5 mm^3. Both intermetallic films are ferromagnets at room temperature with giant magnetostriction. During deposition of intermetallic films the external magnetic field was applied in parallel to the substrate plane, keeping the same direction, but with significantly different intensities for each of compounds. In this case, it was expected that the easy axis $\mathbf{n}_u$ magnetic anisotropy of the films will lie in their plane and will be oriented along the imposed magnetic field, while their magnetic anisotropy constants will be significantly different.

Recently, ferromagnetic films with in-plane uniaxial anisotropy of the magnetic field revealed the effect of a sharp increase in the radio frequency (RF) dynamic magnetic susceptibility [23, 31–33]. It is observed when the external magnetic field H_0 lies in the film plane and directed perpendicular to its easy magnetization axis $\mathbf{n}_u$ (and, therefore, parallel relative to the hard axis direction) and passes through the value $H_0 = H_u$, where H_u is the field of uniaxial intra-planar magnetic anisotropy of the film. In this case, the recording radio frequency magnetic field $he^{i\omega t}$ is directed perpendicular to the field H_0, and its frequency ω is fixed. The effect manifests itself in the form of a relatively narrow resonance-like absorption signal with a maximum at $H_0 = H_u$. A feature of this signal is that when another frequency ω is set being changed over wide limits, the field at which it is observed remains unchanged and is equal to $H_0 = H_u$. This effect, called the "magnetic pseudo-resonance" [23], is caused by the loss of stability of the magnetic system at the critical point $H_0 = H_u$ of the transition from the angular phase to the collinear one with a direction of magnetization parallel to the external field [33].

To search for a pseudo-resonance signal, the TCFC film structure was placed in a Q-meter sensor coil. The signal was recorded by the method of synchronous detection with a bi-directional sweep of the H_0 field, additionally modulated with the frequency of 52.3 kHz and the amplitude of 1.3 Oe. Signal registration was carried out continuously with multiple accumulations (up to 100 times). The received signal is shown in **Fig. 4**. Two components are clearly seen, corresponding to the two pseudo-resonance signals. We note that the shape of these signals differs markedly from the derivative of absorption in a magnetic field that is usual for EPR spectroscopy. The distortions are due to the high sensitivity of the pseudo-resonance signals to the orientation of the modulating field, which in our experimental conditions has a small transverse component. Without dwelling on the details, we confine ourselves to stating the fact that the two observed components of the RF absorption spectrum correspond to two pseudo-resonance

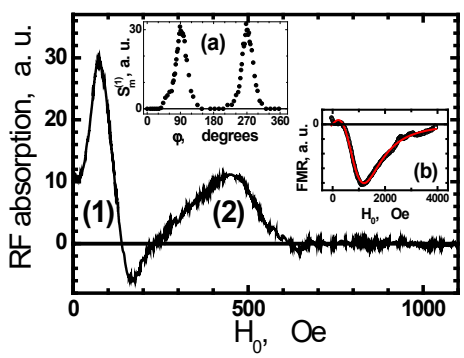

Fig. 4. *Radio-frequency absorption in a ferromagnetic heterostructure film (FeCo/$TbCo_2$/FeCo)/MgO/(FeCo/$TbCo_2$/FeCo) consisting of two three-layer films (in brackets), separated by a layer of MgO, depending on the external magnetic field H_0, oriented perpendicular to the nu axis of the easy magnetization.*

signals, 1 and 2, with maxima at H_0* around 74 Oe and 456 Oe, respectively. Different values of H_0* for these signals mean that the magnetic anisotropy fields H_u in sandwich-type films are significantly different. For signal 1, the dependence $S_m^{(1)}(\varphi)$ of its maximum on angle φ was removed (inset (a) in Fig. 4). It was obtained by scanning the field H_0 in a relatively narrow range of 0–140 Oe at angles φ, including the values φ = 90° and 270°. It can be seen that in both cases the dependencies are almost the same. They turn out to be much smoother than a similar dependence for the LSMO film: their width at half-height reaches 40°. As a result, the average direction of the axis of difficult magnetization for film 1 corresponds to the angle φ = 90° with an accuracy of ±4°. Similar measurements for film 2 with a wider pseudo-resonance line yielded the value φ = 90° ± 12°. From this it follows that in both films of the TCFCM structure the directions of the axes of the intra-plane magnetic anisotropy almost coincide.

It is natural to compare the data obtained for the described heterostructure with what gives FMR at a frequency of 9.78 GHz. Inset (b) is Fig. 4 shows the FMR signal from this structure, which is a derivative of the FMR absorption signal. It was obtained by the method of synchronous detection when sweeping the H_0 field under conditions of its modulation with a frequency of 100 kHz and amplitude of 10 Oe and using 4-fold accumulation. It can be seen that the signal is very broad, there is no resolved structure in it, corresponding to two films with significantly different values of the anisotropy field H_u. Experimentally, it was not possible to identify it for all possible orientations of the sample in the H_0 field. It also could not be detected by modeling the signal with the sum of two lines with the shape characteristic of FMR under the conditions of our experiment. At the same time, it is well described by a single Lorentzian with a width at half-height $\Delta_{1/2}$ = 1024 ± 6 Oe and a resonant field H_0 = 675 ± 2 Oe (the solid curve in inset b in Fig. 4). The unusual sharply asymmetric form of this spectrum is explained by the fact that resonance is observed in low fields ($H_0 \sim \Delta_{1/2}$), when both rotational components of the high-frequency field are effective [34].

Returning to the pseudo-resonance spectrum (Fig. 4), we emphasize once again that it consists of two well-resolved signals corresponding to different values of the field H_u in the films. In addition, from the signals in the inset (a) to Fig. 4, the direction of the n_u axis is also determined, which in this case cannot be done with the help of the FMR spectrum. This suggests that magnetic pseudo-resonance recorded at a frequency of hundreds of MHz may be a useful addition to the ferromagnetic resonance in the microwave range in the study of thin ferromagnetic films with uniaxial planar magnetic anisotropy. Note that the above values of the field H_0*, corresponding to the maxima of the signals of pseudo-resonance 1 and 2, cannot be identified with the values of the fields H_u in isolated ferromagnetic films. In complex structures such as TCFCM, interlayer exchange interactions usually occur, which can lead to renormalization of the anisotropy fields and the corresponding shift of the maximum of the pseudo-resonance in a magnetic field.

5. SPIN CURRENT IN TCFC/$Y_3Fe_5O_{12}$ STRUCTURE

Films from $Y_3Fe_5O_{12}$ (YIG) are very attractive for spintronic structures because of the small magnetic attenuation and the fact that they are an insulator. It was reported that the spin current can be excited in YIG and detected with a Py film [3-5]. **Fig. 5** presents the results of experimental studies of the inverse spin-Hall effect (ISHE) in the TCFC/YIG heterostructure. The YIG epitaxial film with a thickness of 5 μm was grown on a (111) $Gd_3Ga_5O_{12}$ (GGG) substrate. The [$TbCo_2$(5nm)/Cu(0.4nm)/

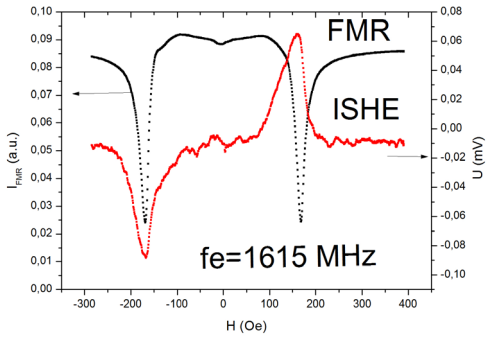

Fig. 5. *The FMR spectrum of an epitaxial YIG film grown on a GGG substrate, on top of which* $[TbCo_2(5nm)/Cu(0.4nm)/FeCo(5nm)/Cu(0.4nm)]_3$ *superlattices were deposited, 32 nm thick. The reverse spin-Hall effect signal appearing from the superlattice is shown by the red line.*

$FeCo(5nm)/Cu(0.4nm)]_3$ ($TCFC_C$) 32 nm thick superlattice was deposited. On the surface of the heterostructure, contact pads were formed to measure the potential difference caused by the ISHE effect. The sample was placed on a strip microwave line located in the gap of the electromagnet, with which FMR was excited in the YIG film. When the magnetizing field was changed, the potential difference ISHE and the intensity of the FMR signal were recorded. Fig. 5 shows the FMR spectrum of a YIG film, taken in a microstrip configuration at a frequency of 1615 MHz at T = 300 K, a generator power of 2 mW and a magnetic field that lies in the plane of the substrate and directed along the hard axis of magnetization. At H = 169 ± 0.2 Oe, a peak is observed, caused by FMR in the YIG film. There is a slight asymmetry of the peak position relative to a change in the polarity of the magnetic field. The peak half-width is 24 Oe. The second peak caused by ferromagnetism of TCFC is not observed due to the small thickness of the layer.

Fig. 5 also shows the dependence of the voltage of the inverse spin-Hall effect measured on the $TCFC_C$ film on the magnetic field. A strong asymmetry of the ISHE peak of ~ 7 Oe is observed. The ISHE peak width was 60 Oe. When the direction of the magnetizing field was changed, a change in the ISHE sign of voltage was observed, the value of which reached 80 μV.

The implementation of ISHE in ferromagnetic metals significantly expands the types of materials that could be used to study the spin current, including the rare-earth materials of the lanthanum group with extremely large spin-Hall angles, such as manganites, ruthenates, and etc.

6. CONCLUSION

Experimental studies of the magnetic properties of heterostructures consisting of epitaxially grown manganite LSMO and rare-earth intermetallic superlattices consisting of exchange-coupled TCFC layers showed that the magnetic interaction in the heterostructure has an antiferromagnetic character. After the deposition of a thin Pt film on top of the LSMO manganite film, an increase in the ferromagnetic resonance line width was observed due to the spin current flowing in Pt, which occurs in the LSMO film at resonance. An electric voltage caused by the inverse spin Hall effect in a TCFC film was experimentally observed under conditions of ferromagnetic resonance in an yttrium iron garnet.

ACKNOWLEDGMENTS

This work was partially supported by the RFBR project 18-57-16001 in the framework of the international laboratory LEMAC-LICS. The authors are grateful to A.E. Mefyod and I.V. Borisenko for help with the work and useful discussions.

REFERENCES

1. Dyakonov MI, Perel VI. Current-induced spin orientation of electrons in semiconductors. *Phys. Lett. A*, 1971, 35:459.
2. Saitoh E, Ueda M, Miyajima H, and Tatara G. Conversion of spin current into charge current at room temperature: Inverse spin-Hall effect. *Appl. Phys. Lett.*, 2006, 88:182509.
3. Miao BF, Huang SY, Qu D, Chien CL. Inverse Spin Hall Effect in a Ferromagnetic Metal. *Phys. Rev. Lett.*, 2013, 111:066602.
4. Hyde P, Lihui Bai, Kumar DMJ, Southern BW, Hu C-M, Huang SY, Miao BF, Chien CL. Electrical detection of direct and alternating

spin current injected from a ferromagnetic insulator into a ferromagnetic metal. *Phys. Rev. B,* 2014, 89:180404(R).
5. Yang F, Hammel PC. FMR-driven spin pumping in $Y_3Fe_5O_{12}$-based Structures. *J. Phys. D: Appl. Phys*., 2018, 51:253001.
6. Gall Y, Ben J, Socha F, Tiercelin N, Preobrazhensky V, Pernod P. Low field anisotropic magnetostriction of single domain exchange-coupled (TbFe/Fe) multilayers. *J. Appl. Phys*, 2000, 87:5783.
7. Quandt E, Ludwig A, Lord DG, Faunce CA. Giant magnetostrictive thin films for applications in microelectromechanical systems. *J. Appl. Phys*., 1998, 83:7267.
8. Haghiri-Cosnet AM, Renard JP. CMR manganites: physics, thin films and devices. *J. Phys. D: Appl. Phys*., 2003, 36:R127.
9. Luo GY, Chang CR, Lin JG. Influence of damping constant on inverse spin hall voltage of $La_{0.7}Sr_{0.3}MnO_3$(x)/platinum bilayers. *J. Appl. Phys*., 2014, 17C508:115.
10. Atsarkin VA, Sorokin BV, Borisenko IV, Demidov VV, Ovsyannikov GA. Resonance spin–charge phenomena and mechanism of magnetoresistance anisotropy in manganite/metal bilayer structures. *J. Appl. Phys. D*, 2016, 49:125003.
11. Vonsovskii SV. *Ferromagnetic resonance; the phenomenon of resonant absorption of a high-frequency magnetic field in ferromagnetic substances.* Ferromagnetic Resonance Academic, New York, 1966.
12. Verhagen TGA, Tinkey HN, Overweg HC, van Son M, Huber M, van Ruitenbeek JM, Aarts J. Temperature dependence of spin pumping and Gilbert damping in thin Co/Pt bilayers. *J.Phys. Condens. Matter*., 2016, 28:056004.
13. Platow W, Anisimov AN, Dunifer GL, Farle M, Baberschke K. Correlations between ferromagnetic-resonance linewidths and sample quality in the study of metallic ultrathin films. *Phys Rev. B*, 1998, 58:5611.
14. Flovik V, Macia F, Kent AD, Wahlstrom E. Eddy current interactions in a ferromagnet-normal metal bilayer structure, and its impact on ferromagnetic resonance lineshapes. *J. Appl. Phys*., 2015, 117:143902.
15. Flores AG, Zazo M, Raposo V, Iniguez J. Ferromagnetic resonance and electric characterization in double perovskite Sr_2FeMoO_6. *J. Appl. Phys*., 2003, 93:8068.
16. Heinrich B, Urban R, Woltersdorf G. Magnetic relaxation in metallic films: Single and multilayer structures. *J. Appl. Phys*., 2002, 91:7523.
17. Heinrich B, Woltersdorf G, Urban R. Role of dynamic exchange coupling in magnetic relaxations of metallic multilayer films (invited). *J. Appl. Phys*., 2003, 93:7545-7550.
18. Beaujour J-M, Ravelosona D, Tudosa I, Fullerton EE, Kent AD. Ferromagnetic resonance linewidth in ultrathin films with perpendicular magnetic anisotropy. *Phys. Rev. B*, 2009, 80:180415(R).
19. Tserkovnyak Ya, Brataas A, Bauer GEW. Enhanced Gilbert damping in thin ferromagnetic films. *Phys.Rev.Lett*, 2002, 88:117601.
20. Ovsyannikov GA, Petrzhik AM, Borisenko IV, Klimov AA, Ignatov YuA, Demidov VV, Nikitov SA. Magnetoransport Characteristics of Strained $La_{0.7}Sr_{0.3}MnO_3$ Epitaxial Manganite Films, *JETP*, 2009, 135:56.
21. Luo GY, Belmeguenai M, Roussigne Y, Chang CR, Lin JG, Cherif SM. Enhanced magnetic damping in $La_{0.7}Sr_{0.3}MnO_3$ capped by normal metal layer. *AIP Adv.*, 2015, 5:097148.
22. Rojas-Sanchez J-C, Reyren N, Laczkowski P, Savero W, Attane J-P, Deranlot C, Jamet M, George J-M, Vila L, Jaffr`es H. Spin pumping and inverse spin Hall effect in platinum: the essential role of spin-memory loss at metallic interfaces. *Phys. Rev. Lett.*, 2014, 112:106602.
23. Atsarkin VA, Demidov VV, Mefed AE, Nagorkin VYu. Magnetic Pseudoresonance in Manganite Thin Films. *Appl. Magn. Reson*., 2014, 45:809.

24. Mosendz O, Vlaminck V, Pearson JE, Fradin FY, Bauer GEW, Bader SD, Hoffmann A. Detection and quantification of inverse spin Hall effect from spin pumping in permalloy/normal metal bilayers. *Phys. Rev. B,* 2010, 82:214403.
25. Rezende TM, Rodrıguez-Suarez RL, Soares MM, Vilela-Le LH, Domınguez DL, Azeved A. Enhanced spin pumping damping in yttrium iron garnet/Pt bilayers. *Appl. Phys. Lett.*, 2013, 102:012402.
26. Emori S, Alaan US, Gray MT, Sluka V, Chen Y, Kent AD, Suzuki Y. Spin transport and dynamics in all-oxide perovskite $La_{2/3}Sr_{1/3}MnO_3/SrRuO_3$ bilayers probed by ferromagnetic resonance. *Phys. Rev. B.*, 2016, 94:224423.
27. Boone CT, Nembach HT, Shaw JM, Silva TJ. Spin transport parameters in metallic multilayers determined by ferromagnetic resonance measurements of spin-pumping. *J. Appl. Phys.,* 2013, 113:153906.
28. Boone CT, Shaw JM, Nembach HT, Silva TJ. Spin-scattering rates in metallic thin films measured by ferromagnetic resonance damping enhanced by spin-pumping. *J. Appl. Phys.*, 2015, 117:223910.
29. Demidov VV, Ovsyannikov GA, Petrzhik AM, Borisenko IV, Shadrin AV, Gunnarsson R. Magnetic anisotropy in strained manganite films and bicrystal junctions. *J. Appl. Phys.*, 2013, 113:163909.
30. Borisenko IV, Demidov VV, Klimov AA, Ovsyannikov G.A, Konstantinyan K.I, Nikitov SA, Preobrazhenskii VL, Tiercelin N, and Pernod P. Magnetic Interaction in the Manganite/Intermetallic Compound Heterostructure. *Technical Physics Letters,* 2016, 42:113.
31. Belyaev BA, Izotov AV, Kiparisov SYa. The peculiarity of the high-frequency susceptibility of thin magnetic films with uniaxial anisotropy. *JETP Lett,* 2001, 74(4):226-230.
32. Vasilevskaya TM, Sementsov DI. Ferromagnetic resonance in a uniaxial magnetic film with bias along the axis of a difficult magnetization. JETP, 2010, 110(5):754.
33. Klimov A, Ignatov Yu, Tiercelin N, Preobrazhensky V, Pernod P, Nikitov S. Ferromagnetic resonance and magnetoelasticde modulation in thin active films with anuniaxial anisotropy. *J. Appl. Phys.*, 2010, 107:093916.
34. Altshuller SA, Kozyrev BM. *Electron Paramagnetic Resonance in Compounds of Intermediate Group Elements.* Moscow, Nauka Publ., 1972.

INFLUENCE OF THE MAGNITUDE AND DIRECTION OF DC-INJECTION CURRENT ON SPIN ACCUMULATION AND THERMOEMF IN NiCo-InSb-NiCo LATERAL SPIN VALVE

Yuriy V. Nikulin, Mikhail E. Seleznev, Alexander G. Veselov, Yuriy A. Filimonov

Kotelnikov Institute of Radioengineering and Electronics of RAS, Saratov Branch, http://www.cplire.ru/rus/sfire
39, Zelenaya str., Saratov 410019, Russian Federation

yvnikulin@gmail.com, mixanich94@mail.ru, labsftwo@mail.ru, yuri.a.filimonov@gmail.com

Abstract. **The influence of the direction and magnitude of the dc-injection current I (5μA-2 mA) on the spin accumulation U_s and the thermo electromotive force U_e in the NiCo-InSb-NiCo lateral spin-valve structure based on textured n-InSb(111) film with thickness d ≈ 500 nm and an electron mobility μH ≈ 2.1 m²/V·s were studied. For non-local injection and detection geometry at T ≈ 300 K it was found that at injection current I less than critical Ic, the value of which is determined by the geometry of the structure, the detected voltage $U_{ac} = U_s + U_e$ increases linearly with I from units to a few hundred microvolts and differs in sign for direct and reverse directions of injection current ($|I| < I_c$ is the region of spin accumulation, $U_{ac} \approx U_s$). At injection currents $|I| > I_c$, a sharp increase of the detected voltage to a few units or tens of millivolts is observed, and the sign of the detected voltage is positive for both directions of the injection current (at $|I| > I_c$ dominates the thermoe-lectric effect, $U_{ac} \approx U_e$, $U_s << U_e$).**

Keywords: **lateral spin valve, semiconductors indium-antimonide, ferromagnetic metals, spin transport**

PACS: 72.25.-b, 73.40.-c

Bibliography - 41 references *Received 12 November 2018; accepted 10 December 2018*

RENSIT, 2018, 10(3):373-380 **DOI: 10.17725/rensit.2018.10.373**

Contents

1. INTRODUCTION

Investigation of the spin-transport phenomena in micro- and nanostructures is of interest due to the possibility of development and optimization of spintronic devices – hard disk, MRAM devices, high sensitive microwave detectors, spin transistor and biosensor [1-9]. Nowdays, multilayer spin-valve structures with vertical arrangement of the injection and detection ferromagnetic electrodes (FM) separated by a thin layer of a paramagnetic metal or insulator are applied as an "active" element in the majority of spintronic devices [10]. However, there is a growing interest to investigation of spin-valve structures with lateral geometry of injection and detection FM electrodes connected by a "bridge" of paramagnetic metal [11-25], semiconductor [26-32], graphen [33, 34] or conducting polymer material [35]. This location of FM electrodes in a lateral spin-valve structure (LSV) gives it possible to separate injection's circuit of spin-polarized current and detection's circuit by means of a non-local geometry of spin injection and accumulation proposed in [36]. The advantage of the non-local geometry is a possibility to generate and detect "pure" spin current – diffusion current of electrons not associated with a charge transfer. Besides, "pure" spin current in LSV can be controlled by changing the magnetization direction of the injection and detection FM electrodes from parallel direction to antiparallel as in vertical spin valves.

The main physical parameters of materials applied for creation FM and NM electrodes in LSV structure are spin polarization of electrons in FM metal, spin diffusion length of electrons in

non-magnetic (NM) material and cleanliness of interface between FM metal and NM material. Thus, to increase the spin accumulation voltage, strong ferromagnetic materials with high spin polarization like NiFe [12-19, 21, 22, 32, 33, 35], FeCo [25], Co [14, 15, 23, 30, 34], CoFeAl [11, 18], Co_2FeSi [20, 24, 31] and nonmagnetic materials with the highest spin diffusion length [11-34] are applied to form FM and NM electrodes.

Currently, LSV structures based on polycrystalline films of ferromagnetic and paramagnetic metals Cu [13-25], Al [14, 25], Ag [12, 17, 25], Au [15, 25] got the most widespread due to simplicity of fabrication such structures. However, spin diffusion length of paramagnetic metals commonly less than few hundreds nanometers [11-25, 37]. By this reason, the magnitude of spin accumulation voltage U_s measured in non-local geometry for FM-NM metal based LSV structures is of few microvolts magnitude at cryogenic temperature [11-25]. Note, that U_s for such LSV can be increased to few hundreds microvolts at cryogenic temperatures by using the tunnel barrier between FM and NM metals [12-25].

It should be expected that U_s can be significantly increased at room temperature if spin transmitting channel is made of material with much higher λ_s and μ than that of paramagnetic metals. By this reason, semiconductors and graphen are the most perspective materials. LSV structures based on monocrystalline InAs, GaAs, InSb and graphen were discussed in [26-34]. Spin diffusion length was estimated to be $\lambda_s \approx 1.5\text{-}4$ μm for LSV structures based on graphen [33, 34], $\lambda_s \approx 1.9$ μm for InAs [30], $\lambda_s \approx 6.2$ μm for GaAs [31] and $\lambda_s \approx 25$ μm for monocrystalline *n*-InSb [26, 27]. The highest value of the spin diffusion length for monocrystalline InSb is due to the highest electron mobility in *n*-InSb ($\mu H \approx 6$ m^2/V·s at 300 K and 70 m^2/V·s at 77 K) in comparison with other semiconductors [38].

Taking to account potential advantages of epitaxial InSb films for creation a spin channel in LSV structure, needs to note, that the requirement of the small lattice mismatch between film and substrate imposes severe restrictions on the choice of a substrate material for growth of epitaxial InSb film and as a result complicates the technology of fabrication LSV structures. So, development of LSV structures with spin transmitting channel produced from polycrystalline InSb films with high electron mobility is of great practical interest. Due to the fact, that polycrystalline films can be grown on any nonorientating substrates, for example, glass, silicon oxide, polycor, this possibility can significantly increase a range of application of ferromagnetic metal – semiconductor based LSV structures. However, LSV structures with spin transmitting channel made of a polycrystalline InSb film until now has not been discussed [11-34].

This work shows, that LSV structure with distance between FM electrodes w ≈ 1.5 μm and spin transmitting channel prepared from textured *n*-InSb(111) film with electron mobility 2.1 m^2/V·s at 300 K can effectively accumulate spin voltage U_s up to few hundreds microvolts at room temperature. The influence of the magnitude and direction of the injected dc-current on spin accumulation voltage U_s and thermoEMF U_e in non-local geometry of injection and detection at room temperature is discussed.

2. MATERIALS AND METHODS

Lateral spin-valve structure NiCo($d \approx 30$ nm)/InSb($d \approx 500$ nm)/NiCo($d \approx 30$ nm) was produced by dc-magnetron sputtering (NiCo), thermal evaporation (InSb), positive photolithography and ion etching on polycor substrate (**Fig. 1**a). At the first step, InSb film with thickness $d \approx 500$ nm (Dektak 150, Veeco) was formed on a polycor substrate by thermal impulse evaporation [39]. XRD analysis (DRON-8, "Burevestnik") shows that InSb film has a strong (111) texture with texture coefficient k ≈ 0.016, i.e. 98.4% of crystallites are oriented in [111] direction perpendicular to the substrate

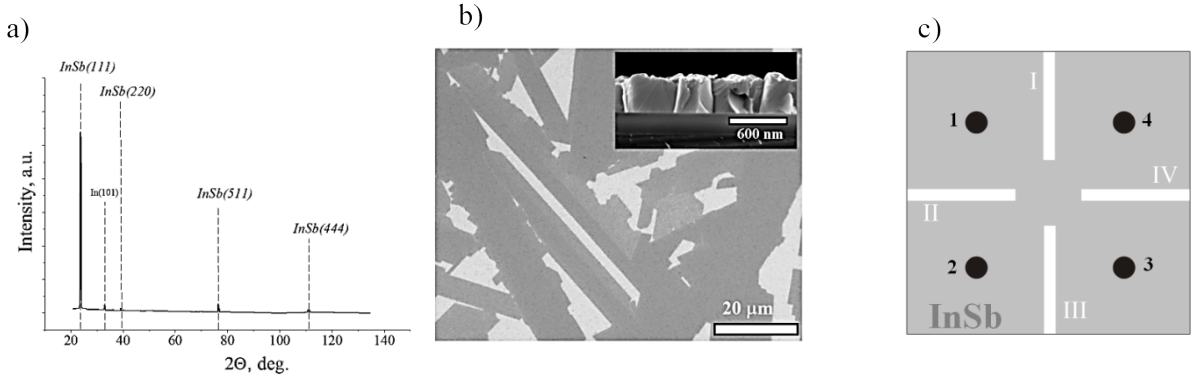

Fig. 1. *(a) X-ray diffraction pattern of n-InSb(111) film with thickness 500 nm; (b) optical picture of the surface of n-InSb(111) film. The inset of the picture (b) shows the cross section image of InSb film with thickness d ≈ 600 nm; (c) schematic image of a sample formed from InSb film on a polycor substrate (10×10 mm²) for Van Der Pauw measurements.*

surface (Fig. 1a). Mass concentrations of the crystal phases correspond InSb-97%, In-2%, In_2O_3 – 1%. The content of the amorphous phase in the film is about 0.4-2%. The average size of the coherent scattering region is 250 nm. According to data of optical (Olympus, MX-4) and scanning electronic (Auriga, Carl Zeiss) microscopies InSb film possesses a mosaic surface morphology and column microstructure (Fig. 1a).

Estimations of the electron mobility μ_H [$m^2/V{\cdot}s$], Hall coefficient R_H [m^3/C], resistivity ϱ [Ohm·m] and charge carrier concentration n [m^{-3}] for InSb film were carried out by the Van Der Pauw technique [40, 41] at room temperature in magnetic field (B ≈ 0.2 **T**) applied perpendicular to surface of InSb film. Fig. 1 shows a schematic image of the measured InSb sample. Digits 1-4 denote conducting point contacts, I-IV – deleted parts of InSb film.

Estimations of μ_H, R_H, ϱ and n were carried out according to [41]:

$$\rho \approx \frac{\pi d}{\ln 2}\left(\frac{R_{12,34}+R_{23,41}}{2}\right)\left(1-\frac{\ln 2}{2}\left(\frac{R_{12,34}-R_{23,41}}{R_{12,34}+R_{23,41}}\right)\right), \quad (1)$$

$$R_H \approx \frac{\Delta U_{24} d}{I_{24} B}, \quad (2)$$

$$\mu_H \approx \frac{R_H}{\rho}, \quad (3)$$

$$n \approx \frac{1}{eR_H}, \quad (4)$$

where d is a thickness of the InSb film, $R_{12,34} \approx \frac{U_{34}}{I_{12}}$ is a relation of voltage, measured between contacts 3 – 4 to current I between contacts 1–2; $R_{23,41} \approx \frac{U_{41}}{I_{23}}$ – is a relation of voltage, measured between contacts 4–1 to current I between contacts 2–3; ΔU_{24} is a voltage change of U_{24} caused by a magnetic field $B \approx 0.2$ T; $e \approx 1.602 \cdot 10^{-19}$ C – charge of electron.

As a result of the measurement, following estimates of μ_H, R_H, ϱ and n of textured n-InSb(111) film with thickness 500 nm were obtained: $\mu_H \approx 2.1$ $m^2/V{\cdot}s$, $R_H \approx 1.06 \cdot 10^{-4}$ m^3/C, $\varrho \approx 49 \cdot 10^{-6}$ Ohm·m and $n \approx 5.8 \cdot 10^{22}$ m^{-3}.

At the second step, the pattern of contacts and spin channel of width $w \approx 1.5$ μm (**Fig. 2***a*) was formed on the surface of the InSb film by a positive photolithography and ion etching. In the third step, NiCo film with thickness $d \approx 30$ nm was dc-sputtered on the surface of the InSb film. Next, ferromagnetic injector and detector electrodes with width $w \approx 1.5$ μm and distance between each other $w \approx 1.5$ μm were formed on the surface of the NiCo film by positive photolithography and ion etching (Fig. 2b).

To verify contact impedance of the indium antimonide–NiCo contact volt-ampere characteristic (VAC) was measured in the current range $|I| \leq 2$ mA. Cruciform structure, consisting of two intersecting microstrips of InSb ($d \approx 500$ nm) and NiCo ($d \approx 30$ nm) with width $w \approx 1.5$ μm was prepared for VAC measurements. Results of the VAC measurements of the InSb-NiCo

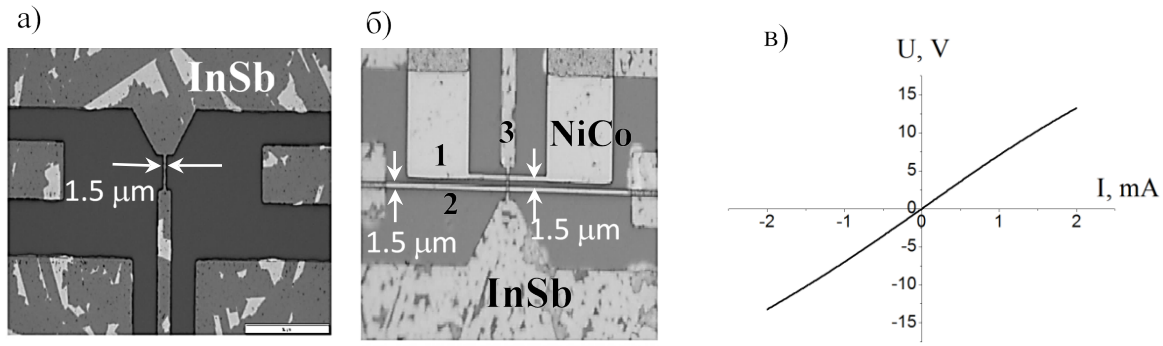

Fig. 2. *(a) System of InSb electrodes with width of the spin transmitting channel w ≈ 1.5 μm; (b) System of NiCo(1,2) electrodes with width w ≈ 1.5 μm and located over the top of the InSb electrodes (3). Distance between FM electrodes is w ≈ 1.5 μm; (c) VAC characteristic of the contact InSb-NiCo measured in currents range |I| ≤ 2 mA.*

contact show that this structure possesses non-rectifying contact in the ferromagnetic metal-indium antimonide interface. As follows from the Fig. 2*c*, VAC is close to linear at $|I| \leq 1.5$ mA and there is a small nonlinearity at $|I| \geq 1.5$ mA of the contact, which may be caused by a thin layer of In_2O_3 between InSb and NiCo films formed during deposition of InSb film.

3. RESULTS AND DISCUSSIONS

Current's measurements in LSV structure were performed in non-local geometry of spin injection and detection at room temperature by a four probe technique. **Fig. 3**a shows a scheme of the measurements. Direct current I with magnitude $I \approx 1$ μA–1.2 mA was injected to the structure in two directions I^+ и I^- at $T \approx 300$ K. Magnetic field $H \approx \pm 0.3$ kOe was applied parallel to FM electrodes. This range of H corresponds to the field where each ferromagnetic electrode shows magnetoresistive effect. For each definite magnitude and direction of the injected current I were determined dependences of the resistance R of the detecting contact on the magnetic field H magnitude, where $R = U_{ac}/I$, $U_{ac} = U_s + U_e$, U_{ac} – detecting voltage, I – current injected to the structure, U_s – voltage of the spin accumulation, U_e – voltage of the thermoelectric effect (Fig. 3b). Values of R_{ap}, R_p, $\angle R = R_{ap} - R_p$ and $U_{ac} = \Delta R \cdot |I|$ were determined from $R(H)$ dependences, where R_{ap} – resistance of the structure, when directions of the magnetizations of detector and injector FM electrodes are closer to anti-parallel, R_p – resistance of the structure in magnetic field H corresponding to saturation field of FM electrodes.

Dependences R_{ap}, ΔR and $U_{ac} = \Delta R \cdot |I|$ on the magnitude and direction of injected current I at T ≈ 300 K are shown in the **Fig. 4***a-c*. As can be seen, values R_{ap} and ΔR don't depend on I at I less than critical current I_c ($I < I_{c+} \approx 1.1$ mA and $I < I_{c-} \approx 0.5$ mA), but U_{ac} increases linearly with I up to $|U_{ac}| \approx 250$–500 μV. It is known that magnitude of the spin voltage U_s depends on the injecting current I linearly [27]:

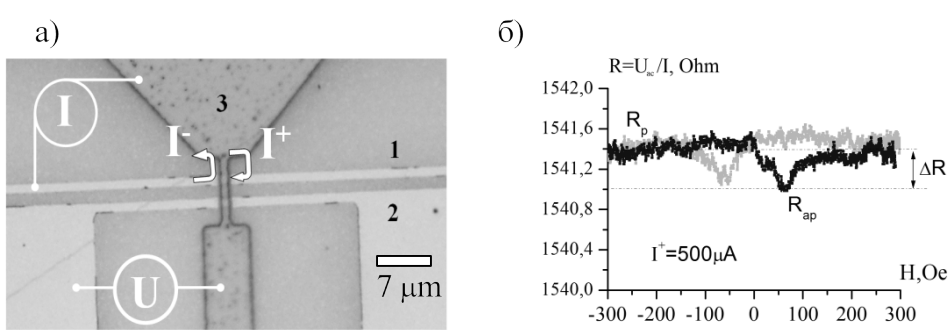

Fig. 3. *(a) Non-local geometry of spin injection and detection for lateral spin-valve structure NiCo-InSb-NiCo. Ferromagnetic electrodes marked as 1 and 2; InSb channel marked as 3; (b) Dependence of parameter R on external field H for injection current I ≈ 500 μA, where $R = U_{ac}/I$, U_{ac} – measured voltage, I – injection current.*

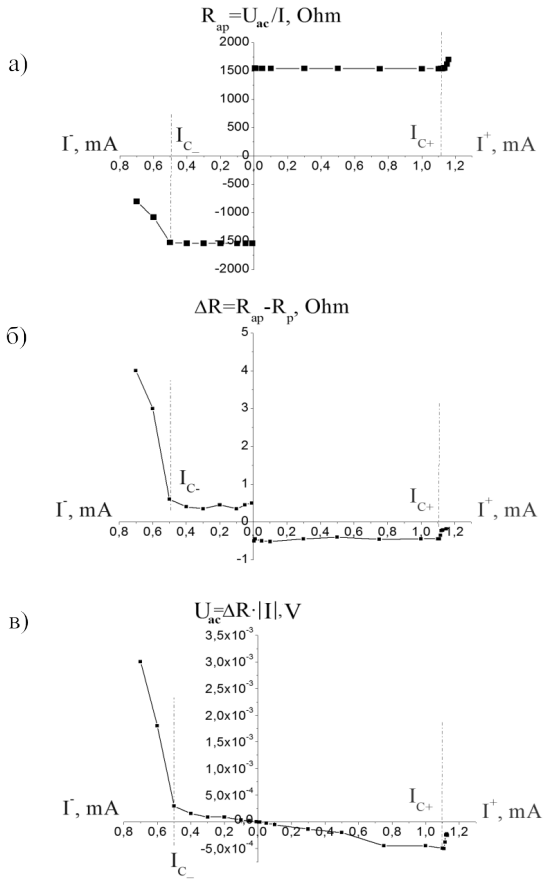

Fig. 4. *Dependences of parameters (a) R_{ap}, (b) $\Delta R = R_{ap} - R_p$ and (c) $U_{ac} = \Delta R \cdot |I|$ on a magnitude and direction of current I injected to the structure at room temperature.*

$$U_s = \frac{P^2 I \lambda_s \rho}{2A} e^{-\frac{w}{\lambda_s}}, \quad (5)$$

where I – injecting current, w – distance between ferromagnetic electrodes, λ_s – spin diffusion length in nonmagnetic material, P – electron polarization near the nonmagnetic material interface, ρ – resistivity of nonmagnetic material, A – cross-sectional area of the spin transmitting channel.

Therefore, we could conclude that the range of injection currents $|I| < I_c$ corresponds to the range in which spin accumulation voltage U_s dominates in the measured voltage U_{ac}, $U_{ac} \approx U_s$, $U_e \approx 0$.

It should note that the value of the critical current is substantially determined by a geometry and shapes of electrodes of the spin-valve structures, by thickness of the ferromagnetic and nonmagnetic films and, in general, by the technology of producing LSV structure. In our case, difference between I_{c+} и I_{c-} can be explained by a shape asymmetry of FM and InSb electrodes and area difference of FM and InSb electrodes.

At injection currents higher than critical value I_c ($I > I_{c+} \approx 1.1$ mA and $I > I_{c-} \approx 0.5$ mA) there is a sharp increase of the detectable voltage U_{ac} for one direction of the injection current ("negative" I_{c-}) and a change of the sign of the $U_{ac}(I)$ dependence for reverse ("positive" I_{c+}) direction of I. Such behavior of $U_{ac}(I)$ dependence can be caused by contribution of thermoEMF U_e to the voltage U_{ac} due to the resistive heating of the LSV structure at large injection currents [14]. When injected current flows through the contact of indium antimonide – ferromagnetic metal, independently on the current's direction, it causes a Joule heating. So, we can assume that the second detection contact play a role of a thermocouple, for which heating is always accompanied by generation of thermEMF of positive polarity. Thus, it can be concluded, that a range of currents $|I| > I_c$ correspond to the range where thermoEMF dominates in detectable voltage U_{ac}, i.e. $U_{ac} \approx U_e$, $U_s << U_e$.

4. CONCLUSION

Influence of the direction and magnitude of injection current I (5 μA–2 mA) on the spin accumulation voltage in the lateral spin-valve structure ferromagnetic metal (NiCo) – indium antimonide with spin transmitting channel formed of a texture film InSb (111) with electron mobility 2.1 $m^2/V \cdot s$ was investigated. For non-local geometry of the injection and detection at $T \approx 300$ K were determined current dependences of parameters R_{ap}, $\Delta R = R_p - R_{ap}$ и $U_{ac} = \Delta R \cdot I$, where U_s – spin accumulation voltage, U_e – voltage of a thermoelectric effect, R_{ap} resistance of the structure at "quasi" antiparallel direction of the magnetizations of the detection and injection ferromagnetic (FM) electrodes, R_p – resistance of LSV structure in the saturation magnetic field H corresponding to the parallel magnetization of FM electrodes.

It was established that at $T \approx 300$ K and injection currents I less than critical I_c which magnitude is determined by a geometry of the LSV structure, the magnitude of R_{ap} and ΔR, almost independent on I, but U_{ac} linearly increase with current from units to few hundreds microvolts (the range of spin accumulation, $U_{ac} \approx U_s$). At injection currents $|I| > I_c$ there are a sharp increase in magnitude of ΔR and U_{ac} for one current's direction and sign change of $\Delta R(I)$ and $U_{ac}(I)$ dependences for other current's direction due to resistive heating of the structure at large injection current ($|I| > I_c$ – the currents range, where thermoelectric effect dominates, $U_{ac} \approx U_e$, $U_s << U_e$).

Obtained results could be of interest at creation high sensitive microwave detectors based on the lateral spin-valve ferromagnetic metal-indium antimonide structures [17].

ACKNOWLEDGMENTS

This work was supported by RFBR, projects № 16-37-60052, 16-29-14058.

REFERENCES

1. Fang B, Carpentieri M, Hao X, Jiang H, Katine JA, Krivorotov IN, Ocker B, Langer J, Wang KL, Zhang B, Azzerboni B, Amiri PK, Finocchio G, Zeng Z. Giant spin-torque diode sensitivity in the absence of bias magnetic field. *Nature Commutications,* 2016, 7(11259):1-7.
2. Gui YS., Xiao Y, Bai LH, Hemour S, Zhao Y P, Houssameddine D, Wu K, Guo H, Hu CM. High sensitivity microwave detection using a magnetic tunnel junction in the absence of an external applied magnetic field. *Appl. Phys. Lett.*, 2015, 106 (152403):1-6.
3. Fan X, Cao R, Moriyama T, Wang W, Zhang HW, Xiao JQ. Magnetic tunnel junction based microwave detector. *Appl. Phys. Lett.*, 2009, 122501:1-4.
4. Li X., Zhou Y, Zheng C, Chan PH., Chan M, Pong PWT. Field–angle and DC-bias dependence of spin-torque diode in giant magnetoresistive Microstripe. *Appl. Phys. Lett.*, 2016, 109 (192402):1–6.
5. Kumar PSA, Lodder JC. The spin-valve transistor. *J. Phys. D: Appl. Phys.*, 2000, 33:2911-2920.
6. Fu L, Gui YS, Bai LH, Guo H, Abou-Rachid H, Hu CM. Microwave holography using a magnetic tunnel junction based spintronic microwave Sensor. *J. Appl. Phys.*, 2015, 117 (213902):1-6.
7. Tulapurkar AA, Suzuki A, Fukushima A, Kubota H, Maehara H, Tsunekawa K, Djayaprawira DD, Watanabe N, Yuasa S. Spin-torque diode effect in magnetic tunnel junctions. *Nature*, 2005, 438:339-342.
8. Deen DA, Pokhil TG, Singleton E, Patwari MSU. Lateral spin valve reader with large–area tunneling spin injector. US Patent, № US9685178B1, 20 June 2017.
9. Hall DA, Gaster RS, Lin T, Osterfeld SJ, Han S, Murmann B, Wang SX. GMR biosensor arrays:A system perspective. *Biosensors and Bioelectronics*, 2010, 25(9):2051-2057.
10. Wu Y. *Nano Spintronics for Data Storage. Encyclopedia of Nanoscience and Nanotechnology*, Edited by H.S. Nalwa, Stevenson Ranch, Calif., 2004, 10:1-50.
11. Hu S, Nomura T, Uematsu G, Asam N, Kimura T. First- and second-harmonic detection of spin accumulation in a multiterminal lateral spin valve under high-bias ac current. *Phys. Rev. B.*, 2016, 94(014416):1-5.
12. Fukuma Y, Wang L, Idzuchi H, Takahashi S, Maekawa S, Otani YC. Giant enhancement of spin accumulation and long–distance spin precession in metallic lateral spin valves. **Nature Materials**, 2011, 10:527-531.
13. Otani Y, Kimura T. Manipulation of spin currents in metallic Systems. *Phil. Trans. R. Soc. A.*, 2011, 369:3136-3149.
14. Casanova F, Sharoni A, Erekhinsky M, Schuller IK. Control of spin injection by direct current in lateral spin valves. *Phys. Rev. B.*, 2009, 79(184415):1-6.

15. Ji Y, Hoffmann A, Jiang JS, Pearson JE, Bader SD. Non-local spin injection in lateral spin valves. *J. Phys. D: Appl. Phys.*, 2007, 40:1280-1284.
16. Kimura T, Hamrle J, OtaniY, Tsukagoshi K, Aoyagi Y. Spin-dependent boundary resistance in the lateral spin–valve structure. *Appl. Phys. Letters*, 2004, 85:3501-3503.
17. Kuhlmann N, Swoboda C, Vogel A, Matsuyama T, Meier G. All-metal lateral spin valve operated by spin pumping. *Phys. Rev. B.*, 2013, 87(104409):1-5.
18. Nomura T, Ohnishi K, Kimura T. Large spin current injection in nano-pillar-based lateral spin valve. *AIP Conference Proceedings*, 2016, 1763(020011):1-5.
19. Nonoguchi S, Nomura T, Kimura T. Longitudinal and transverse spin current absorptions in a lateral spin-valve structure. *Phys. Rev. B.*, 2012, 86(104417):1-5.
20. Oki S, Kurokawa T, Honda S, Yamada S, Kanashima T, Itoh H, Hamaya K. Robust spin-current injection in lateral spin valves with two-terminal Co_2FeSi spin Injectors. *AIP Advances*, 2017, 7(055808):1-7.
21. Erekhinsky M, Sharoni A, Casanova F, Schuller IK. Surface enhanced spin-flip scattering in lateral spin valves. *Appl. Phys. Lett.*, 2010, 96(022513):1-3.
22. Kimura T, Hamrle J, Otani Y. Estimation of spin-diffusion length from the magnitude of spin–current absorption: Multiterminal ferromagnetic/nonferromagnetic hybrid structures. *Phys. Rev. B.*, 2005, 72(014461):1-6.
23. Smith AK, Jamali M, Stecklein G, Crowell PA, Wang JP. Demonstration of nonlocal lateral spin valve devices fabricated with a versatile top-down fabrication process. *IEEE Magnetics Lett.*, 2015, 6:1-5.
24. Yamasaki K, Oki S, Yamada S, Kanashima T, Hamaya K. Spin-related thermoelectric conversion in lateral spin-valve deviceswith single–crystalline Co_2FeSi electrodes. *Appl. Phys. Express*, 2015, 8(043003):1-4.
25. Idzuchi H, Fukuma Y, Otani YC. Spin transport in non-magnetic nanostructures induced by non-local spin injection. *Physica E*, 2015, 68:239-263.
26. Viglin NA, Ustinov VV, Demokritov SO, Shorikov AO, Bebenin NG, Tsvelikhovskaya VM, Pavlov TN, Patrakov EI. Electric measurement and magnetic control of spin transport in InSb-based lateral spin devices. *Phys. Rev. B*, 2017, 96(235303):1-10.
27. Viglin NA, Ustinov VV, Tsvelikhovskaya VM, Pavlov TN. Electric Injection and Detection of Spin-Polarized Electrons in Lateral Spin Valves on Ferromagnetic Metal-Semiconductor InSb Heterojunctions. *JETP Letters,* 2015, 101(2):113-117.
28. Kim YJ. Electrical injection and detection of spin polarization in InSb/ferromagnet nanostructures. *PhD Thesis*, 2012, Blacksburg, Virginia.
29. Saha D, Holub M, Bhattacharya P, Liao YC. Epitaxially grown MnAs/GaAs lateral spin valves. *Appl. Phys. Lett.*, 2006, 89(142504):1-3.
30. Wang Z, Pan D, Wang L, Wang T, Zhao B, Wu Y, Yang M, Xu X, Miao J, Zhao J, Jiang Y. Room temperature spin transport in InAs nanowire lateral spin valve. *RSC Adv.*, 2016, 6(79):75736-75740.
31. Bruski P, Manzke Y, Farshchi R, Brandt O, Herfort J, Ramsteiner M. All-electrical spin injection and detection in the Co_2FeSi/GaAs hybrid system in the local and non-local configuration. *Appl. Phys. Lett.*, 2013, 103(052406):1-5.
32. Last T, Wahle M, Hacia S, Fischer SF, Kunze U. Local Hall Effect and Ballistic Transport in Multi-terminal InAs-Based Lateral Spin-Valve Tunnelling Devices. *J. Superconductivity: Incorporating Novel Magnetism*, 2005, 18(3):385-389.
33. Lin CC, Penumatcha AV, Gao Y, Diep VQ, Appenzeller J, Chen Z. Spin Transfer Torque in a Graphene Lateral Spin Valve Assisted by an External Magnetic Field. *Nanoletters,* 2013, 13(11):5177-5181.

34. Tombros N, Jozsa C, Popinciuc M, Jonkman HT, van Wees BJ. Electronic spin transport and spin precession in single graphene layers at room temperature. *Nature*, 2007, 448:571-575.
35. Kawasugi Y, Ara M, Ushirokita H, Kamiya T, Tada H. Preparation of lateral spin-valve structure using doped conducting polymer poly(3,4-ethylenedioxythiophene) poly(styrenesulfonate). *Organic Electronics*, 2013, 14:1869-1873.
36. Johnson M, Silsbee RH. Interfacial charge-spin coupling: Injection and detection of spin magnetization in metals. *Phys. Rev. Lett.*, 1985, 55(17):1790-1793.
37. Coey JMD. *Magnetism and magnetic materials.* New York, Cambridge university press, 2010, 633 p.
38. Sluchinskaya IA. *Osnovy materialovedeniya i techniki poluprovodnikov* [Base principals of the semiconductors material science and industry]. Moscow, Mir Publ., 2002, 376 p.
39. Gulyaev YV, Veselov AA, Veselov AG, Buriylin EI, Dzhumaliev AS, Zyuryukin YA, Kiryasova OA, Ryabushkin SL. *ZhTF*, 2004, 74(8):113-115.
40. Van der Pauw LJ. A method of measuring the resistivity and Hall coefficient on lamellae of arbitrary shape. *Philips Tech. Rev.*, 1958, 20(8):220-224.
41. Kuchis EV *Galvanomagnitniye effektiy i metody ih issledovaniya* [Galvanomagnetic effects and methods of investigations]. Moscow, Radio i Svyaz Publ., 1990, 264 p.

PROBLEMS OF CREATING MATERIALS AND FILM STRUCTURES BASED ON FERRITS FOR SPINTRONICS DEVICES

Valery A. Ketsko, Maria N. Smirnova, Maria A. Kopieva, Evgeny N. Beresnev

Kurnakov Institute of General and Inorganic Chemistry, Russian Academy of Sciences, http://igic.ras.ru
Moscow 119991, Russian Federation

ketsko@igic.ras.ru, smirnova_macha1989@mail.ru, mkopieva@mail.ru, benko@igic.ras.ru

Abstract. **The review presents the main directions of the search for materials and film structures based on them for spintronics devices, provides data on materials for these purposes available in the literature. The problems that need to be solved when creating spintronics structures are analyzed. A new method for the synthesis of ferrite films on semiconductor substrates without elastic stresses and unwanted interactions of components at the interface is presented. A method for the synthesis of powdered ferrites, based on burning the gel, characterized by phase homogeneity and dimensional unimodality, which makes it possible to use the material as a target for the synthesis of films, is considered. The prospects for the practical use of submicron films of ferrite garnets with a SiO_2 buffer layer on Si with a Hilbert damping parameter $\alpha \approx 10^{-3}$, which can be used in spin-wave device structures on silicon substrates, are considered.**

Keywords: **spintronics, ferrites, homogeneous powders, new method for creating film structures, properties of structures**

UDC 546.027

Bibliography - 46 references *Received November 1, 2018; adopted December 10, 2018*

RENSIT, 2018, 10(3):381-394 **DOI: 10.17725/rensit.2018.10.381**

Contents

1. INTRODUCTION

It is known that the increase in the speed of processing and transmitting information in modern microelectronics devices is approaching the limit due to the fundamental physical limitations on the further reduction of the size of active elements. In this regard, in order to expand the capabilities of electronic devices, it is necessary to search for and create new technological approaches that would ensure further progress in this field of science and technology.

Using, along with the charge of an electron, its spin will allow in the future to create instrument film devices that are integrally controlled by magnetic and electric fields, which can be: spin field-effect transistors, ultrafast frequency tuning filters, coatings and screens absorbing electromagnetic radiation in a wide wavelength range , as well as matching devices in antenna systems and receiving modules of the microwave range, tunable delay lines, noise suppressors, etc. These structures can be applied in satellite communications and radiolocation systems, cellular telephony, digital television systems, etc.

An important characteristic of new electronic devices in terms of future technologies is their energy efficiency. When using them, there is no need for high current

densities, energy losses are sharply reduced and the signal transmission rate increases.

2. BASIC DIRECTIONS OF SEARCH OF MATERIALS AND FILM STRUCTURES OF SPINTTRONICS

At present, the search for new materials and film heterostructures with both semiconductor and magnetic characteristics at temperatures above room temperature is conducted in two main directions [1-3].

The first direction is connected with the creation of a "ferromagnet-semiconductor" film composite structure, obtained by sequential layer spraying of the structure components. Such a path is quite attractive due to the variety of existing magnetic and semiconductor materials, which can be combined to make a directed search for structures with the necessary properties. Such a hybrid structure should be considered as exchange-related. It should be noted that in this case the contact of a ferromagnet (FM) with a semiconductor (PP) is accompanied by two effects: the Hall effect in a semiconductor under the action of the magnetic field of the ferromagnet, and the formation of a Schottky barrier due to the distortion of the band structure [1, 4], which is accompanied by the accumulation near the film – substrate interface is a significant number of charge carriers. In this case, a strong exchange interaction near the interface region between charge carriers in PP and magnetic atoms in FM can lead to the appearance of a unified spin system. The disadvantage of this approach is a small spin relaxation time, which limits the use of such structures.

As an example, we can cite a number of works in which the results of studies of FM films on zinc oxide substrates are presented. Thus, in the works, the authors, using various methods of synthesis (sol-gel [5], reactive sputtering [6], laser evaporation [7]) obtained ferromagnetic (T_C above 350 K) films ($0 < x < 0.25$ [5], $0.035 < x < 0.115$ [6], $x < 0.4$ [7]), in which there were no cobalt clusters. In [8], films ($x = 0.05$-0.25) deposited on a sapphire substrate by the method of pulsed laser evaporation were ferromagnetic and retained magnetic ordering at temperatures above room temperature.

At the same time, other authors argue that solid solutions with wurtzite structure are predominantly paramagnetic [9-11]. At the same time, in films ($x = 0.25$) obtained by the method of pulsed laser decomposition [9], ferromagnetism is caused by the presence of cobalt clusters, and in polycrystals ($x = 0.05$, 0.1 and 0.15) synthesized by the solid phase method [10], and in single crystals, grown by the melt technique [11], due to the presence of impurities.

In some papers, information is given on the existence of ferromagnetism (T_C above 300 K) in 3*d*-doped wide-gap semiconductors GaN [4], AlN [12], ZnO [13-16], TiO_2 [17], SnO_2 [18-21].

In a number of works [21-24], the occurrence of ferromagnetism in undoped 3*d*-elements SnO_2 has been reported. It is assumed that this effect may occur either with a large number of defects in the crystal lattice, or its appearance is associated with the size factor.

The authors of [25] investigated phase equilibria in the Co-Zn-O system and showed that in solid solutions $Zn_{1-X}Co_XO_{1+\delta}$, where $x \leq 0.2$, there is only antiferromagnetic ordering, and the manifestation of ferromagnetism in ceramics is most likely associated with the violation of homogeneity or the presence of impurities.

The second direction of the search is based on the creation of homogeneous materials with both semiconductor and magnetic properties, which must satisfy three basic criteria: the simplicity and reliability of synthesis

methods, the possibility of including products derived from these materials into standard semiconductor circuits; preservation of the structure and physicochemical properties of the original semiconductor arrays in the obtained magnetic semiconductor materials without deterioration of their functional characteristics; preservation of the magnetic orientation in semiconductors with n- and p-mobile charge carriers at temperatures above room temperature.

The first open ferromagnetic semiconductor is europium monoxide EuO [26]. Ferromagnetic ordering in EuO and its semiconductor conductivity is associated primarily with the unusual electronic structure of the doubly charged europium ion. Being in the lowest oxidation state for rare-earth metals, Eu^{2+} is characterized by the maximum possible number of unpaired electrons at the 4*f*-electronic level. This provides ferromagnetism with a colossal atomic magnetic moment (7 μB). At the same time, it should be noted that the creation of heterostructures for microelectronic devices based on EuO is difficult due to the low Curie temperature (69.4 K) and the instability of the material in air. In [3], it is said that TC can be enhanced by dissolving samarium monoxide SmO or ytterbium YbO in EuO. Thus, the T_S was increased to 130 K. However, the authors could not significantly raise the Curie temperature due to the fact that the solubility of the oxides SmO and YbO was not high enough (for example, for SmO it was 14 mol%). In addition, solid solutions of $Eu_{1-x}Sm_xO$ or $Eu_{1-X}Yb_XO$, as well as EuO, turned out to be metastable. It should be noted that the functional characteristics of EuO depend on oxygen nonstoichiometry. At the same time, despite the indicated drawbacks, the work on obtaining EuO-based heterostructures continues to this day.

In [28], the authors synthesized EuO – Fe (Co) composites, including in the form of thin films, whose Curie temperatures corresponded to the indicated transition ferromagnetic metals, while the composites themselves remained semiconductors with a band gap $E_g \approx 0.75$ eV.

High Curie temperatures were found in chalcogenide ferromagnetic semiconductors with a spinel structure with the general formula AB_2C_4 (where A is Cd, Hg. Zn, Cu; B is Cr, Fe; C is S, Se, Te) [29]. However, it has not yet been possible to obtain film structures in such materials.

Based on the principles of isovalent substitution of cations in the structure, a solid solution $Ga_{1-x}Mn_xAs$ (where x is up to 5%) was obtained, which had a higher Curie temperature of 170 K compared to EuO [3]. Such substances, which are characterized by a disordered distribution of impurity magnetic ions in the crystal structure, are called diluted magnetic semiconductors – DMS (diluted magnetic semiconductors).

As follows from a brief analysis of the presented results, the range of materials that would satisfy the necessary criteria for their use in spintronic devices is extremely limited. At the same time, recently, the number of publications related to the synthesis and research of materials and film structures based on ferrites with a spinel and garnet structure, which can be used in spintronics devices, has significantly increased [30-32].

3. MAGNETIC SEMICONDUCTOR MATERIALS BASED ON FERRITES

Interest in the creation of electronic devices containing ferrite films on semiconductor substrates increased significantly after the discovery of $Mg(Fe_{0.8}Ga_{0.2})_2O_4$ magnetic semiconductors in the Mg-Fe-Ga-O system [3].

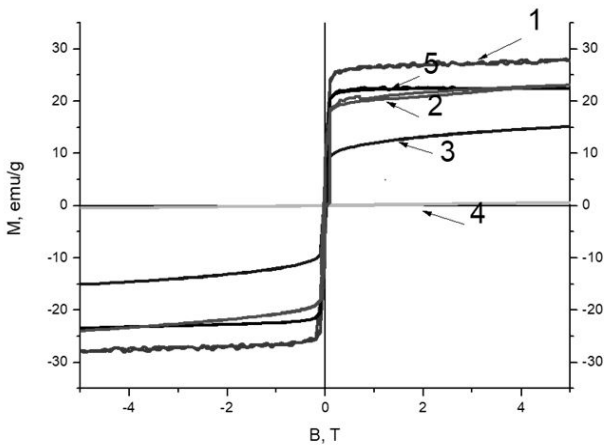

Fig. 1. *Field dependences of the specific magnetization solid solution the $Mg(Fe_{1-x}Ga_x)_2O_4$ at 300 K: 1- $Mg(Fe_{0.8}Ga_{0.2})_2O_4$, 2 - $Mg(Fe_{0.7}Ga_{0.3})_2O_4$, 3 - $Mg(Fe_{0.65}Ga_{0.35})_2O_4$, 4 - $Mg(Fe_{0.2}Ga_{0.8})_2O_4$, 5 - $MgFe_2O_4$.*

As a result of a detailed study of the Mg-Fe-Ga-O system, the authors found that the most optimal combination of functional properties is a solid solution of the composition $Mg(Fe_{0.8}Ga_{0.2})_2O_4$. This material is characterized by Curie temperature (T_C) ~ 450 K, saturation magnetization (M_S) ~ 28 A · m^2 · kg^{-1}, specific electrical conductivity ~ 10^{-8} S/m, band gap ΔE ~ 1.9 eV.

In **Fig. 1** and **Fig. 2** presents the results of studies of the functional characteristics of the $Mg(Fe_{1-x}Ga_x)_2O_4$ solid solution at 300 K.

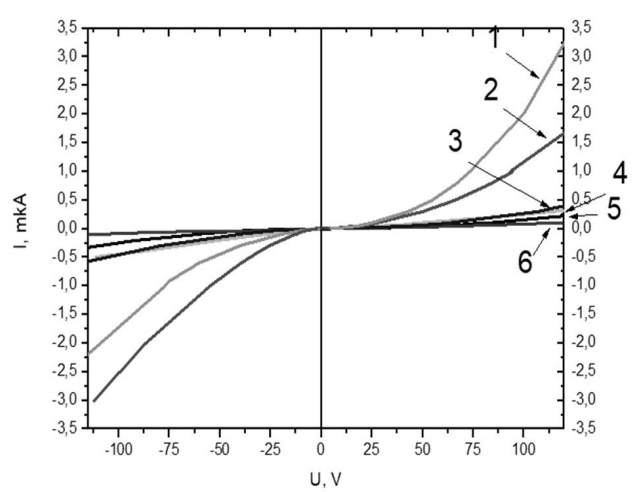

Fig. 2. *Current-voltage characteristics of the solid solution $Mg(Fe_{1-x}Ga_x)_2O_4$ at 300 K: 1- $Mg(Fe_{0.8}Ga_{0.2})_2O_4$, 2 - $Mg(Fe_{0.7}Ga_{0.3})_2O_4$, 3 - $Mg(Fe_{0.65}Ga_{0.35})_2O_4$, 4 - $Mg(Fe_{0.2}Ga_{0.8})_2O_4$, 5 - $MgFe_2O_4$, 6- $MgGa_2O_4$.*

As can be seen from Fig. 1, the magnitude of specific magnetization (MS) reaches saturation only for $Mg(Fe_{0.8}Ga_{0.2})_2O_4$ and $MgFe_2O_4$ at values of the applied external magnetic field of 0.1–0.3 *T*. In this case, the magnitude of M_S in $Mg(Fe_{0.8}Ga_{0.2})_2O_4$ (M_S = 28) is higher compared to M_S of magnesium ferrite $MgFe_2O_4$ (M_S = 23). At the same time, in $Mg(Fe_{0.7}Ga_{0.3})_2O_4$ and $Mg(Fe_{0.65}Ga_{0.35})_2O_4$, M_S does not reach saturation values even in external fields up to 4*T*, which indicates magnetic inhomogeneity of materials.

However, a significant disadvantage of both $Mg(Fe_{0.8}Ga_{0.2})_2O_4$ and ferrites in general is the high (850–950°*C*) crystallization temperature, as well as the significant mismatch of the crystallographic parameters of their lattices with commercial semiconductors such as Si, GaN and GaAs. At these temperatures, elastic stresses arise in the heterostructures, initiated by the processes of crystallization of the films, and undesirable interactions of the components at the interface occur, which leads to a significant decrease in their functional characteristics.

As an example in **Fig. 3** shows the results of study the cross section of the $Mg(Fe_{0.8}Ga_{0.2})_2O_4$/Si heterostructure after

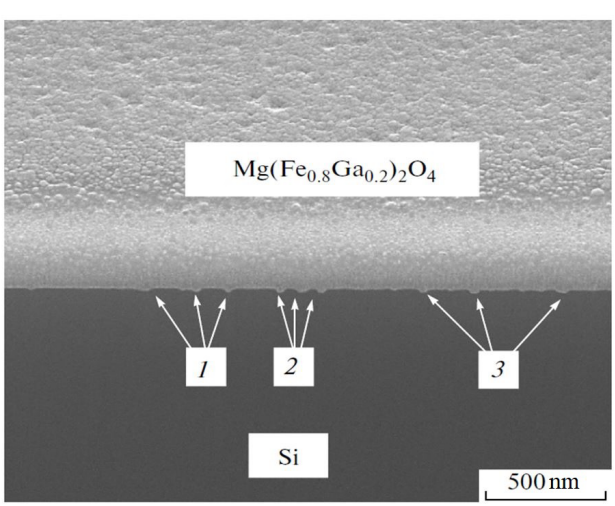

Fig. 3. *SEM imaging the cross section of the $Mg(Fe_{0.8}Ga_{0.2})_2O_4$/Si heterostructure after crystallization at 1173 K for 10 min (Figures 1, 2, 3 show the areas of interaction $Mg(Fe_{0.8}Ga_{0.2})_2O_4$ with Si).*

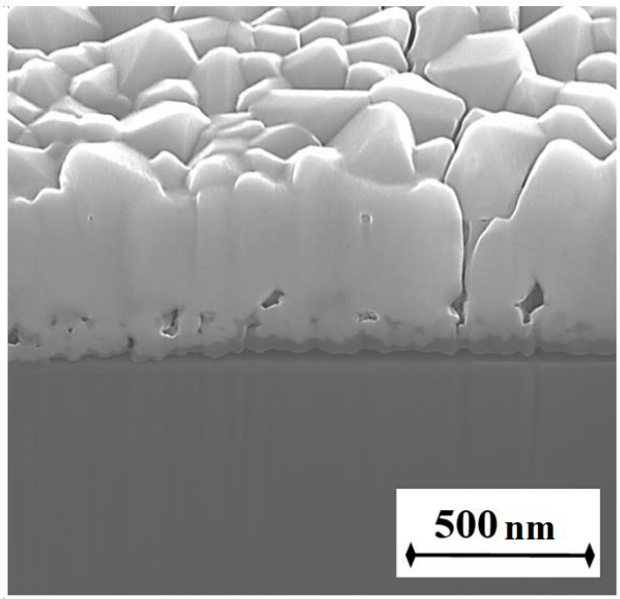

Fig. 4. *SEM imaging the cross section of the $Mg(Fe_{0.8}Ga_{0.2})_2O_4/Si$ heterostructure after crystallization at 1173 K for 30 min.*

the film crystallizes at 1173 K for 10 min. It can be seen from the figure that an intensive interaction occurs at the film/substrate interface, leading to a decrease in the primarily magnetic characteristics of the substituted ferrite.

In **Fig. 4** shows the SEM image of the cross section of the $Mg(Fe_{0.8}Ga_{0.2})_2O_4/Si$ heterostructure after crystallization at 1173 K for 30 min. It can be seen that the film contains numerous defects, local delaminations from the substrate are also seen.

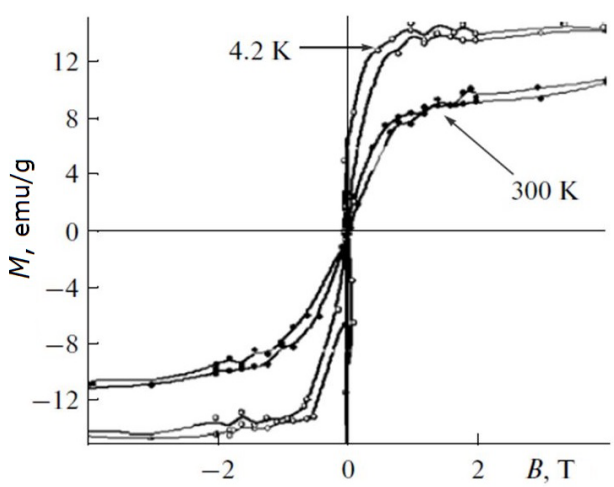

Fig. 5. *Magnetization curves of $Mg(Fe_{0.8}Ga_{0.2})_2O_4$ film on Si with a thickness of 200 nm after its crystallization at 800 K for 30 min* [6].

In **Fig. 5** shows the results of studies of the magnetization curves of the $Mg(Fe_{0.8}Ga_{0.2})_2O_4$ film on Si with a thickness of 200 nm after its crystallization at 800 K for 30 min. It can be seen from the figure that M_S is much less than the analogous value for powdered $Mg(Fe_{0.8}Ga_{0.2})_2O_4$ and does not reach saturation at room temperature in an external magnetic field exceeding 4*T*.

4. A NEW WAY OF OBTAINING FERRITE FILMS ON SEMICONDUCTOR SUBSTRATES

The authors of [33] proposed a method for obtaining microelectronic-quality ferrite films on semiconductor and dielectric substrates without elastic stresses and undesirable interactions of components at the interface. The film structures were obtained by ion-beam sputtering, which allows the transfer of the metal oxide target material to the substrate without changing the cationic composition, ensuring the density of the submicron thickness layer close to the density of the bulk target material, and achieving high adhesion of the deposited layer due to the presence of a high-energy component in the flow adatoms.

For an effective implementation of this method, they applied an integrated approach, which consists in the fact that a method of synthesizing a target material was originally developed, which allows minimizing surface and bulk film defects in the process of its creation, to obtain a uniform thickness and area while ensuring the chemical stability of the interface film/substrate. Then, at the second stage, when creating the film structures, the original idea of the film crystallization process was implemented without heating the substrate.

Note that in most of the works, the quality (phase homogeneity, dimensional unimodality, etc.) of the target material

for the synthesis of films is not given due attention. However, it is this factor that can have a significant effect on the quality of the heterostructures obtained.

To achieve this goal, a method for the synthesis of powdered ferrites was developed, which uses gel burning [34]. The method is based on heat treatment of mixtures containing nitrates of the respective metals and "organic fuel", which must meet certain requirements. First, to form complex compounds with metal salts, which contributes to increasing the solubility of the starting components and prevents precipitation upon evaporation of water. As a result, a uniform distribution of ions in the gel precursor is achieved, the heat treatment of which leads to the formation of a single-phase highly dispersed powdered oxide. Secondly, the organic component of the reaction mixture should generate enough heat to burn/smolder the gel in a self-sustaining mode, which, in turn, eliminates the subsequent high-temperature annealing in order to crystallize the final product. The choice of an effective "organic fuel" took into account these requirements, as well as the individual characteristics of the objects of study.

Let us consider in more detail the process of synthesizing a homogeneous powder that is unimodal in particle size $Mg(Fe_{0.8}Ga_{0.2})_2O_4$ powder by burning a gel using glycine as an "organic fuel" and its mixture with hexamine. Due to its symmetry, the glycine molecule can serve as a bidentate ligand for divalent and trivalent *d*-metals, which contributes to the homogenization of the gel precursor, and, as a consequence, the phase and dimensional uniformity of the final powdered material. The second component of the fuel mixture - hexamine, has attractive calorific properties (calorific value of 4215 kJ/mol), which ensures the initiation of gel burning and the flow of this process in a self-sustaining mode.

Note that the initial solution of metal nitrates was prepared by dissolving metallic magnesium, gallium and carbonyl iron. In a molar ratio of 1:0.4:1.6 in diluted (1:3) nitric acid. Then a mixture of glycine ($H_2N–CH_2–C(O)OH$) and hexamine ($C_6H_{12}N_4$) were added to the solution.

The resulting solutions were evaporated in the reactor with stirring at ~ 100°*C* to the state of gels. At a temperature of > 100°*C*, an intense combustion reaction began (**Fig. 6**). At temperatures of ~ 135-165°*C* (Fig. 6), a sharp mass loss was observed, accompanied by a significant exothermic effect (DSC curve, Fig. 6). It is associated with burning gels.

It is obvious that the actual temperature of combustion of the samples is significantly higher than the specified temperature range. In this regard, the authors of [34] developed a calculation method based on the DSC results to determine the temperature of burning gels. As a result, it turned out that the real temperature of short-term burning is 1040°*C*. At the same time, in the literature, as a rule, only the adiabatic combustion temperature of the samples is indicated, which is several thousand degrees.

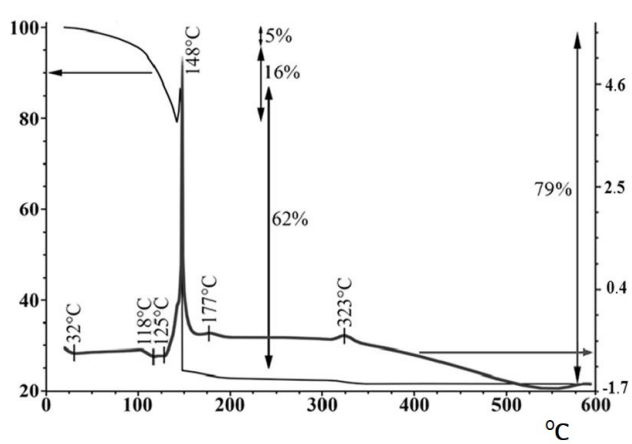

Fig. 6. *TGA-DSC of gel (air flow).*

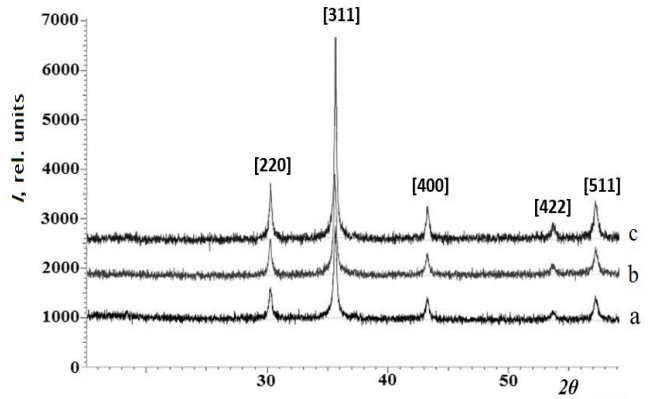

Fig. 7. *XRD patterns of $Mg(Fe_{0.8}Ga_{0.2})_2O_4$ powder: a - after synthesis; b - annealing at 600°C; c - annealing at 700°C.*

On X-ray diffractograms of the powders (**Fig. 7**a), after burning and cooling, the reflections of crystalline $Mg(Fe_{0.8}Ga_{0.2})_2O_4$ were recorded. Further heat treatment at 600°*C* and 700°*C* (Fig. 7b, c) contributes to an increase in the degree of crystallinity of the powder and allows one to obtain a single-phase, nano-sized powder with a relative unimodality of particle size distribution without carbon-containing impurities.

Targets for film production were prepared from the synthesized powders.

In this case, the synthesis of ferrite films took place in several stages. Initially, a layer of ferrite from 10 to 20 nm thick was deposited with an ion beam method of oxygen ions with an energy of 1500 to 1600 eV and a beam current density of 0.1 to 0.25 mA/cm^2. The interval of thicknesses was chosen from the following considerations: when the film thickness is less than 10 nm, the magnetic properties of the films after crystallization practically do not appear, and when the layer thickness is more than 20 nm, it is necessary to increase the crystallization temperature of the film.

Then, in the quasi-pulse mode, ferrites crystallized. The speed (150–200°*C*/min) and the exposure time (700–720°*C* for 2–3 min) of the reactor were selected so that the substrate did not heat up during the crystallization of

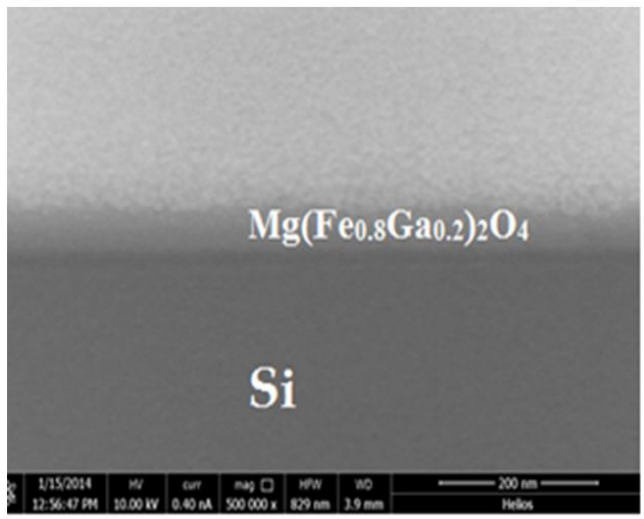

Fig. 8. *SEM image the cross section of $Mg(Fe_{0.8}Ga_{0.2})_2O_4/Si$ heterostructure after crystallization in the quasi-pulse mode.*

the film. After rapid cooling of the reactor, the film was thinned to a thickness of ~ 2 nanometers. As a result of such operations, a ferrite film containing numerous defects (see Fig. 4), formed as a result of its crystallization, was removed.

Next, re-deposition of the film on the germinal crystal layer of ferrite was performed. Thus, a quasi-epitaxial growth of the ferrite film took place, and its subsequent crystallization in the quasi-pulse mode was not accompanied by the formation of defects.

In **Fig. 8** shows the SEM image of the cross section of the $Mg(Fe_{0.8}Ga_{0.2})_2O_4/Si$ heterostructure after quasi-pulse crystallization. It is seen that the interface border is smooth, and there are no defects in the film itself.

In **Fig. 9** shows the SEM images of the surface of the $Mg(Fe_{0.8}Ga_{0.2})_2O_4$ film on the

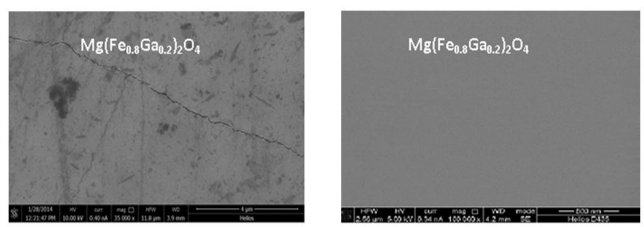

Fig. 9. *SEM images of the surface of the $Mg(Fe_{0.8}Ga_{0.2})_2O_4$ film on the Si substrate after its crystallization in the isothermal (left) and quasi-pulse (right) modes.*

silicon substrate after its crystallization by the isothermal method (left) and in the quasi-pulse mode (right).

It can be seen from the figure that the $Mg(Fe_{0.8}Ga_{0.2})_2O_4$ surface after crystallization in the isothermal mode consists of numerous defects and cracks over the entire film area, and vice versa, the $Mg(Fe_{0.8}Ga_{0.2})_2O_4$ surface remains nano-sized after quasi-pulse crystallization.

It should be noted that the proposed method of creating film structures is quite complex in execution. Its implementation is possible only with the availability of appropriate high-tech sputtering equipment and personnel with high qualifications.

In some cases, when creating film structures, it is possible to use another approach - the use of barrier layers at the interface, which will interfere with the processes of interaction of components during the crystallization of films. At the same time, the question remains whether the composition of the buffer layer affects the functional properties of the structures obtained. The physical properties of film structures were analyzed by the example of films of yttrium iron garnet (YIG, $Y_3Fe_5O_{12}$) on Si with buffer layers of SiO_2 and AlO_x [35].

5. FILM STRUCTURES OF $Y_3Fe_5O_{12}$ ON Si

It is known that epitaxial $Y_3Fe_5O_{12}$ films of micron thickness are usually grown by the method of liquid-phase epitaxy (LPE) on gallium-gadolinium garnet (GGG) substrates due to the small lattice mismatch ≈ 0.06%. At the same time, $Y_3Fe_5O_{12}$ films on silicon or quartz substrates are characterized by higher values of the Hilbert attenuation parameter ≈ 10^{-2} [36], which is caused by the mismatch of the crystal lattices and the temperature expansion coefficients of $Y_3Fe_5O_{12}$ and Si, which excludes their epitaxial growth. However, if we separate the processes of precipitation and crystallization of $Y_3Fe_5O_{12}$, and form a buffer layer on the Si surface in the form of a thin film of SiO_2 or AlO_x, which will prevent third-party chemical reactions during annealing, but at the same time provide high adhesion of the deposited layer to the surface, then we can expect high quality polycrystalline ferrite garnet films. In this case, at the deposition stage, diffusion exchange will be excluded between the substrate, which is perfect in structure and the substrate and film of the material being crystallized, and the role of diffusion processes in the crystallization of the film will be leveled by the high density of the material being deposited.

In **Fig. 10** shows the appearance of the surface of the YIG film in the composition of the $Y_3Fe_5O_{12}$ (260nm)/AlO_x/SiO_x/Si (100) heterostructure (Fig. 10*a*), its cross section (Fig. 10*b*) and its elemental composition (Fig. 10*c*).

From Fig. 10 that the $Y_3Fe_5O_{12}$ film is characterized by the presence of large and

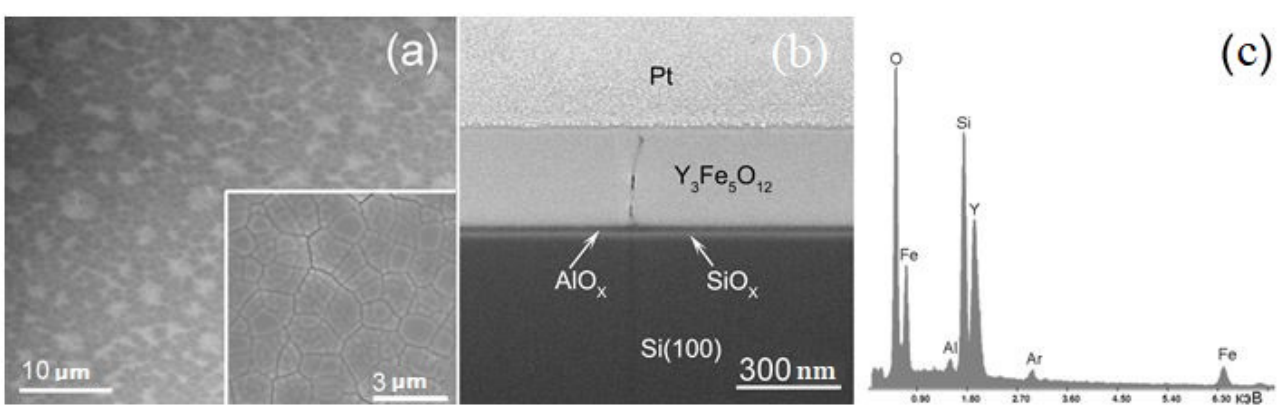

Fig. 10. *SEM image of the surface of the $Y_3Fe_5O_{12}$/AlO_x/SiO_x/Si(100) film heterostructure (Fig. 10a, inset shows a section of the surface with a high resolution).*

small fracture meshes. The characteristic dimensions of large grids of cracks are up to 2 μm, and small ones that are contained inside large ones do not exceed 0.3 μm, which correlates with the thickness of the $Y_3Fe_5O_{12}$film (about 0.3). In this case, the $Y_3Fe_5O_{12}$ film is polycrystalline and consists of single-crystal blocks with characteristic sizes up to 0.3 microns. The interface areas of the grain boundaries, especially when the boundaries of large and small areas coincide, are enriched with defects, which is reflected in the contrast in the appearance of the surface (Fig. 10*a,b*). The fine mesh of cracks does not grow through the entire thickness of the $Y_3Fe_5O_{12}$ film, and the large one extends up to the buffer layer (Fig. 10*b*). It can be seen that the interfaces in the $Y_3Fe_5O_{12}$ (260nm)/AlO_x/SiO_x/Si (100) heterostructure are solid, clear and plane-parallel. In this case, no violations that could be caused by intense interactions with the buffer layer and the substrate are recorded. The elemental composition of the heterostructure (Fig. 10*c*) contains only elements corresponding to the composition $Y_3Fe_5O_{12}/AlO_x/SiO_x$/Si (100). Similar results were obtained for heterostructures with the composition $Y_3Fe_5O_{12}/SiO_2$/Si (111). It should be noted that the formation of cracked grids is also fixed for films of ferrite garnets obtained by the method of magnetron sputtering on Si or quartz substrates [38, 39].

In **Fig. 11** shows X-ray diffraction patterns of film heterostructures $Y_3Fe_5O_{12}$(260nm)/AlO_x(40nm)/SiO_x(10nm)/Si (100) (Fig. 11, curve 1) and $Y_3Fe_5O_{12}$(260nm)/SiO_2(800nm)/Si (111) (Fig. 11, curve 2). For $Y_3Fe_5O_{12}$ films with a thickness of about 200 nm, diffraction patterns identify narrow reflexes of high intensity, which are related to the cubic symmetry of the space group (230) [40]. In this case, the lattice constant of submicron films was about 1.2378 nm, which is somewhat larger

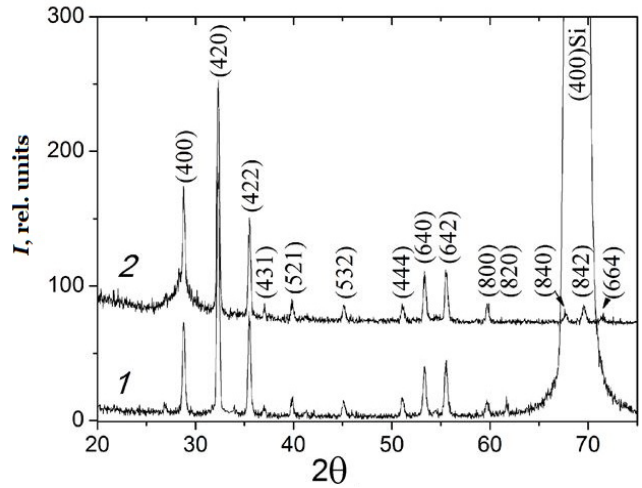

Fig. 11. *X-ray diffraction patterns of typical heterostructures $Y_3Fe_5O_{12}$(200нм)/AlO_x(40нм)/SiO_x(10нм)/Si (100) (Fig. 11, curve 1) and $Y_3Fe_5O_{12}$ (200nm)/SiO_2 (800nm)/Si (111) (Fig. 11, curve 2).*

than that of a bulk YIG single crystal (1.2376 nm [41]). One can see a good agreement of the X-ray diffraction spectra of both samples. In the case of a relatively thick thermally grown layer of SiO_2 (Fig. 11, curve 2), the substrate is completely shielded from X-rays, but this does not lead to a significant deformation of the diffractogram reflections. This is evidence in favor of the non-diffusion mechanism of crystallization of the samples under study. It should also be noted that in films of ferrite garnets obtained by the method of ion-beam sputtering-deposition, the lattice constant always turns out to be greater than the value characteristic of bulk single crystals. The reason for this can be either the intrinsic defect structure of the YIG films, which forms as the crystallization progresses, and the adhesive, rather than epitaxial, bond with the substrate, which does not involve a gradual relaxation of the elastic stresses as the film thickness increases.

According to the magnetization curves, ferrite-garnet films with a thickness of more than 100 nm, regardless of the composition of the buffer layer, are characterized by a saturation magnetization value close to that of the $Y_3Fe_5O_{12}$ single crystal, i.e. 1740 Gs and

a coercive force of 30 ... 40 O. This indicates that the films obtained are characterized by the stoichiometric composition of $Y_3Fe_5O_{12}$.

To determine the magnetic properties, measurements were made of the Kerr effect for films differing in buffer layers and thickness. In the polar configuration, the rotation of the Kerr angle θ_K for the $Y_3Fe_5O_{12}$(260nm)/AlO_x / SiO_x/S (100) heterostructure is 1530 degrees /cm (**Fig. 12***a*). It is known that in $Y_3Fe_5O_{12}$the contribution from Fe^{3+} ions in tetrahedral and octahedral sublattices has the opposite sign of the Faraday angle θ_F [42] and the resulting rotation θ_F at the incident light wavelength λ = 640 nm is 750 degrees/cm [35]. For a laser wavelength of 640 nm, the garnet ferrite film is optically transparent. Therefore, for submicron ferrite-garnet films, in the light reflection configuration, the Kerr rotation angle θ_K will be comparable to twice the angle of rotation of the polarization plane in a magnetic field θ_F $Y_3Fe_5O_{12}$ with a transparent thin buffer layer AlO_x. Accordingly, we can assume, taking into account the linear relationship between θ_F and saturation magnetization, that in this case the magnitude of the sublattice magnetization correspond to bulk ferrite garnet, and, therefore, the concentration of Fe^{3+} ions in tetrahedrons and octahedra is close to the stoichiometric composition of $Y_3Fe_5O_{12}$. For a ferrite garnet film on a relatively thick buffer layer of SiO_2, the angle $\theta_K \approx 820$ deg/cm is about 2 times smaller than for a sample with a buffer layer of AlO_x (Fig. 12*b*). Such a difference may be due to a relatively thick layer of SiO_2, which leads to an additional reflection of the incident beam of light at different interfaces, and the rotation of θ_K mainly occurs only in one direction - upon reflection from the Si (100) substrate.

In a magnetic field applied along the normal to the garnet surface, the films are characterized by a saturation field H_s of about 1.3 kOe (Fig. 12*a*), and in a field directed along the film plane, the value of the saturation field is about 0.06 kOe (Fig. 12*b*). Therefore, in these samples, the axis of easy magnetization is close in location to the film plane and determines the planar nature of the magnetic anisotropy. The coercive field in polycrystalline ferrite garnet films does not exceed 30 Oe and is typical of ferrite garnet films obtained on Si [43].

In **Fig. 13** shows the characteristic dependence of the amplitude of the FMR signal for ferrite-garnet films 260 nm thick on the external magnetic field and on the orientation of the samples, given by the polar θ_H and azimuthal φ_H angles. This makes it possible to measure the values of the resonant field and, according to the phenomenological model [44],

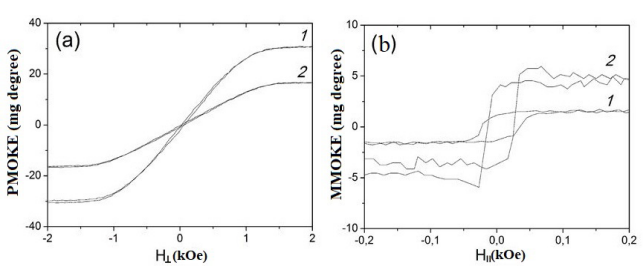

Fig. 12. *Field dependences of the polar (a) and meridional (b) Kerr effect for the characteristic $Y_3Fe_5O_{12}$(200nm)/AlO_x(40nm)/SiO_x (10nm)/Si (100) film heterostructures (Fig. 12a,b, curve 1) and $Y_3Fe_5O_{12}$(200nm)/SiO_2(800nm)/Si (111) (Fig. 12a,b, curve 2).*

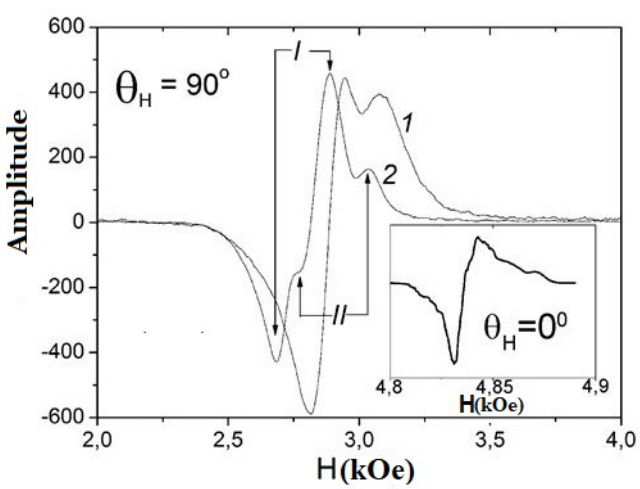

Fig. 13. *FMR spectra of characteristic $Y_3Fe_5O_{12}$(200nm)/ AlO_x(40nm)/SiO_x(10nm)/Si (100) film heterostructures (Fig. 13, curve 1) and $Y_3Fe_5O_{12}$(200nm)/SiO_2(800nm)/Si (111) (Fig. 13, curve 2) in a magnetic field oriented along the surface of the sample. The inset in Fig. 13 shows the FMR spectrum for sample $Y_3Fe_5O_{12}$(200nm)/SiO_2(800nm)/Si(111) in a magnetic field normally oriented to the sample surface.*

determine the values of the effective magnetic anisotropy constant K_{eff} for these samples, including the uniaxial anisotropy constant K_u and the demagnetization energy $2\pi M_S^2$. For the buffer layers under consideration, the value of Kerr was $-1 \cdot 10^5$ erg/cm^3. Note that the negative sign Kerr corresponds to the orientation of the axis of easy magnetization lying in the sample plane, and, therefore, correlates with the results obtained using the magneto-optical Kerr effect (Fig. 13).

From Fig. 13 that the FMR line for ferrite-garnet films, in the case of the direction of an external magnetic field along the sample plane, contains several resonances. This fact is the subject of a separate study. In the case of a garnet ferrite film on the AlO_x buffer layer, these resonances are difficult to distinguish. However, for a garnet ferrite film crystallized on a SiO_2 layer, the FMR line contains lines of two resonances, marked as I and II. The amplitude of the second resonance line decreases with a change in the direction of the external magnetic field from the plane of the sample surface to the normal to it. At $\theta_H = 0°$, only one contribution from the first resonance to the total signal is observed (inset to Fig. 13). Using the value for the width of the resonance curve ΔH, obtained for the resonant frequency of FMR, we can estimate the dimensionless damping parameter Hilbert α, which is determined by [35] from the relationship: $\Delta H \approx 2\pi f\alpha/\gamma$, where f is the FMR frequency, $\gamma = 1.7588 \cdot 10^7$ Oe^{-1} is the gyromagnetic ratio.

For samples with buffer layers in an external magnetic field applied parallel to the sample surface, the width of the first resonance line ΔH_1 is in the range of 150-200 Oe, while ΔH_2 is 270 O. However, for the perpendicular direction of the magnetic field ΔH_1 for ferrite films-granate on the AlO_x buffer layer is 150 Oe and 11 Oe for samples with a buffer layer of SiO_2 (inset to Fig. 13), which corresponds to the value of the Hilbert damping parameter $\alpha = 2.8 \cdot 10^{-3}$. The value of $\Delta H = 11$ Oe for the considered submicron films of ferrite-garnet, obtained by the method of ion-beam sputtering on silicon substrates, is 3-4 times higher than for films, by the method of pulsed laser evaporation PLD [44] and 3 times less than with films of ferrite garnets obtained by magnetron sputtering on GGG substrates [45].

The relaxation of spin-wave excitation processes in the samples under consideration is determined by their polycrystalline nature, the state of grain boundaries and the influence of the interface regions on the state of the film as a whole with its thickness specified by a limited range of values comparable to the value of 10 ... 100 lattice constants. In this case, in films of ferrite-garnet, inhomogeneous effective fields are created mainly due to the anisotropy of the crystal structure (random orientation of crystallites) and the anisotropy induced by stresses [46]. For the anisotropy field, Ha ~ $4\pi M_S$, and the width of the FMR line is determined by the expression $\Delta H = 0.5 H_a$ [35]. Since the field of uniaxial anisotropy is $H_U = 370$ Oe, an increase in the FMR line width in the structure of polycrystallites may be $\Delta H \approx 190$ O, which is in good agreement with the experimental value (Fig. 13). Due to the fact that $H_U \sim 4\pi M_S$, it should be expected that the interaction between the crystallites is weak, and the crystallites are resonantly excited in an external magnetic field independently of each other [35]. Therefore, the presence of two resonances in the FMR line (Fig. 13) may be due to two types of crystallites and intercrystallite boundaries differing in size (Fig. 13*a,b*), which are formed during deposition and subsequent crystallization. In addition, the value of the damping parameter is also affected by the buffer layer. It is known that a thermally oxidized SiO_2 layer on Si is

amorphous [46]. This provides a more stable structure of the SiO_2 layer, compared to the AlO_x layer obtained by precipitation at room temperature. Therefore, the ferrite-garnet film on the buffer layer of SiO_2 is less strained as compared to the film containing AlO_x. As a consequence, the ferrite-garnet film on the SiO_2 buffer layer in an external magnetic field perpendicular to the sample plane is characterized by a smaller contribution of randomly oriented crystallites to the total width of the FMR ΔH line.

The practical significance of applying the method of ion-beam sputtering to obtain submicron films of ferrite garnets on a SiO_2 buffer layer on silicon with the Hilbert decay parameter $\alpha \approx 10^{-3}$ is obvious. Film structures can be claimed in a large area of silicon spin-wave device structures.

6. CONCLUSION

A team of authors to create ferrite films on semiconductor substrates without elastic stresses and interactions of components at the interface created by crystallization of structures can give additional impetus for accelerated development of work in both spintronics and magnon-plasmon structures.

A distinctive feature of this method is that with its help it is possible to create structures not only of ferrites, but also of other film heterostructures with mismatched lattice parameters, group methods of microelectronics.

ACKNOLEDJMENTS

This work was supported by the RFBR projects No. 16-08-00933 and 16-29-05204.

REFERENCES

1. Zakharchenya BP, Korenev VL. Integrating magnetism into semiconductor electronics. UFN, 2005, 175 (6): 629-635 (in Russ.).
2. Joshi VK. Spintronics: A contemporary review of emerging electronics devices. *Engineering Science and Technology, an International Journal,* 2016, 19(3):1503-1513.
3. Nipan DG, Stogny AI, Ketsko VA. Oxide magnetic semiconductors: coatings and films. *Uspekhi khimii*, 2012, 5: 458-475 (in Russ.).
4. Sonoda S, Shimizu S, Sasaki T, Yamamoto Y. Molecular beam epitaxy of wurtzite (Ga, Mn)N films on sapphire(0001) showing the ferromagnetic behaviour at room temperature. *J. Cryst. Growth.*, 2002, 237:1358-1362.
5. Yang SG, Pakhomov AB, Hung ST, Wong CY. Room temperature magnetism in sputtered (Zn, Co)O films. *IEEE Transact. Magn.*, 2002, 38:2877.
6. Lim S-W, Hwang D-K, Myoung J-M. Observation of optical properties related to room-temperature ferromagnetism in co-sputtered $Zn_{1-x}Co_xO$ thin films. *Solid State Commun.*, 2003, 125:231-235.
7. Ramachandran S, Tiwari A, Narayan J. $Zn_{0.9}Co_{0.1}O$-based diluted magnetic semiconducting thin films. *Appl. Phys. Lett.*, 2004, 84:5255-5257.
8. Kim JH, Kim H, Kim D. Magnetic properties of epitaxially grown $Zn_{1-x}Co_xO$ thin films by pulsed laser deposition. *J. Appl. Phys.*, 2002, 92:6066-6071.
9. Lawes G, Risbud AS, Ramirez AP, Seshadri G. Absence of ferromagnetism in Co and Mg substituted polycrystalline ZnO. *Phys. Rev. B: Condens. Matter*, 2005, 71:045201-1-045201-5.
10. Kane MH, Salini K, Summers CJ. Magnetic properties of bulk $Zn_{1-x}Mn_xO$ and $Zn_{1-x}Co_xO$ single crystals. *J. Appl. Phys.*, 2005, 97:023906.
11. Mathias BT, Bozorth RM, van Vleck JH. Ferromagnetic Interaction in EuO. *Phys. Rev. Lett.*, 1961, 7(5):160-165.
12. Kumar D, Antifakos J, Blamire MG, Barber ZH. High Curie temperatures in ferromagnetic Cr-doped AlN thin films. *Appl. Phys. Lett.*, 2004, 84:5004-5006.
13. Ueda K, Tabata H, Kawai T. Magnetic and electric properties of transition-metal-doped ZnO films. *Appl. Phys. Lett.*, 2001, 79:988-1000.
14. Venkatesan M, Fitzgerald CB, Lunney JG, Coey JMD. Anisotropic Ferromagnetism in Substituted Zinc Oxide. *Phys. Rev. Lett.*, 2004, 93(17):7206-7209.
15. Sharma P, Gupta A, Rao KV. Ferromagnetism above room temperature in bulk and transparent thin films of Mn-doped ZnO. *Nat. Mater.*, 2003, 2:673-677.

16. Buchholz DB, Chang RPH, Song JH, Ketterson JB. Room-temperature ferromagnetism in Cu-doped ZnO thin films. *Appl. Phys. Lett.*, 2005, 87:1-082504-3.
17. Wang Z, Wang W, Tang J. Extraordinary Hall effect and ferromagnetism in Fe-doped reduced rutile. *Appl. Phys. Lett.*, 2003, 83:518-520.
18. Ogale SB, Choudhary RJ, Buban JP. High temperature ferromagnetism with a giant magnetic moment in transparent co-doped SnO(2-delta). *Phys. Rev. Lett.*, 2003, 91:077205-4.
19. Coey JMD, Douvalis AP, Fitzgerald CB, Venkatesan M. Ferromagnetism in Fe-doped SnO_2 thin films. *Appl. Phys. Lett.*, 2004, 84:1332-1334.
20. Hong NH, Sakai J, Prellier W, Hassini A. Transparent Cr-doped SnO_2 thin films: ferromagnetism beyond room temperature with a giant magnetic moment. *J. Phys.:Condens. Matter.*, 2005, 17:1697-1702.
21. Hong NH, Sakai J. Ferromagnetic V-doped SnO_2 thin. *Physica B.*, 2005, 358:265-268.
22. Wang CM, Jianga GeJ. Magnetic behavior of SnO_2 nanosheets at room temperature. *Appl. Phys. Lett.*, 2010, 97:42510.
23. Sundaresan A, Bhargavi R, Rangarajan N. Ferromagnetism as a universal feature of nanoparticles of the otherwise nonmagnetic oxides. *Phys. Rev. B.*, 2006, 74:161306-1-161306-4.
24. Mohanty S, Kar M, Ravi S. Ferromagnetism in mechanically milled pure SnO_2. *Intern. Journal of Modern Physics,* 2013, 27:1350025-1-1350025-11.
25. Nipan DG, Ketsko VA, Koltsova TN, Stogniy AI, Yanushkevich KI, Pankov VV, Khoviv AM. Solid solutions in the Zn-Co-O system: physicochemical properties. *Zh. Neorg Khimii*, 2006, 51 (12):2083-2089 (in Russ.).
26. Mathias BT, Bozorth RM, Vleck J.H. Ferromagnetic Interaction in EuO. *Phys. Rev. Lett.*, 1961, 7(5):160-165.
27. Appelbaum I, Huang B, Monsma DJ. Electronic measurement and control of spin transport in silicon. *Nature*, 2007, 447:295-299.
28. Schmehl A, Vaithyanathan V, Herrnberger A. Epitaxial integration of the highly spin-polarized ferromagnetic semiconductor EuO with silicon and GaN. *Nature Materials,* 2007, 6:882-887.
29. Ivanov V.A. Novotortsev VM, Kalinnikov VT. Spintronics and spintronic materials. *Izvestiya AN. Ser. Khimii*, 2004, 11:2255-2303 (in Russ.).
30. Randoshkin VV, Chervonenkis AY. *Prikladnaya magnitooptika.* Moscow, Energoatomizdat Publ., 1990, 320 p.
31. Mezin NI, Starostyuk NYu, Yampolskii SV. Growth and Properties of Yttrium Iron Garnet Films with a Higher Iron Content. *J. Magn. Magn. Mater.*, 2017, 442(15):189-195.
32. Popova Elena, Deb Marwan, Bocher Laura, Gloter Alexandre, Stéphan Odile, Warot-Fonrose Bénédict, Berini Bruno, Dumont Yves, Keller Niels. Interplay between epitaxial strain and low dimensionality effects in a ferromagnetic oxide. *Journal of Applied Physics,* 2017, 121:115304-1-115304-11.
33. Smirnova MN, Stogny AI, Bespalov AV, Golikova OL, Novitsky NN, Geraskin AA, Ermakov VA, Ketsko VA. The method of obtaining the heterostructure $Mg(Fe_{1-x}Ga_x)_2O_4/Si$ with a stable phase boundary. *Patent for IZ № 2657674*.
34. Beresnev EN, Smirnova MN, Goeva LV, Simonenko NP, Kopeva MA, Kuznetsova OB, Ketsko VA. Investigation of the process of decomposition of the gel and the formation of MgFe1.6Ga0.4O4 powder. *Zh. Neorg. Khimii,* 2016, 61 (8):1078-1083 (in Russ.).
35. Stogny AI, Novitsky NN, Golikova OL, Bespalov AV, Gieniusz R, Maziewski A, Stupakiewicz A, Smirnova MN, Ketsko VA. Formation by the method of ion-beam sputtering of submicron films of iron-yttrium garnet on silicon with buffer layers of silicon oxide or aluminum oxide. *Neorgan. Mater.*, 2017, 53 (10):1069-1074 (in Russ.).
36. Bhoi B, Venkataramani N, Aiyar RPRC, Prasad Sh. FMR and magnetic studies on polycrystalline YIG thin films deposited using pulsed laser. *IEEE Transactions on Magnetics*, 2013, 49(3):990-994.
37. Popova E, Keller N, Gendron F, Guyot M, Brianso MC, Dumond Y, Tessier M. Structure and magnetic properties of yttrium–iron–garnet thin films prepared by laser deposition. *J. Appl. Phys.*, 2001, 90(3):1422-1428.
38. Yang QH, Zhang HW, Wen QY, Liu YL. Effects of off-stechiometry and density on the magnetic and magneto-optical properties of yttrium iron

garnet films by magnetron sputtering method. *J. Appl. Phys.*, 2010, 108:073901-1-073901-5.

39. Boudiar T, Capraro S, Rouiller T, Blanc-Mignon MF, Payet-Gervy B, Berre MLe, Rousseau JJ. YIG thin films for magneto-optical and microwave applications. *Phys. Stat. Sol. (C),* 2004, 1(12):3347-3351.
40. International Centre for Diffraction Data. 1998, *JCPDS*. Card 43-0507.
41. Landolt-Börnstein. *Numerical Data and Functional Relationships in Science and Technology*. New Series. Group III. 27/e, 1991, Springer-Verlag, Berlin.
42. Zvezdin AK, Kotov VA. *Magnitooptika tonkikh plenok*. Moscow, Nauka Publ., 1988, 192 p.
43. Yang QH, Zhang HW, Wen QY, and Liu YL. Effects of off-stoichiometry and density on the magnetic and magneto-optical properties of yttrium iron garnet films by magnetron sputtering method. *J. Appl. Phys.*, 2010, 108:073901-1-073901-5.
44. Manuilov SA, Khartsev SI, Grishin AM. Pulsed laser deposited $Y_3Fe_5O_{12}$ films: Nature of magnetic anisotropy I. *J. Appl. Phys.*, 2009, 106:123917-1-123917-11.
45. Yamamoto S, Kuniki H, Kurisu H, Matsuura M, Jang P. Post-annealing effect of YIG ferrite thin-films epitaxially grown by reactive sputtering. *Phys. Stat. Sol. (A)*, 2004, 201(4):1810-1814.
46. Schlömann E. Inhomogeneous Broadening of Ferromagnetic Resonance Lines. *Phys. Rev.,* 1969, 182:632-645.

PHYSICO-CHEMICAL ANALYSIS OF SEMICONDUCTOR-FERROMAGNET SYSTEMS AS A BASIS OF SYNTHESIS OF MAGNETIC-GRANULATED SPINTRONIC STRUCTURES

[1,2]Sergey F. Marenkin, [1]Irina V. Fedorchenko, [1]Alexander D. Izotov, [1]Mikhail G. Vasil'ev

[1]Kurnakov Institute of General and Inorganic Chemistry of RAS, http://www.igic.ras.ru/
Moscow 119991, Russian Federation

[2]National Research Technological University "MISiS", http://misis.ru/
Moscow 119049, Russian Federation

marenkin@rambler.ru, irina@igic.ras.ru, izotov@igic.ras.ru, mgvas@igic.ras.ru

Abstract. **An analytical review devoted to the physicochemical principles of the synthesis of granular structures in semiconductor-ferromagnet systems is represented. In these systems, as semiconductors, compounds are $A^{II}B^{IV}C^{V}_2$, $A^{III}C^{V}$, $A^{II}_2C^{V}_3$ and $A^{II}C^{V}_2$ and manganese compounds (MnP, MnAs and MnSb) as ferromagnets. It is shown that in magnetostransmitter devices magneto-granular structures are an alternative to superlattices, and the effects of GMR and TMR are also possible. Advantages of magneto-granular structures are considered, such as: less labor-intensive methods of production, milder requirements for the dimension of a ferromagnet and a non-magnet, the possibility of forming a stable interface, soft requirements to the thickness of layers than in the case of superlattices, etc. It is shown that, due to the high mobility of charge carriers, the use of semiconductors as a matrix is more preferable than metals or dielectrics. The basic principles for the creation of granular structures with high values of magnetoresistance based on eutectic-type systems are formulated. During the crystallization of the eutectic, the simultaneous crystallization of all the phases that make up the eutectic takes place, leading to the formation of a specific fine-dispersed structure. The use of ultrahigh supersaturations leads to significant supercooling, which contributes to metastable crystallization. This causes a synergistic effect that stimulates nanostructuring, and promotes the creation of granular structures. The results of investigations of semiconductor-ferromagnet systems are presented and the possibility of obtaining magnetogranular structures with high magnetoresistance in them is shown.**

Keywords: **spintronics, magneto-granular structures, semiconductors, ferromagnets**

UDC 548.4;548.73;548.735.6

Bibliography - 45 references *Received Oktober 10, 2018; accepted November 16, 2018*

RENSIT, 2018, 10(3):395-402 **DOI: 10.17725/rensit.2018.10.395**

Contents

1. INTRODUCTION

Granular structures are an alternative to superlattices in spintronic devices. Currently, spintronics is one of the most dynamically developed areas of electronics. This is due to the fact that it is more energy-efficient to control the electron spin than the electron charge. In this regard, research on the creation of spin diodes, transistors and other traditional electronics devices is intensively carried out in Russia and abroad. However, while research on the creation of such devices are at the model levels [1, 2]. Actually existing spintronic devices are magnetic memory devices. Magnetic memory devices are produced in large quantities, because are part of all modern computers [3, 4]. Magnetic memory

devices are based on two effects, the effects of giant (GMR) and tunnel (TMR) magnetoresistance. [5, 6]. Effects were found on superlattices, which consisted of nanolayers of a magnetic and non-magnetic ones. Heterogeneous magnetically ordered systems are considered as analogues of superlattices, better known in the literature as magnetically granulated structures [7-11]. The effects of GMR and TMR are also observed on such structures [12–16]. Magnetogranular structure consists of a nonmagnetic matrix and ferromagnetic nanoparticles. Metals, semiconductors and dielectrics can be used as matrix materials [17–23].

The nature of the GMR effect in magnetically granular structures and superlattices is similar. **Figure 1** shows the scheme of the appearance of the HMS effect. Despite the fact that the magnitudes of the effects of GMR and TMR in magnetically granulated structures are smaller than in superlattices, however, these structures have several advantages [24]. Of the advantages, there are: less labor-intensive methods of obtaining, softer requirements for the size of a ferromagnet and non-magnetics, better possibilities for creating a stable phase boundary between a ferromagnet and a nonmagnet, softer requirements for the thickness of layers, etc. Therefore, the synthesis and study of the properties of magnetically granular structures are rather intensive. Nonmagnetic metals or dielectrics, usually oxides, are used as the matrix material. Iron, cobalt, nickel or alloys based on them are chosen as ferromagnets. In our works,

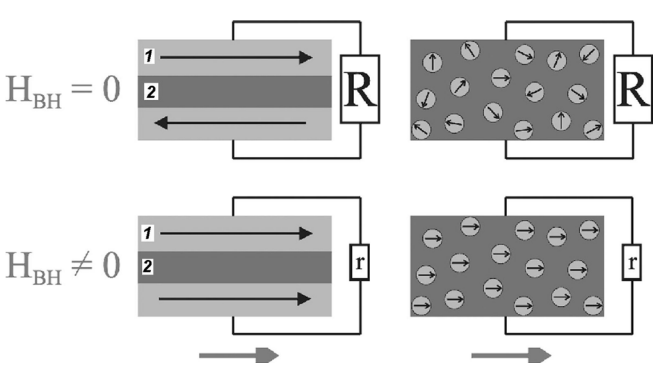

Fig. 1. *Pattern for GMR effect - a) in superlattices, б) in granular structures. (1 – ferromagnetic, 2 - nonmagnetic).*

semiconductors are used as the matrix material. Semiconductors have high mobility of charge carriers; this allows increasing the spin relaxation time and increasing the polarization efficiency of the spin transport.

2. PHASE EQUILIBRIA IN SEMICONDUCTOR-FERROMAGNET SYSTEMS

For the synthesis of a magnetically granular structure in semiconductor-ferromagnet systems, components are needed that would form a eutectic between themselves and have minimal inter-solubility. During eutectic crystallization, simultaneous crystallization of all phases that make up the eutectic occurs, which forms a specific fine structure. The use of ultra-high supersaturation, leads to a significant overcooling of the medium, and cause metastable crystallization. Both of these factors cause a synergistic effect that contributes to nanostructuring when creating a granular structure.

Manganese compounds (MnP, MnAs, MnSb) were chosen as ferromagnetic components of eutectic type systems. These compounds are semi-metallic ferromagnets with high Curie temperatures [25, 26]. Compounds $A^{II}B^{IV}C^{V}_2$, $A^{II}C^{V}$, $A^{II}_2C^{V}_3$ and $A^{II}C^{V}_2$, which include an element of the fifth group, were chosen as semiconductors. The crystal structure of these semiconductors is significantly different from the crystal structure of MnP, MnAs and MnSb, which suggests the possibility of the formation of systems of the eutectic type or systems with significant areas of delamination.

The study of semiconductor-ferromagnet systems was performed using a complex of physicochemical analysis methods: XRD, DTA and DSC. Microstructural studies were performed using SEM, AFM and optical microscope "Epicuant". The results of these studies are presented in **Table 1.** The table shows the composition, melting points and types of eutectic microstructures. As can be

Table 1

The results of the study of systems $A^{II}B^{IV}C^{V}_2$, $A^{II}_3C^{V}_2$, $A^{II}C^{V}_2$, $A^{III}B^{V}$ - manganese pnictides.

System	Eutectic coordinates		Microstructure of eutectic
	Composition, mol.%	T_m °C	
$ZnSiAs_2$ - MnAs	87 MnAs	847	needle
$ZnSnAs_2$ - MnAs	45 MnAs	744	needle
$ZnGeAs_2$ - MnAs	39 MnAs	816	lamellar
$CdGeAs_2$ - MnAs	18 MnAs	620	needle
$Zn_{0,9}Cd_{0,1}As_2$- MnAs	43 MnAs	756	lamellar
$Zn_{0,1}Cd_{0,9}As_2$- MnAs	24 MnAs	615	needle
GaSb - MnSb	41 MnSb	632	lamellar
InSb – MnSb	6.5 MnSb	515	needle
Zn_3As_2 – MnAs [44]	50 MnAs	815	lamellar
$ZnAs_2$ – MnAs [45]	27 MnAs	716	needle

seen from the data in the table, the systems were of the eutectic type, the microstructures of the eutectics depending on the composition were plate-like, columnar, needle-shaped [27, 28].

3. SYNTHESIS AND PROPERTIES OF MAGNETIC GRANULATED STRUCTURES

Based on the works of Ya.B. Zeldovich on nucleation, under conditions of significant supersaturation [29, 30], composites were synthesized with nanoclusters of MnAs and MnSb ferromagnets with T_C = 290–600 K. Subsequently, the effect of the dispersion factor on the electrical and magnetic properties in a wide range of temperatures and magnetic fields was studied on these composite alloys [31]. In the $ZnGeAs_2$-MnAs system, two types of samples were prepared. Upon receipt of the first type, the melt crystallized under normal conditions; in the off-furnace mode, the cooling rate was ~ $1.5 \cdot 10^{-2}$ deg/s. The melts of the second type crystallized in quenching mode. The cooling rate was ~ $1 \cdot 10^{2}$ deg/s. Salt solutions with high thermal conductivity were used as a quenching medium. Microstructural studies have shown that the synthesized alloys were of the eutectic type, the size of the manganese arsenide crystallites in them depended on the cooling rate. With an increase in speed of 4 orders of magnitude, the average crystallite size of manganese arsenide changed by 3 orders of magnitude from $5 \cdot 10^{4}$ to $\leq 6 \cdot 10^{1}$ nm. In samples of the second type, unlike samples of the first type, the DSC curves showed no thermal effect of the structural transformation α–β MnAs, while the Curie temperature shifted towards higher values, from 318 to 351 K, respectively. Significant differences in the properties show the increasing role of surface phenomena with increasing dispersion.

The magnetoresistance was measured on granular structures of alloys: $ZnGeAs_2$ and $CdGeAs_2$ with MnAs. In **Fig. 2** (a) shows the change in resistance from the magnetic field for the $ZnGeAs_2$ alloy with MnAs. At the beginning, the resistance dropped sharply with increasing magnetic field, and then saturation was observed. The magnitude of the magnetoresistance reached 60%. The type of magnetoresistance practically corresponded to the results observed by A. Fert and P. Grünberg when opening the GMR effect on superlattices [5, 6]. For $CdGeAs_2$ alloys with MnAs, the change in resistance had a different appearance. The resistance increased sharply with increasing magnetic field and there was no saturation (Fig. 2b). The known models of magnetoresistance cannot explain this nature of the change in resistance. As an attempt to find an explanation, alloys of $ZnGeAs_2$ solid solutions with $CdGeAs_2$ were prepared with the subsequent introduction of manganese arsenide. To determine the boundaries of solid

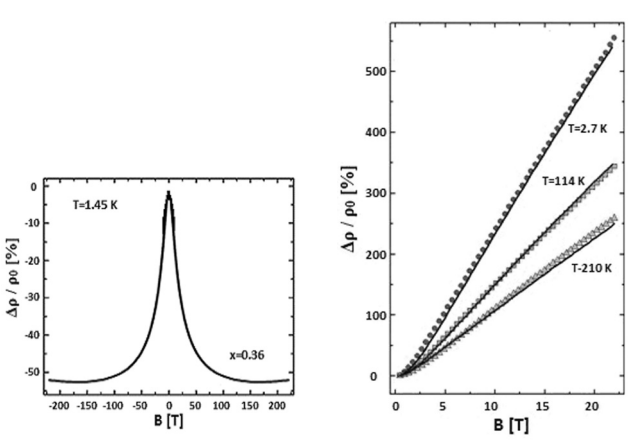

a *b*

Fig. 2. *Magnetic field/resistance dependence for alloys: a) $ZnGeAs_2$ with MnAs, b) $CdGeAs_2$ with MnAs.*

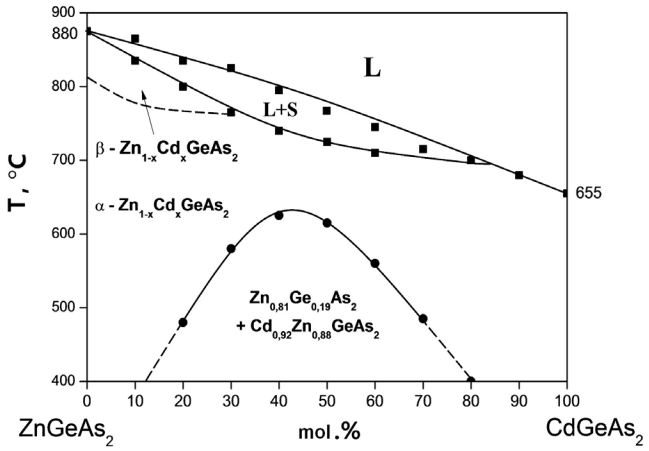

Fig. 3. *Phase diagram of $ZnGeAs_2$ – $CdGeAs_2$ system.*

solutions, the $ZnGeAs_2$-$CdGeAs_2$ system was studied. The results were unexpected [32, 33]. Despite the proximity of the crystal structures of compounds, the formation of solid solutions between them occurs in narrow boundaries (**Fig. 3**) with a large decay region. Therefore, magnetic field measurements were performed on alloys of solid solutions with a composition close to the compositions of $ZnGeAs_2$ and $CdGeAs_2$ compounds. The nature of the change in resistance (**Fig.** 4) from the magnetic field, as in the case of solid solutions from the side of $ZnGeAs_2$, and from the side of $CdGeAs_2$ did not change, but the magnitude of the effects decreased, as if their convergence occurred. The different type of change in resistance from the magnetic field for composite alloys $ZnGeAs_2$ and $CdGeAs_2$ with MnAs corresponds to the difference in the microstructures of their eutectic eutectics. In the first case, it is lamellar; in the second, needle-like, a form effect is observed. The needle-like view of the granular structure of $CdGeAs_2$ with MnAs is a classical solenoid, which leads either to the appearance of percolation processes or to the formation of a complex spin-valve structure. In both cases, a positive effect of magnetoresistance is possible [34, 35].

The interesting results were obtained on granular structures of alloys of the Ga(In) Sb–MnSb systems. Of greatest interest were the data of the magnetoresistance of granular

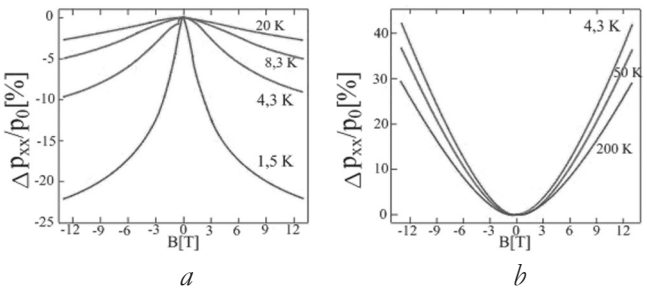

Fig. 4. *Magnetic field/ resistance dependence for alloys: a) $Zn_{1-x}Cd_xGeAs_2$ c MnAs, b) $Cd_{1-x}Zn_xGeAs_2$ c MnAs.*

structures. The average size of ferromagnetic MnSb clusters in granular structures was 24 nm [36-40]. **Fig. 5** presents the temperature dependence of the magnetization of the eutectic alloy of the GaSb-MnSb system. The Curie temperature ~ 600 K was determined by the MnSb clusters. The dependence of resistance in a magnetic field had a complex form. At small values of the magnetic field (up to a saturation of 0.8 *T*), the resistance dropped sharply, and at large values it grew slowly. At low magnetic fields, negative magnetoresistance was observed, and at high magnetic fields, which was observed both at low temperatures of 5 K and at room 300 K (**Fig. 6**). The same type of change in resistance from the magnetic field was observed by A. Fert and P. Grünberg when the GMR effect was discovered [5, 6]. The change in the mechanism of charge carrier scattering occurs due to the fact that at low magnetic fields

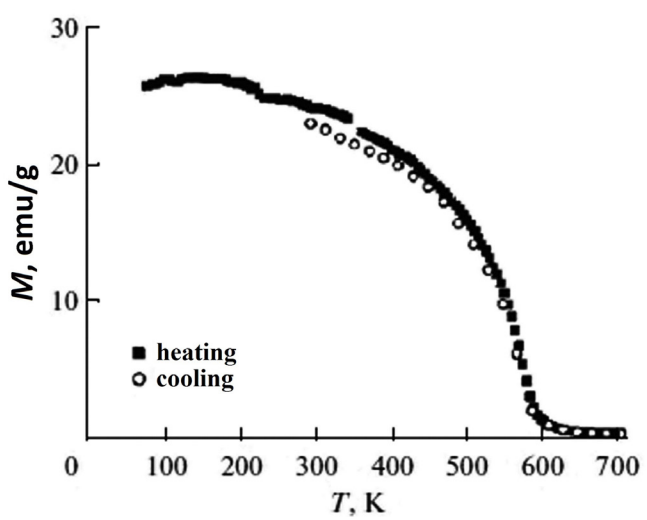

Fig. 5. *Temperature dependence of the specific magnetization for eutectic alloy of GaSb + MnSb system at B = 0.1 T.*

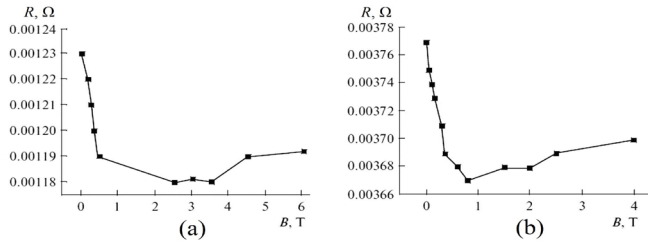

Fig. 6. *Magnetic field's magenetude/resistance dependence of the GaSb + MnSb granular structure at T = 5 (a) u 300 K (b).*

up to saturation, scattering associated with the spin-dependent effect predominates, and at high magnetic fields, the resistance changes due to the Lorentz force. The change in resistance is insignificant in magnetic fields above saturation, but it is positive. Using pulsed laser deposition, using composite alloys of eutectics of the GaSb-MnSb and InSb-MnSb systems as a target, films were obtained. GaSb films with MnSb were synthesized on leucosapphire substrates, the film thickness was 80-100 nm. According to electron and atomic force microscopy data, the films were homogeneous [38, 41]. The electrical conditions of deposition largely influenced their electrical properties. The best samples had a hole type with a specific resistance of $7 \cdot 10^{19}$ cm^{-3} at 300 K. The dependences of the specific magnetization and resistance on the magnetic field are presented in **Fig. 7***a,b* respectively. The type of change in film resistance coincided qualitatively with bulk samples (Fig. 6). There was only a difference in the magnitude of the saturation magnetic field. In films, it is lower than ~ 0.2 *T*, and in bulk samples it was ~ 0.8 *T*.

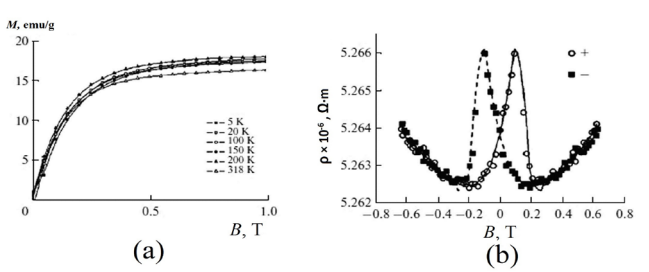

Fig. 7. *Specific magnetization (a) and the specific resistance (b) magnetic field dependences for GaSb + MnSb structure's film.*

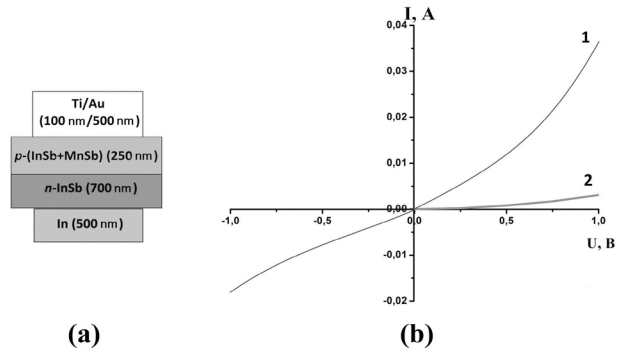

Fig. 8. *a) Pattern for diode structure; b) (volt-current plot) of the p-(96%InSb+4%MnSb)/n-InSb diode structure at 300 K (1 - B = 0 T and 2 - B = 0.15 T).*

Films of the InSb + MnSb composite with hole type conductivity were formed on single-crystal n-type InSb substrates by pulsed laser deposition and diode structures were formed [42, 43]. **Fig. 8***a* shows the formation of these diode structures, Fig. 8*b* shows the current-voltage characteristic (VAC) of the *p*-(96% InSb + 4% MnSb)/*n*-InSb diode structure at 300 K: 1 - *B* = 0 *T*; 3 - *B* = 0.15 *T* in the perpendicular field of the heterojunction plane.

Diodes based on this granular structure showed high sensitivity to a magnetic field. The magnitude of the current in a magnetic field of 0.15 *T*, applied perpendicular to the plane of the diode structure, decreased more than 9 times from 0.35 A to 0.04 A at a voltage of 1 *V*.

4. CONCLUSION

It is shown that the use of semiconductors as a matrix of magnetically granulated structures due to the high mobility of charge carriers is preferable to metals or dielectrics. The basic principles of creating granular structures with high values of magnetoresistance based on eutectic type systems are formulated. During eutectic crystallization, simultaneous crystallization of all phases takes place, and a specific fine-dispersed structure of eutectic alloys is formed. The use of ultra-high supersaturation leads to metastable crystallization, which causes a synergistic effect leading to nanostructuring, which is necessary when creating granular structures.

ACKNOLEDJMENTS

The work was performed as part of the state assignment of the Institute of General and Inorganic Chemistry of the Russian Academy of Sciences in the field of fundamental scientific research (subject No. 0088-2014-0003) with partial support from the Presidium of the Russian Academy of Sciences I.35 program "Scientific Foundations for Creating New Functional Materials" and the RFBR No. 16-03-00150.

REFERENCES

1. Iqbal MZ, Qureshi NA, Hussain G. Recent advancements in 2D-materials interface based magnetic junctions for spintronics. *Magn. Magn. Mater.*, 2018, 457:110-125.
2. Van Dorpe P, Liu Z, Roy WV, Motsnyi VF, Sawicki M, Borghs G, De Boeck J. Very high spin polarization in GaAs by injection from a (Ga, Mn)As Zener diode. *Appl. Phys. Lett.*, 2004, 84:3495-3497.
3. Fert A. Proiskhozhdenie, razvitie i perspektivy spintroniki [The origin, development and prospects of spintronics]. *UFN*, 2008, 178(12):1336-1348 (in Russ).
4. Ognev AV, Samardak AS, Vorob'ev YuD, Chebotkevich LA. Magnitnaya anizotropiya Co/Cu/Co plenok s kosvennoy obmennoy svyaz'yu [Magnetic anisotropy of Co/Cu/Co films with indirect exchange coupling]. Fizika tverdogo tela [Solid State Phisics], 2004, 46(6):1054-1057 (in Russ.).
5. Baibich MN, Broto JM, Fert A, Nguyen Van Dau F, Petroff F, Etienne P, Creuzet G, Friederich A, Chazelas J. Giant Magnetoresistance of (001)Fe/(001)Cr Magnetic Superlattices. *Phys. Rev. Lett.*, 1988. 61:2472-2475.
6. Grünberg P, Schreiber R, Pang Y, Brodsky MB, Sowers H. Layered Magnetic Structures: Evidence for Antiferromagnetic Coupling of Fe Layers Across Cr Interlayers. *J. Appl. Phys.*, 1987, 61(8):3750-3752.
7. Xiong P, Xiao G, Wang JQ, Xiao JQ, Jiang JS, Chien CL. Extraordinary Hall effect and Giant Magnetoresistance in the Granular Co-Ag System. *Phys. Rev. Lett.,* 1992, 69:3220-3223.
8. Berkowitz AE, Mitchell JR, Carey MJ, Young AP, Rao D, Starr A, Zhang S, Spada FE, Parker FT, Hutten A, Thomas G. Giant magnetoresistance in heterogeneous Cu-Co and Ag-Co alloy films. *J.Appl.Phys.*, 1993, 73(10):5320-5325.
9. Chien CL, Xiao JQ, Jiang JS. Giant negative magnetoresistance in granular ferromagnetic systems (invited). *J. Appl. Phys.*, 1993, 73(10):5309-5314.
10. Milner A, Gerber A, Groisman B. Spin-dependent electronic transport in granular ferromagnets. *Phys.Rev.Lett.,* 1996, 76(3):475-478.
11. Dubiel B, Wolf D, Czyrska-Filemonowicz A. TEM and electron holography analyses of granular and thin layered Cu–Co magnetic materials. *Ultramicroscopy*, 2010, 110 (5):433-437.
12. Polyakov VV, Polyakova KP, Seredkin VA, Patrin GS. Magneto–Optical Kerr Effect Enhancement in Co-Ti-O Nanocomposite Films. *Solid State Phenomena*, 2012, 190:506-509.
13. Aronzon BA, Kovalev DYu, Varfolomeev AE, Likal'ter AA, Ryl'kov VV, Sedova MA. Conductivity, magnetoresistance, and the hall effect in granular Fe/SiO_2 films. *Phys. Solid State*, 1999, 41(6):857-863.
14. Oksuzoglu RM, Elmali A, Weirich TE, Fuess H, Hahn H. Evolution of the surface roughness (dynamic scaling) and microstructure of sputter-deposited $Ag_{75}Co_{25}$ granular films. *J. Phys. Condens. Matter.*, 2000, 12:9237–9245.
15. Du J, Zhang B, Zheng RK, Zhang XX. Memory effect and spin-glass-like behavior in Co-Ag granular films. *Phys. Rev. B.*, 2007, 75:14415.
16. Socolovsky LM, Denardin JC, Brandl AL, Knobel M. Magnetotransport, magnetic, and structural properties of TM–SiO_2 (TM = Fe,

Co, Ni) granular alloys. *Mater.Charact.*, 2003, 50:117-121.
17. Yarzhemsky VG, Murashov SV, Izotov AD. Electronic structure and exchange interaction in the magnetic semiconductors $Ga_{1-x}Mn_xAs$ and $In_{1-x}Mn_xAs$. *Inorganic Materials,* 2016, 52(2): 89-93.
18. Yarzhemsky VG, Murashov SV, Izotov AD. Calculation of the electronic structure and exchange interaction in the InSb and GaAs semiconductors codoped with Mn and Ni. *Inorganic Materials*, 2017, 53(11):1131-1135.
19. Wang CZ, Zhang P, Zheng L, Xiao X, Rong Y. Influence of annealing on microstructure and magnetic-transport of FeCo–Al_2O_3 nanogranular films. *Thin Solid Films*, 2008, 516:3422-3430.
20. Ognev AV, Samardak AS, Vorob'ev YuD, Chebotkevich LA. Structure and magnetic anisotropy of Co/Cu/Co films. *Phys. Solid State*, 2004, 46(8):1490-1495.
21. Pashkova ON, Izotov AD, Sanygin VP, Filatov AV. Ferromagnetism of GaSb (2% Mn) alloy. *Russian Journal of Inorganic Chemistry*, 2014, 59(11):1324-1327.
22. Novotortsev VM, Kochura AV, Marenkin SF. New ferromagnetic based on manganese-alloyed chalcopyrites $A^{II}B^{IV}C^{V}_2$. I*norganic Materials*, 2010, 46(13):1421-1433.
23. Pashkova ON, Izotov AD, Sanygin VP, Filatov AV. Cluster magnetism in doped InSb. *Russian Journal of Inorganic Chemistry,* 2014, 59(7):689-692.
24. Marenkin SF, Izotov AD, Fedorchenko IV, Novotortsev VM. Sintez magnitogranulirovannykh struktur v sistemakh poluprovodnik-ferromagnetik [Synthesis of magnetically granulated structures in semiconductor – ferromagnet systems]. *Zhurnal neorganicheskoi khimii* 2015, 60(3):343-348 (in Russ.).
25. Motizuki K, Ido H, Itoh T, Morifuji M. *Electronic Structure and Magnetism of 3d-Transition Metal Pnictides.* Springer Series in Materials Science. Springer-Verlag Berlin Heidelberg, 2009, 148 p.
26. Reis MS, Rubinger RM, Sobolev NA, Valente MA, Yamada K, Sato K, Todate Y, Bouravleuv A, von Ranke PJ, Gama S. Influence of the strong magnetocrystalline anisotropy on the magnetocaloric properties of MnP single crystal. *Phys. Rev. B.*, 2008, 77:1044391-1044398.
27. Marenkin SF, Kochura AV, Fedorchenko IV, Izotov AD, Vasil'ev MG, Trukhan VM, Shelkovaya TV, Novodvorsky OA, Zheludkevich AL. Growth of eutectic composites in the InSb-MnSb system. *Inorganic Materials*, 2016, 52(3):268-273.
28. Marenkin SF, Trukhan VM, Trukhanov SV, Fedorchenko IV, Novotortsev VM. Phase equilibria and electrical and magnetic properties of a eutectic in the GaSb-MnSb system. *Russ. J. Inorg. Chem.*, 2013, 58(11):1324-1329.
29. Zeldovich YaB. *Izbrannye trudy. Khimicheskaya fizika i gidrodinamika* [Selected Works. Chemical physics and hydrodynamics]. Moscow, Nauka Publ., 1984, 374 p.
30. Krapuhin VV, Sokolov IA, Kuznetsov GD. *The technology of electronic materials.* Moscow, MISiS, 1995, 493 p.
31. Marenkin SF, Aronov AN, Fedorchenko IV, Zheludkevich AL, Khoroshilov AV, Kozlov VV. *Inoranic Materials,* 2018, 54(12): [in press].
32. Marenkin SF, Aronov AN, Trukhan VM, Shelkovaya TV, Fedorchenko IV, Domuchovski V, Lahderanta E. Phase Equilibria in the $ZnGeAs_2$–$CdGeAs_2$ System. *Russian Journal of Inorganic Chemistry,* 2014, 59(2):126-129.
33. Fedorchenko IV, Aronov AN, Kilanski L, Domukhovski V, Reszka A, Kowalski BJ, Lahderanta E, Dobrowolski W, Izotov AD, Marenkin SF. Homogeneous limit of $Cd_{1-x}Mn_xGeAs_2$ alloy: Electrical and magnetic propertie. *J. Alloys Comp.*, 2014, 599:121-126.
34. Svalov AV, Savin PA, Kurlyandskaya GV, Gutiérrez J, Vas'kovskiy VO. Spin-valve

magnetoresistive structures based on Co/Tb multilayer films. *J. Tekhn. Phys*., 2002, 47(8):987-990.

35. Gidnev SA, Kalinin YU, Sitnik AV, Stogney OB. *Nelineinye yavleniya v nano I microgeterogennih sistemah* [Nonlinear phenomena in nano and microheterogeneous systems]. Moscow, Binom, Laboratoriya znanyi Publ., 2012, 352 p.
36. Kochura AV, Aronzon BA, Lisunov KG, Lashkul AV, Sidorenko AA, De Renzi R,. Marenkin SF, Alam M, Kuzmenko AP, Lähderanta E. Structural and magnetic properties of $In_{1-x}Mn_xSb$: Effect of Mn complexes and MnSb nanoprecipitates. *J. Appl.Phys*., 2013, 113:083905.
37. Novotortsev VM, Kochura AV, Marenkin SF, Fedorchenko IV, Drogunov SV, Lashkul A, Lähderanta E. Synthesis and magnetic properties of the InSb-MnSb eutectic. *Russ. J. Inorg. Chem*., 2011, 56(12):1951-1956.
38. Marenkin SF, Novodvorsky OA, Shorokhova AV, Davydov AB, Aronzon BA, Kochura AV, Fedorchenko IV, Khramova OD, Timofeev AV. Growth of magnetic eutectic GaSb-MnSb films by pulsed laser deposition. *Inorganic Materials,* 2014, 50(9):897-902.
39. Novotortsev VM, Zakharov IS, Kochura AV, Marenkin SF, Laiho R, Lahderanta E, Lashkul A, Veresov AG, Molchanov AV, Yur'ev GS. Ferromagnetism of manganese-doped InSb alloys. *Russ. J. Inorg. Chem*., 2006, 51(10):1627-1631.
40. Rabinovich O, Legotin S, Didenko S, Yakimov E, Osipov Yu, Fedorchenko I. Heterostructure optimization for increasing LED efficiency. *Japanese Journal of Applied Physics,* 2016, 55:05FJ131-05FJ134.
41. Marenkin SF, Novodvorsky OA, Baranov VV, Trukhan VM, Shoukavaya TV, Struts AM. The synthesis, electric and magnetic properties of films with eftectic composition of GaSb-MnSb system. *Reports of the Belarusian State University of Informatics and Radioelectronics.* Minsk, Belarusian State University of Informatics and Radioelectronics Publ., 2016, 5(99):5-10.
42. Khramova OD, Mikhalevsky VA, Parshina LS, Novodvorsky OA, Marenkin SF, Lotin AA, Cherebilo EA, Aronzon BA, Aronov AN, Panchenko VYa. Effect of magnetic field on the voltage-current characteristic of the *p*-(InSb+MnSb)/*n*-InSb diode structure. *Opt. Quant. Electron*., 2016, 48(7):361.
43. Mikhalevsky VA, Novodvorsky OA, Parshina LS, Khramova OD, Lotin AA, Cherebylo EA, Marenkin SF, Aronov AN, Kochura AV, Aronzon BA, Panchenko VYA. Magnetoresistance in InSb:Mn-InSb p-n junction at room temperature. *Moscow International Symposium on Magnetism*, 1-5 July, 2017, 494.
44. Marenkin SF, Fedorchenko IV, Trukhan VM, Trukhanov SV, Shoukavaya TV, Vasil'Ev PN, Zhaludkevich AL. State diagram of the Zn_3As_2-MnAs system. *Russ. J. Inorg. Chem*., 2015, 60(3):1578-1582.
45. Marenkin SF, Ril AI, Fedorchenko IV. Phase diagram of $ZnAs_2$–MnAs system. *Mendeleev Commun*., 2018, 28(2):219-221.

ON THE CHEMICAL STABILITY OF THE STRUCTURE AND PHYSICAL CHARACTERISTICS OF THE HIGH-TEMPERATURE SPINTRONIC COMPOSITE EuO:Fe UNDER NORMAL CONDITIONS

Arnold S. Borukhovich

Russian State Vocational Pedagogical University, http://www.rsvpu.ru/
Yekaterinburg 620083, Russian Federation

Vitaly G. Bamburov

Solid State Chemistry Institute of Ural Division of RAS, http://www.ihim.uran.ru/
Yekaterinburg 620990, Russian Federation

a.borukhovich@gmail.com, bam@ihim.uran.ru

Abstract. **The possibility of forming a limited solid solution $Eu_{1-x}Fe_xO$ in the structure of a spintronic composite material EuO:Fe obtained by the high-temperature solid-phase reduction method of a mixture of higher metal oxides is discussed. Its prevailing role in the formation of outstanding physical properties of this composite as a high-temperature spin injector is described from experimental and theoretical data.**

Keywords: **europium monoxide; solid solution; ferromagnetism; super paramagnetic; nanoparticles; NMR (Mössbauer effect); magnetization; spintronics**

UDC 548.4;548.73;548.735.6

Bibliography - 18 references

Received May 30, 2018; accepted Juni 28, 2018

RENSIT, 2018, 10(3):403-410

DOI: 10.17725/rensit.2018.10.403

Contents

1. INTRODUCTION

It is considered [1] that metallic iron does not dissolve in europium monoxide and does not form an independent crystalline phase with it as a solid solution (SS) $Eu_{1-x}Fe_xO$. However, this does not mean that such SSs are not able to originate at least partially or in limited regions of compositions in more complex multiphase composites containing europium and iron oxides. In particular, in the spintronic composite material synthesized from higher oxides of europium (Eu_2O_3) and iron (Fe_2O_3) by the high-temperature solid-phase reduction method [2]. It has been experimentally confirmed [3] that several more independent crystalline phases co-exist in such composite in addition to the above-mentioned SS: from nano sized super paramagnetic particles of metallic iron to oxides of both metals in different oxidation states. However, it is the presence of this SS that determines the outstanding physical characteristics of this composite - its high specific magnetization (40-60 emu/g at room temperatures, Tr) and the Curie temperature, T_c = 480 K. Under the conditions of its inherent semiconductor conductivity at the range of compositions $0.15 < x < 0.25$, this composite material is promising in the creation of semiconductor spintronic devices capable of stable operation at the room temperature, while ensuring an increased degree of spin current transfer, P ≈60% [4]. To the latter in a great extent contributes the chemical stability of this composite, located both in bulk and

in thin-film states in normal environmental conditions. This is evidenced by the complete identity of the experimental data obtained on samples of different synthesis series after long (several years) time intervals of their storage. The data are presented below.

2. EXPERIMENTAL DATA

In support of the above, we present the results of the experimental studies of resonance (nuclear magnetic resonance, NGR) and magnetic parameters of this composite, according to data from [5, 6]. Moreover, NGR spectroscopy of composite samples was studied using a standard SM-2201 spectrometer with ^{57}Fe and $^{151}Sm_2O_3$ sources. Their magnetic parameter at low temperatures was studied on a SQUID magnetometer of MPHS-XL7 type, and at elevated temperatures - on a magnetic balance using the Faraday method.

Thus, the spectra of nuclear magnetic resonance (or the Mössbauer effect) of a bulk sample of the EuO:Fe composite for the ^{57}Fe isotope, taken at room temperature are presented in **Fig. 1**. It's characterized by a typical ferromagnetism and contain at least two sixes of Zeeman lines: one with H_{eff} = 32.8Tl, δ = 0, ΔE = 0, the other with H_{eff} = 19.2Tl, δ = +0.20 mm/s, ΔE = 0.005 mm/s.

They relate to α-Fe nanoparticles and Eu-Fe-O clusters, respectively. The relative intensity of the sextets I(α-Fe) ≈ 0.72; I(Eu-Fe-O) ≈ 0.28. From which it may be concluded that the presence of iron in the composite, basically, corresponds to its free (metallic) state. The fraction of ferromagnetic clusters in it is much smaller, which agrees with the impossibility of formation of solid substitution solutions of Eu on Fe at the EuO lattice. The display of the ionic state of iron in the composite should be considered as impurity centers forming Eu-Fe-O clusters as a result of a possible chemical interaction of them with an europium cations at accordance by the mechanism of indirect *d-f*-exchange [7].

In the same conditions the Mössbauer spectra of ^{57}Fe of the composite films (**Fig. 2**) represent a singlet with an isomeric shift of δ = +0.20 mm/s and with a very weak splitting, typical for the display of super paramagnets of α-Fe nano particles. This data exemplifies that the high-temperature magnetism of the composite is caused by the presence of the ferromagnetic ordering of Eu-Fe-O clusters and super paramagnetic α-Fe nanoparticles in it. As shown below, this is fully confirmed by magnetic studies of the composite.

The cation state of the europium atoms in the composite illustrates the NGR spectrum of ^{151}Eu, **Fig. 3**. It is an overlap of two lines characterized by isomeric shifts of δ = 12.6 mm/s and δ = +0.02 mm/s, and width at half height of 3.7 mm/s and 4.1 mm/s, respectively. The

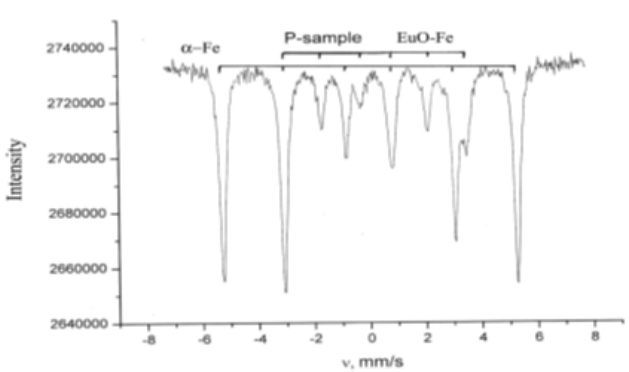

Fig. 1. *NGR spectra of ^{57}Fe powder of the EuO:Fe composite at room temperature.*

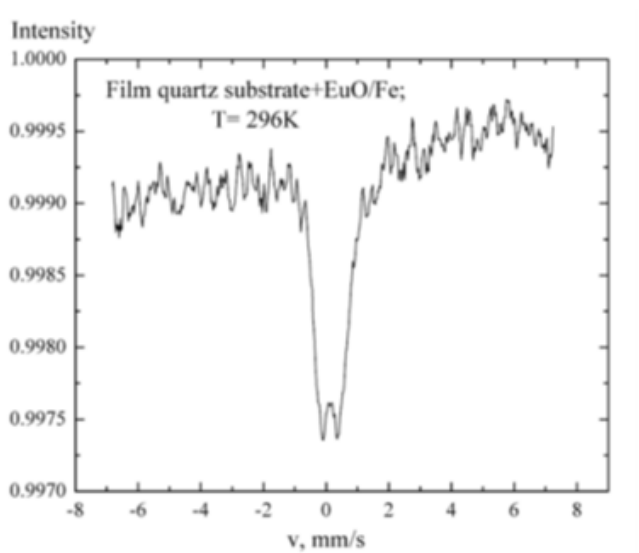

Fig. 2. *Mössbauer spectra of ^{57}Fe thin films of a composite on Quartz.*

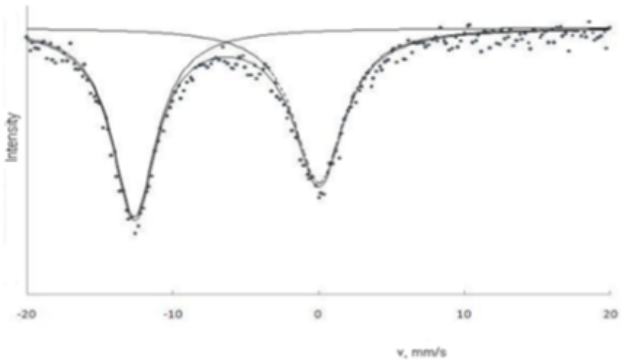

Fig. 3. *The Mossbauer spectrum of ^{151}Eu powder of the composite at room temperature.*

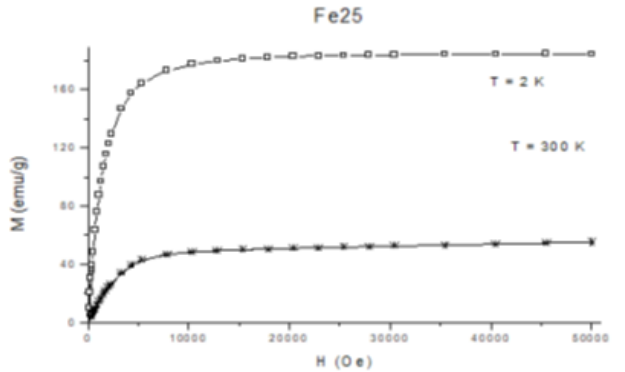

Fig. 4. *Dependence of the magnetic saturation moment of the $(EuO)_{0.75}Fe_{0.25}$ composite by H.*

first line corresponds to the paramagnetic ion of the Eu^{2+} matrix; the second line is responsible for the manifestation of the valence state of Eu^{3+}. Note that such isomeric shifts of NGR spectra of ^{151}Eu at the composite correspond to the positions of these cations in the lattices of EuO and Eu_2O_3 [8]. The obtained spectra and the position of the isomeric shifts of the Eu^{2+} and Eu^{3+} ions in them agree well with the NGR investigation of the micro crystals of the magnetic semiconductor EuS interspersed in thin films of the TiO_2, Al_2O_3 and SiO_2 oxides [9].

The presence of Eu^{3+} ions in the composite, on the one hand, can be considered as an impurity phase of Eu_2O_3 due to the conditions of its synthesis – high temperature reduction of a sesquioxide or a mixture (Eu_2O_3 + Fe_2O_3) by carbon. Based on the results of chemical and X-ray spectral analysis, the presence of this phase in the composite did not exceed 1% by weight.

On the other hand, comparison of state line intensities of the Eu^{3+} ions (~0.55) in the spectrum with that for the ion state Eu^{2+} (~ 0.45) may indicate the appearance in the composite of some "inductive" effect associated with the effect of iron atoms on the electron density on ^{151}Eu nuclei. This, as noted above, can correspond to the manifestation of an indirect (via the *p*-state of oxygen) *d-f* exchange between iron and europium to form Eu-Fe-O clusters. A possible transfer of the electron density from Eu^{2+} to the iron (even partial) will lead to the polarization of the spins of these ions, which under these conditions is equivalent to the manifestation of their ionic state in the cluster as Eu^{3+}, and the states of the iron ion as Fe^{+}. As a result, the ferromagnetic moment of such an $Eu^{3+}Fe^{+}O$ cluster at T > 70 K (the temperature of the ferromagnetic disordering of the EuO phase) caused by the spin polarization of the paramagnetic europium ions from the nearest environment of the impurity Fe^{+} ion and localized on might become increased comparing to magnetic moment of atomic iron.

Let us now analyze the magnetic characteristics of the samples of the composite, measured for a wide range of temperatures and magnitudes of the external magnetic field. **Fig. 4** shows the field dependence from the ferromagnetic saturation moment $M(H)$ of a composite composition $(EuO)_{0.75}Fe_{0.25}$ at T = 2 K and T = 300 K, and in **Fig. 5** (a, b) its temperature dependences, $M(T)$.

From these data, it follows that the composite is actually a heterogeneous mixture at least of three ferromagnetic ally ordered phases. In this case, the value of the magnetization of the

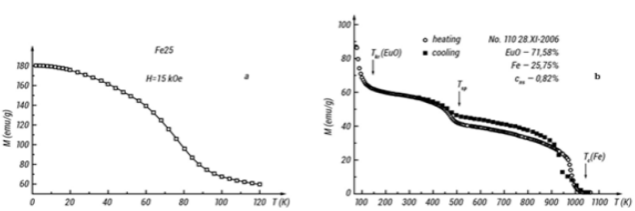

Fig. 5. *Temperature dependences of the magnetization of a composite at low (a) and elevated temperatures (b).*

Fe-component for this concentration range almost linearly corresponds to its share presence in the composite [2].

At the room temperature, the ferromagnetic saturation moment of this composition composite is close to the value of $M \approx 60$ emu/g, which completely corresponds to the Fe-component, although it exceeds it in absolute terms by approximately 10÷15 units. At low temperatures the ferromagnetic moment predominates mainly due to the contribution of the divalent europium ion in the composite against which the contribution of iron to M is ≤ 30%. Throughout the temperature range the samples of the composite exhibit the properties of magnetically soft ferromagnetism. A feature of the $M(T)$ dependence in Fig. 5(b) is its inflection in the region of $T \approx 480$ K which is characteristic of the ferromagnetic disordering of the magneto-structural phase. If a transition of the "ferro-para" of the EuO phase takes place in the region of $T \approx 70$ K, and a similar for the Fe-component of the composite observed at $T \approx 1000$ K, then a certain ferromagnetic (super paramagnetic) constituent (i.e., ferromagnetic phase) of the composite must undergo a disorder in the above temperature range. It should be responsible for the increased value of its specific magnetization (magnetic saturation moment) at the room temperature range and above (up to 480 K). As follows from the above NMR-spectra of a composite, such a ferromagnetically ordered structural phase can only be the presence of a cluster (solid solution) of $Eu^{3+}Fe^{+}O$ with a Curie temperature in it, $T_c = 480$ K.

The behavior of the magnetization of the composite films received "flash technique" in the way [3], correlates well with the data in Fig. 5 - the characteristic features of the $M(T)$ dependences also appear in the films. Their magnetization reversal curve under normal conditions in the easy direction is close to rectangular, saturation is achieved in fields of $H \approx 0.5$Tl. However, the opening of the hysteresis loop is not observed. The magnitude of the magnetic moment of the composite thus reaches $M \approx 4\mu_B$ and correlates in these conditions with magnetically active Fe-centers in it. This value of M exceeds the characteristic value of the magnetic moment of pure iron almost by ≈20%, which completely corresponds to the contribution made to it from the environment of the paramagnetic moments of europium ions.

At the same time, studies of the $M(T)$ dependence upon cooling of the composite films at low temperatures in an external magnetic field (the FC condition) and without a field ($H = 0$, the ZFC condition) revealed another feature. Namely, the presence of an inflection of this dependence in the temperature region of $T = 25÷30$ K (**Fig. 6**) in the latter case. This so-called "blocking temperature" (T_{bl}) - is the transition from the anti ferromagnetically ordered state (at $T < T_{bl}$) to super paramagnetic (at $T > T_{bl}$) of α-iron nanoparticles in the composite. Physically this means that the magnetic moments of such nanoparticles at $T \leq T_{bl}$ are anti ferromagnetically in relation to ferromagnetically ordered state of the ions of the Eu^{2+} matrix. This leads to a general decrease in the magnetic moment of the composite at $T = 0$ K to a value of $M = 180$ emu/g. For comparison: under the same conditions, "pure" EuO monoxide has a record value of $M = 240$ emu/g for ferromagnets. However, at $T > T_{bl}$, the situation changes to the directly opposite – super paramagnetic of α-Fe nanoparticles

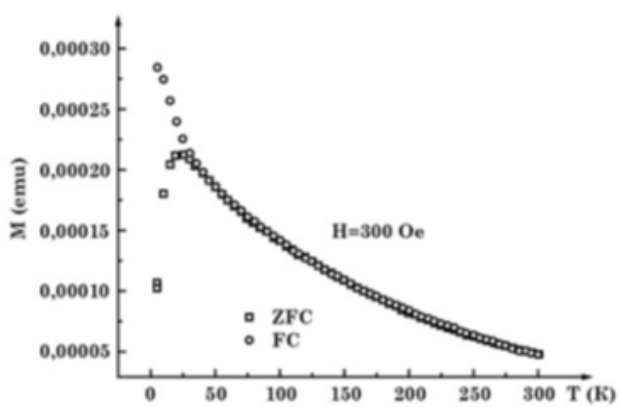

Fig. 6. *The magnetization of the $(EuO)_{0.75}Fe_{0.25}$ composite film on a silicon substrate under conditions of ZFC and FC.*

promotes the growth of the magnetic moment of the EuO:Fe cluster (solid solution) in the composite with decreasing magnetization and disordering of the Eu^{2+} cations of the matrix. According to the magnetic data presented, the total ferromagnetic moment of such a cluster (solid solution) at room temperature is numerically more than 10 emu/g exceeding the ferromagnetic moment inherent in pure iron at these temperatures. Due to this, in general, taking into account a last parameter, this composite is the record among all known ferromagnetic materials, especially semiconductor materials, which are recommended for spintronics. When using a composite as a spin injector, these qualities will, in particular, contribute to an increase of the degree of spin current transfer in spintronic structures created with his participation [4].

3. THEORY

For a possible theoretical justification and understanding of the regularities behavior of the EuO:Fe composite experimental parameters, a model calculation of the electronic band structure of the $Eu_{1-x}Fe_xO$ solid solution, which is structurally included at the composite composition, was performed [10]. The calculation method included the use of the linear method of associated plane waves (FLAPW, code WIEN2k) with the generalized gradient approximation (GGA) of the exchange-correlation potential [11]. In recent years, a similar calculation method has been applied to the EuO and a EuS phase doped with rare earth metals and provides good correlation with experiment [12, 13]. At the calculations a super lattice, obtained by translating the unit cell of EuO along the crystallographic axes when one of the europium cations is replaced by an iron ion, was constructed. Without going into here, especially in carrying out such calculations of systems with strongly correlated electrons, such as Europium compounds, and performing certain corrections of the band-state spectrum [14], we will analyze only the results of the theoretically modeling of the band states density of iron-doped europium oxide, indicating their good agreement with the above experimental data presented. These results are illustrated in **Fig. 7**, where along with the final picture of the spectrum of the solid solution, the partial density of the electronic 3d states of iron is allocated.

It follows that zone states formed mainly by the 2*p* orbitals of oxygen atoms are located below the energies -2eV, whereas at states above 0.5 eV there are band states formed by the 5*d* orbital's of europium atoms (the energy of states is relative to the Fermi level). The band states formed by the 4*f*-orbitals of europium are situated at the near Fermi region. Wherein the activation energy of the conductivity, ΔE, between the Fermi level near the 4f-zone ceiling and the bottom of the 5*d* band is 0.8 eV, which agrees well with the experimental value of ΔE = 0.75 eV [3]. Also the calculations reproduce well the interval between the maxima of the 2*p* O- and 4*f* Eu-states, equal to 2.5 eV [15].

The most significant changes in the spectrum of the EuO band states when doped with iron are the appearance of two bands of states with a positive spin-up direction at the energy near -6 eV and one band with a negative spin down direction at Fermi level. The magnetic moments values obtained on Fe ions were 3.74 μ_B, and on Eu^{2+} cations, they were from 6.86 to 6.88 μ_B. To explain these values, we consider the partial density of the 3*d* states of iron atoms

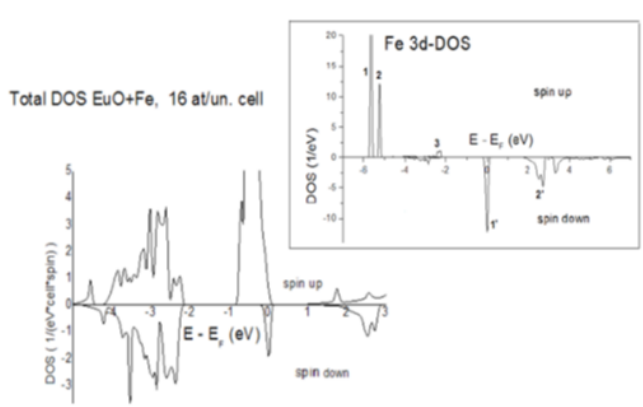

Fig. 7. *The density of electronic states of TP $Eu_{1-x}Fe_xO$ with the separation of the partial density of the electronic 3d-states of iron.*

which additively enters the band spectrum of this SS. The bands of spin-up band states noted on Fig. 7 by the numerals 1 and 2 have the type of local symmetry t_{2g} and e_g and contain 3+2 electrons. Another peak of the density of 3*d* Fe- states (peak 3) is located at the top of the valence 2*p* O - band, but it is a consequence of the hybridization of 2*p* O- and 3*d* Fe - states. Band 1' corresponds to spin down 3*d* Fe-states with e_g-type local symmetry: it contains one electron. Band 2'corresponds to the empty zone of spin-down 3d Fe states. It follows that the iron ions in the monoxide structure retain 6 electrons, i.e. they are in the charge state 2^+ and will have a magnetic moment equal to 4 μ_B which corresponds to the data given above. The spin up band of the 4*f*-states in the near Fermi region contains ~ 7 electrons, i.e., the magnetic moment of the Eu atoms is ~ 7 μ_B, which also corresponds to the values given above.

The reason for the presence of large magnetic moments on iron atoms is a large exchange splitting of the states of iron ions – at around 5 eV (Fig. 7), so that the majority of spin-down states of iron are not populated by electrons. As a result, the magnetic moment on Fe^{2+} cations is ~1.7μ_B higher than the magnetic moment of pure iron. Accordingly, at room temperature, the numerical value of the saturation magnetization of the composite due to doping reaches values of 40÷60 emu/g [2]. Since the 3*d* orbitals of iron are much less localized in space than the 4*f* states of europium, the appearance of iron atoms in the structure of the monoxide leads to an increase in the exchange interaction between the *f*- and *d*-cations and, as a consequence, to an increase in the Curie temperature of the composite. Note also that in the energy range from about 0.9 to 1.3 eV, i.e., near the bottom of the conduction band, there are no spin-down band states. This may mean that even in the presence of iron atoms a 100% spin polarization of the charge carriers is possible what corresponds to the previously indicated values of the spin polarization *P* in pure EuO [16]. Thus, the existence of a ferromagnetically ordered phase in the form of a similar SS in the EuO:Fe composite is completely responsible for the experimental observation in it at room temperature of a record-breaking degree of spin current transfer.

Let us also trace the possible correspondence of the performed calculation of the band spectrum of the solid solution to the electronic parameters of the composite, related to the manifestations of its other structural components. First, this concerns the data of the NGR-studies of the composite and the possibility of carrying out in it an "induction" effect - transfer of the electron density from Eu^{2+} ions to impurity ions Fe^{2+} introduced in the matrix lattice. The presence of such a transfer, which can be interpreted as the transition of a part of the europium ions Eu^{2+} to the Eu^{3+} state, and some iron ions to the Fe^+ state, does not contradict the results of calculations of the electronic band structure of the solid solution, although they do not directly follow from them. Approximately 0.03 of the 4*f*-states (per europium atom) remain empty. On the other hand, it can be noted that the band of 3*d*-states of iron (with a negative value of the spin projection, spin-down) is asymmetric relative to the Fermi level. I.e., the number of states occupied by electrons (to the left of the Fermi energy) is somewhat larger (their zeroing corresponds to an energy of -0.15 eV) than the number of empty states in this zone (to the right of the Fermi energy, zeroing at 0.1 eV). Both of these circumstances indicate that there is actually a slight transfer of the electron density from the 4*f* Eu^{2+} state to the 3*d* Fe^{2+} state (about 0.03 electron per impurity Fe-node).

These calculations, like the vast majority of similar calculations by the methods of the electron density functional theory, correspond to the temperature of $T = 0$ K. Obviously, a certain "smearing" of the Fermi level with an increase in the temperature can be accompanied by a somewhat higher transfer of the electron density from 4*f* Eu- states to 3*d* Fe-states wherein.

The second example concerns the experimental data of Fig. 6 – the presence of a "blocking" temperature – the spin reorientation of the magnetic moments of free iron nanoparticles in the composite structure and its transition from an antiferromagnetic to a superparamagnetic state at $T > 25$ K. Such a spin reorientation is in many ways analogous to spin-orientation transitions in rare-earth metals observed at low temperatures [17]. Nevertheless, the very indication of the theory of the antiparallelity of the spins of iron nanoparticles at the SS with respect to the spin state of the Eu^{2+} - cations at T = 0 K implies the presence of T_{bl} at $T > 0$ K. What also can be attributed to the merit of these calculations.

4. CONCLUSION

Thus, the comparison of the calculation results of electronic band structure of the $Eu_{1-x}Fe_xO$ SS with the experimental data of the EuO:Fe spintronic composite, which is one of its structural constituents, is indicative of both surprisingly good agreement between each other and a correct and justified choice of theoretical model for doping a monoxide lattice, and the method used at calculating its electronic band structure. It is shown that the presence of this SS in the composite provides its elevated Curie temperature. At the same time, iron cations are in a high-spin state, on the $1.7\mu_B$ higher than the intrinsic magnetic moment of pure iron. It is also shown that iron and europium cations in the monoxide structure have an oxidation degree close to 2^+. Both in pure and in Fe-doped monoxide, the states near the bottom of the conduction band (the 5*d*-state of europium) are 100% spin-polarized. What is quite possible to provide, as already noted, an increased (record-to-date) degree of spin current transfer from the composite when it is used as an injector of spin carriers in semiconductor devices of spin electronics. It is shown that in Fe-doped monoxide there is an insignificant electron density transfer from Eu^{2+} ions to Fe^{2+} ions, but the main factor ensuring the presence of Eu^{3+} ions observed in the experiments - iron nanoparticles, apparently provides is apparently the presence of Eu_2O_3 nanoclusters in the composite structure. Their presence, as well as the presence of superparamagnetic α-iron nanoparticles, apparently provides the samples of this composite in the bulk and thin-film states with long-term chemical stability of their physical parameters under normal conditions. As evidenced by the available experience with this spintronic material [18]. Its further advancement in high-temperature spintronics and the creation of appropriate devices, in particular, a spin transistor, is possible with the development of thin-film composite technology in the method of molecular epitaxy from higher oxides of europium and iron. As the most economically justified and corresponding to industrial production of films of composites of a given composition with a corresponding set of physical and physical-chemical characteristics. In contrast from the less effective and a more costly of the "flash technique" method of synthesis of the thin films of such a composite, based on the preliminary synthesis of bulk material - a precursor [3].

In conclusion, we note that this combination of phase components, which form the outstanding properties of this composite as a high-temperature spintronic material, may be reproduced only when it is synthesized from the higher oxides of metals. Attempts to synthesize the aforementioned single-phase SS from the metals corresponding to the properties of this composite have so far been unsuccessful.

REFERENCES

1. Ahn KA, Shafer MW. *J Appl. Phys.*, 1070, 41:1260.
2. Borukhovich AS, Ignat'eva NI, Bamburov VG et al. *Doklady RAS*, 2005, 402:181.
3. Borukhovich AS, Galyas AI, Demidenko OF et al. *Inorganic Materials*, 2009, 45:254.
4. Borukhovich AS. *J. Mod. Phys.*, 2013, 4:306.

5. Borukhovich AS, Ignat'eva NI, Galyas AI et al. *Journal of Nanoelectronics and Optoelectronics,* 2008, 3:82.
6. Borukhovich AS, Ignat'eva NI, Stognii AI et al. *JETPh Letters*, 2009, 89:215.
7. Altshuler TS, Gorunov YI, Bresler MC. *JETPh*, 2006, 130:729.
8. Nemov SA, Marchenko AV, Seregin PP et al. *Physic and Chemistry of the Glass,* 2007, 33:897.
9. Tanaka K, Tatehata N, Fujita K et al. *Journal of Appl. Phys.*, 2001, 89:2213.
10. Anoshina OV, Zhukov VP, Borukhovich AS. *Sol. State Phys.*, 2015, 57:2173.
11. Perdew JP, Burke S, Ernzerh MJ. *Phys. Rev. Lett.,* 1996, 77:3865.
12. An JM, Barabach SV, Osolins V. *Phys. Rev. B,* 2010, 83:064105.
13. An JM, Belashchenko KD. *Phys. Rev. B*, 2013, 88:054421.
14. Anisimov VI, Solovyev IV, Korotin MA et al. *Phys. Rev. B*, 1993, 48:16929.
15. Eastman DE, Holtzberg F, Methfessel S. *Phys. Rev. Lett.*, 1969, 23:226.
16. Auslender MI, Irkhin VY. *Solid State Commun*, 1984, 50:1003.
17. Belov KP, Zvezdin AK, Kadomtseva AM et al. *Orientational transitions in rare earth magnetics.* Moscow, Nauka Publ., 1979, 320 p.
18. Borukhovich AS, Troshin AV. *Europium Monoxide-Semiconductor and Ferromagnet for Spintronics.* Springer International Publishing, 2018, 190 p.

SPIN ELECTRON CONDENSATE. SPIN NUCLIDE ELECTRON CONDENSATE

Gennady V. Mishinsky

Joint Institute for Nuclear Research, http://www.jinr.ru/
6, Joliot Curie str., Dubna 141980, Moscow Region, Russian Federation
mysh@jinr.ru

Abstract. **Atomic electrons pair in orthobosons in a strong magnetic field. In orthoboson, the spins of the electrons are parallel S = 1, and their energies are equal. The atomic electron orthobosons form a Bose-Einstein spin electron condensate, in which the magnetic moments of electrons are directed in one direction. Such an atom is called the transatom. The magnetic moments of electrons generate a giant, directed, inhomogeneous and anisotropic magnetic field inside and outside the transatom. This field interacts with the magnetic and orbital moments of the protons and neutrons of the atomic nucleus and changes the structure of the latter and turns the atomic nucleus into a transnucleus. A transnuclear transatom is a spin nuclide electron condensate. This is a new state of matter, based on the properties of that matter we can create new technologies.**

Keywords: **quantum physics, atomic physics, nuclear physics, spin Bose–Einstein condensate, low energy nuclear reactions, spintronics, abnormal phenomena**

PACS: 03.75.Mn; 03.75.Nt; 25.60.Pj; 32.10.-f; 76.30.-v

Bibliography - 25 references *Received November 10, 2018; accepted December 08, 2018*

RENSIT, 2018, 10(3):411-424 **DOI: 10.17725/rensit.2018.10.411**

Contents

1. INTRODUCTION

The concept of the spin nuclide electron condensate (SNEC) is associated with the creation of the theory of low-energy transmutation of chemical elements (transformation of some elements into others, then transmutation). Transmutation reactions occur in a weakly excited condensed medium [1-5]. Numerous and diverse, simple and complex experiments on low-energy transmutation of chemical elements demonstrate the obviousness of those processes. This article gives a brief description of the possibility of the existence of spin electron and spin nuclide electron condensates. Their properties and possible technologies based on these properties are discussed.

The main property of transmutation reactions is that "extraneous" chemical elements appear in their products, which were absent in initial material prior to beginning of said processes. In addition, in the reaction products there is an increased yield of some elements and groups of elements and a different ratio of isotopes of chemical elements that is different from the natural ratio.

The isotopes of elements obtained in transmutation reactions are non-radioactive. During the course of these reactions, γ- and β-radiation were also not detected. In special experiments with radioactive isotopes, their transformation into stable isotopes is demonstrated.

Other peculiarity of transmutation process is the registration in them of excess heat (in some experiments, electrical) energy, the value of which cannot be explained by chemical reactions.

It is noted that in transmutation reactions occurring in relatively element-light medium, along with "extraneous" light elements, heavy elements are produced that cannot be obtained in pairwise, nuclear reactions. Moreover, in some experimental methods, the yield of transmutation products reaches tens of percent of the total mass of the condensed medium, which is incomparable with the yield of products in conventional nuclear reactions. Thus, it should be assumed that in the transmutation reactions there occurs interaction of many atoms simultaneously, and, accordingly, of many nuclei. The latter means that atoms should attract each other, and the structure of atomic electron shells should automatically lead to the approach of nuclei to the distances of the nuclear forces and the beginning of the processes of nuclear transformations. In this case, the probability of nuclear reactions becomes equal to the probability of atomic transformations.

Thus, it becomes obvious that in order to carry out low-energy transmutation reactions, it is necessary that the structures of atoms and nuclei change dramatically. The simplest and most known way to change the structure of electron levels in an atom is to place the latter in a magnetic field.

2. ELECTRONIC OSCILLATIONS. FORMATION OF TRANSATOM

For clearness, the Bohr concept of elliptic motion of electrons in a plane will be used in reasoning and drawings. The internal electron orbitals of the atom, in the absence of a strong magnetic field, do not have a constant orientation in outer space, since they precess under the action of other charges and cease to lie in one plane. The electron moves around the nucleus not in a plane, but along a trajectory similar to "thread in the clew" [6]. Therefore, in spite of the fact that the orbital moments for *p, d* ... of electronic states differ from zero ($\ell \neq 0$), the medium values of orbital moments for *x, y* and *z*-components are equal to zero: $(0|\ell_x|0) = (0|\ell_y|0) = (0|\ell_z|0) = 0$. Because of this, first, the magnetic field created by orbital motion of an electron is zeroed, and, secondly, the forces of Coulomb repulsion between atomic electrons do not have a preferred direction, their medium values for the *x-, y-*, and *z*-components are equal to zero.

In a strong external magnetic field, apparently, more than 30 *T*: First, ℓ-*s* and *j-j* bonds of each electron in the whole atom are torn apart, not only on external but also on internal orbitals. **Fig. 1**a shows the splitting of energy, electronic levels in the sodium atom. The external magnetic field **B**, which has a constant orientation, rigidly aligns electron orbitals with respect to its direction in accordance with their orbital magnetic moments. The average values of the orbital moments for *x-, y-* and *z*-components cease to be zero. The orbital and orbital magnetic moments of electrons precess around the magnetic field **B**. The orbital magnetic moments create their own magnetic fields, rotating around the field **B**. Fig. 1b shows schematically two orbitals with equal orbital moments ℓ and their projections m_ℓ on the

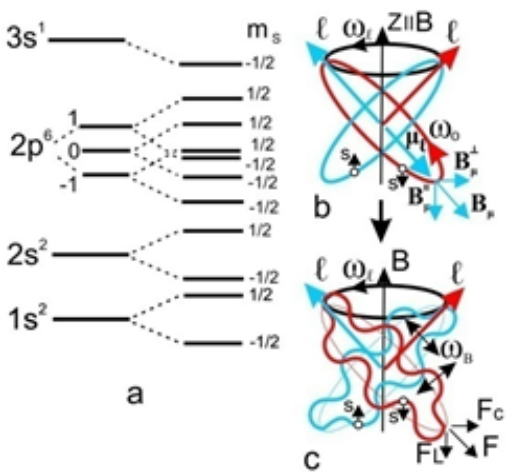

Fig. 1. *a - sodium electronic shell in strong magnetic field* **B***, b - precession of orbitals, c - electron oscillations.*

Z axis parallel to **B**, but with different directions of electron spins $s = \pm 1/2$.

Secondly, the Coulomb repulsive forces, which forced, in the absence of field **B**, the electron orbitals to freely precess, now cause the electrons to oscillate near the orbitals (Fig. 1c). Oscillation is an additional degree of freedom of the spatial motion of electron. A new degree of electron freedom generates a new quantum number for them n_b. The frequency of oscillations ω_B is related to the frequency of electron rotation on the orbital $\omega_0 = E_0/\hbar$ and the precession frequency of its orbital momentum ω_ℓ by the following relation [7, 8]:

$$\omega_B = n_b\sqrt{\omega_0^2 + \omega_\ell^2}, \quad n_b = 1, 2, 3, ...$$

Apparently, the value of the oscillation quantum number n_b depends on the value of the magnetic field. The greater the magnetic field, the greater n_b can be. Initially $n_b = 1$. Owing to the exchange interaction, the two electrons can form an orthoboson with oscillation quantum numbers 1 and –1. In the orthoboson, the spins of the electrons are parallel $S = 1$, and their energies are equal. Orthobosons create a spin electron condensate in an atom. An atom with such a condensate is called a transatom.

The spin μ_e and orbital μ_ℓ magnetic moments of each individual electron interact independently interact with an external magnetic field **B**. The spin magnetic moments of electrons do not precess around **B**, since they are oriented only in two ways: $m_S = -1/2$ over the field and $m_S = +1/2$ against the field. Electron states with identical orbital ℓ and magnetic moments m_ℓ are split into two levels with antiparallel electron spins $s = \pm 1/2$. The frequency of transitions between these levels $m_s = \pm 1/2$ is the same for all electron pairs $\omega = 2\cdot\mu_e B/\hbar$ (Fig. 1a) and it does not depend on the charge of the nuclei *Z*.

The orbital magnetic moment μ_ℓ of each individual electron precesses around magnetic field **B** with frequency $\omega_\ell = \mu_\ell \cdot B/\hbar$ ($\mu_\ell = \ell\cdot\mu_e$) and it creates its own intra-atomic magnetic field with a magnetic induction vector $\mathbf{B}_\mu$, which is calculated by the formula [9]:

$$\mathbf{B}_\mu = \mu_0 \frac{3\mathbf{n}(\boldsymbol{\mu}_\ell \cdot \mathbf{n}) - \boldsymbol{\mu}_\ell}{r^3}, \quad (\mathbf{B}_S \textit{ for } \boldsymbol{\mu}_e), \qquad (1)$$

where $\mu_0 = 1.26\cdot10^{-6}$ H/m is magnetic constant; $\mu_e = 9.29\cdot10^{-24}$ J/T = $5.79\cdot10^{-5}$ eV/T, *r* is the distance from electron to the point at which the field is calculated; and **n** is a unit vector in the *r* direction. The magnetic induction vector $\mathbf{B}_\mu$ rotates with the same frequency as μ_ℓ and it can be decomposed into two components: a magnetic field $B_\mu^{\parallel}$ directed parallel to the homogeneous field **B** and a magnetic field $B_\mu^{\perp}$ directed perpendicular to the field **B** (Fig. 1b) [10]. The internal magnetic field $B_\mu^{\perp}$ stimulates transitions between the levels $m_s = 1/2 \rightarrow m_s = -1/2$. The $1/2 \rightarrow -1/2$ transitions are possible, since they occur in states with the formation of orthobosons. An interlevel transition is performed with the emission of a photon with energy $E_f = 2\mu_e\cdot B$. The photon energy amounts, with an external magnetic field in the range of 10÷100 T, to 10^{-3}÷10^{-2} eV, which corresponds to a frequency of 0.3-3 THz or a wavelength of 1-0.1 mm. Thus, in a strong magnetic field, the spin-orbit interaction of internal electrons leads to intra-atomic electron magnetic resonance (IAMR). The IAMR and photons E_f, propagating in the medium, stimulate the forced transitions with the same energy both inside the atom in which they were generated and in other surrounding atoms. Then the orthobosons transit to the low-lying levels with the emission of photons with characteristic energy for a given element. Transitions to low-lying levels will be carried out by electron orthobosons, probably, with the emission of two photons. Since transitions occur between internal electron levels of the atom, the energies of these photons depend on the charge of nucleus *Z* and lie in the range from hard ultraviolet to hard *X*-rays of 10^2-10^5 eV. Thus, orthobosons are formed in the

entire atom and spin electron Bose–Einstein condensate is produced.

3. ELECTRON PAIRING INTO ORTHOBOSON

If we transfer the conditions for electron pairing to an atom, as at superconductivity in metals, then we must observe three basic requirements:

1. The Pauli principle must be fulfilled, according to which fermions cannot be in exactly equal states.
2. Electrons should be attracted by each other (Cooper condition [11]). This attraction between electrons can be arbitrarily small.
3. The sum of pulses of two electrons in a pair must be equal to zero $P_{ee} = 0$, i.e. electrons in the pair must have equal in magnitude and opposite in the direction pulses: $\mathbf{P}_{e1} = -\mathbf{P}_{e2}$.

Atomic electrons with equal quantum numbers n, ℓ and m_ℓ, but and with antiparallel spins $s = \pm 1/2$, occupy different energy states in a strong magnetic field, for them $\mathbf{P}_{e1} \neq -\mathbf{P}_{e2}$ (Fig. 1a). Therefore, electrons cannot form a boson with $S = 0$. Consequently, paired atomic electrons should be in equal energy states, which requires equal direction of their spins ↑↑ $S = 1$.

The second condition − presence of attraction between paired electrons, is provided by the exchange interaction [12]. It is remarkable that the exchange interaction has the character of attraction in an atom for electrons with parallel-directed spins ↑↑ only. The exchange interaction is associated with the indistinguishability of electrons (the principle of identity). It is characterized by the magnitude of exchange energy "A". The exchange energy represents an additional contribution to the total system energy. It differs from zero only in case if wave functions of electrons overlap. The more the wave functions of electrons overlap, the greater is the exchange energy. In the atom, the energy of the Coulomb repulsion of electrons "C" and the exchange energy "A" are positive. In contrast to the Coulomb electrostatic energy "C", the contribution of the exchange energy "A" to the total system energy can have different signs depending on whether the wave function of the spatial motion of two electrons is symmetric or antisymmetric, or, correspondingly, the spin part of wave function is antisymmetric or symmetric. The correction ΔE to the total system energy, connected with the interaction of electrons, is calculated in perturbation theory and, depending on whether the spatial part of the wave function is symmetric or antisymmetric, is equal to:

$$\Delta E = C + A, \quad (2)$$

or

$$\Delta E = C - A, \quad (3)$$

where '+' refers to the symmetric spatial wave function and the antisymmetric ↑↓ spin state S = 0, and '−' refers to the antisymmetric spatial wave function and the symmetric ↑↑ spin state S = 1.

Owing to the exchange interaction, the two electrons obtain rigidly correlated oscillations. The sum of their pulses is zero $P_{ee} = 0$, $\mathbf{P}_{1B} = -\mathbf{P}_{2B}$ (Fig. 2e). The projections of the oscillation pulse moments for each electron in a pair by the selected direction (Z axis) are not defined. However, these moments, just like the pulses themselves, are equal and opposite to each other in the direction: $n_b^1 \hbar = r_1 \cdot P_{1B} = r_2 \cdot (-P_{2B}) = -n_b^2 \hbar$. With an average $<r_1>$ equal to the mean $<r_2>$, this is equivalent to the equality of the modules, but with opposite signs, the quantum numbers of electron oscillations $n_b^1 = -n_b^2$, $n_b = 1, 2, 3, \ldots$ [10]. Therefore, the Pauli principle for them is satisfied.

Opposite oscillation quantum numbers of electrons make it possible to create an antisymmetric wave function of their spatial motion. Therefore, two electrons can be in the same energy state and have parallel spins $S = 1$, thereby forming an coupled pair — orthoboson. In the orthoboson, in the first order of perturbation theory, the exchange Coulomb energy of electrons is equal to the energy of their Coulomb repulsion $A = C$

[13]. Therefore, the exchange Coulomb energy of orthoboson completely compensates the energy of their Coulomb repulsion $\Delta E = 0$ (3). It turns into the quantum paradox - "The Waves extinguish the Wind".

For clearness, **Fig. 2** shows the formation of orthoboson in the helium atom. The spatial wave function of electrons of the ground state of parahelium is symmetric. The electrons are in equal energy states. The exchange energy for them is equal to the energy of their Coulomb repulsion $A = C$. These energies are added together (2) (Fig. 2a). The spatial wave function of electrons of orthohelium is antisymmetric. The electrons are in different energy states. The exchange energy for them is different from the Coulomb repulsion energy $A \neq C$. It is subtracted from the latter (3) (Fig. 2b). Due to the Pauli principle, electrons cannot be in the same energy states with parallel spins (Fig. 2c). Let's turn on a strong magnetic field. Correlated oscillations of electrons with oscillation quantum numbers 1 and –1 (n_b and $-n_b$) appear in a strong magnetic field. The spatial wave function of electrons is antisymmetric, but electrons are in the same energy states (Fig. 2d). The exchange energy for them is equal to the Coulomb repulsion energy $A = C$ and it is subtracted from the latter (3) → $\Delta E = 0$. In Fig. 2d, for clearness, the oscillation quantum numbers of electrons $n_b = \pm 4$. For oscillation quantum numbers $n_b = \pm 1$, the energy of two electrons is $6E_a$, where $E_a = 54.4$ eV is ionization energy of the He^+ helium ion

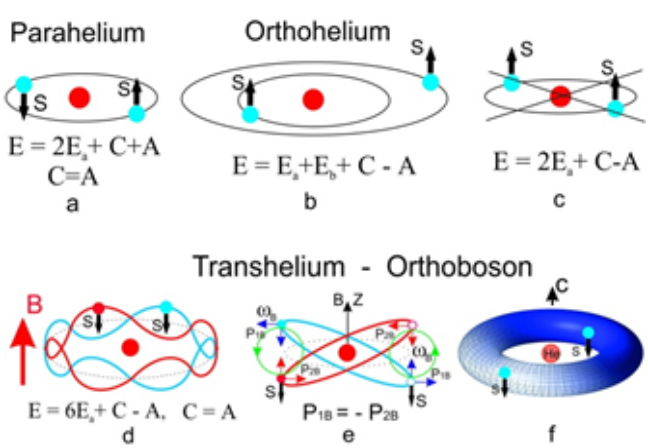

Fig. 2. *Parahelium. Orthogelium. Transhelium - Orthoboson.*

[13]. Electron oscillations in the orthobosons are carried out both in the longitudinal and in the transverse magnetic field **B** directions. Since electrons in a pair oscillate in antiphase, such a motion allows two electrons in identical energy states to be in nonintersecting spatial regions (Fig. 2e). The trajectories of two moving paired electrons can be represented as a closed double helix like screw molecule of DNA and located on the toroidal surface (Fig. 2f). Another quantum paradox emerged, while the wave functions of electrons in the orthoboson overlap to the maximum, their real, spatial clouds do not intersect.

4. PROPERTIES OF ORTHOBOSONS

1. Since the magnetic moments of electrons μ_e in a Bose-condensate are directed in the same direction, they create a giant directional inhomogeneous and anisotropic magnetic field $\mathbf{B}_S$ 10^5–10^{10} T inside and around the transatom (1). This magnetic field and the electrostatic electric field of a spin electron condensate form inside the first electron orthobosonic orbitals with a radius R_Z an electromagnetic well with a magnetic field inhomogeneity of 10^2–10^6 T at the nucleus diameter [10]. **Fig. 3** shows, in relative units, the dependence of magnetic induction vector $\mathbf{B}_S$ on the distance to the nucleus $C(R_Z)$ along the axis C (Fig. 2f). Distance $C(R_Z)$ is normalized to R_Z. Negative values of $\mathbf{B}_S$ mean that the magnetic field in central region of the atom is directed opposite

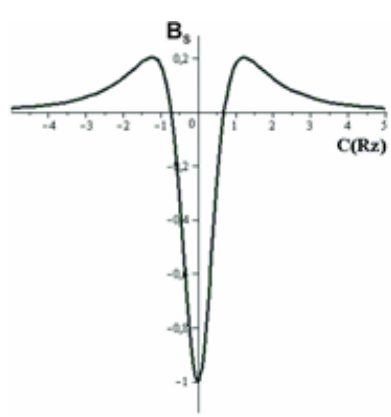

Fig. 3. *Dependence of magnetic induction vector* $\mathbf{B}_S$ *along axis* $C(R_Z)$.

to the direction of the magnetic moment of electron.

The internal magnetic field $\mathbf{B}_S$, interacting with the spin and orbital magnetic moments of protons and neutrons in the atomic nucleus, changes its structure and turns the atomic nucleus into a transnucleus. Transnucleus with transatoms represent a new state of matter: spin-nuclide-electron condensate [10].

The external ultrastrong magnetic fields and the electron Bose-condensates of transatoms allow them to attract each other, thereby creating binuclear and multinuclear molecules − transmolecules.

2. The exchange energy of paired electrons has the character of attraction and it completely compensates, in the first order of perturbation theory, the energy of their Coulomb repulsion. Oscillations of paired electrons in the transatom increase by three times their binding energy and decrease by three times the radius of their orbitals compared to the binding energy and the radius of the single electron of the multiply charged ion [13]. The radius of the orbital of such an electron is less than the radius of the K-orbital. Therefore, electrons in the Bose condensate are located on the orbital closest to atomic nucleus. The wave functions of electrons in transatoms and transmolecules significantly overlap with wave functions of transnuclei. This property of transatoms and transmolecules in low energy transmutation reactions allows to increase the probabilities of weak processes responsible for the transformation of protons into neutrons and vice versa. Thus, radioactive isotopes are not formed in transmutation reactions.

3. The exchange Coulomb energy of any two charged particles paired in orthoboson has the character of attraction and it completely compensates the energy of their Coulomb repulsion. For strongly interacting identical particles, including atomic nuclei, this fact energy compensation leads to an automatic launch of nuclear reactions without Coulomb barrier. This is due to the fact that the ultrastrong internal magnetic field $\mathbf{B}_S$ of transmolecules, consisting of identical transnuclei allows the latter, due to exchange interaction, to form an orthoboson. Since the exchange energy of identical transnuclei compensates for their Coulomb repulsion, they can enter into nuclear interactions without Coulomb barrier. Thus, the nuclear reactions occur after the formation of transmolecules automatically. This explains the possibility of low energy nuclear reactions with atomic cross sections.

Moreover, transnuclei in the transmolecule move in inhomogeneous and anisotropic space created by an ultrastrong magnetic field. Thus, motion integrals are not conserved in the interaction of the transnuclei: momentum conservation law, angular momentum (spin) conservation law, and energy conservation law are violated.

5. "CAPSULES", ORTHOHELIUM

The appearance of a strong magnetic field in a condensed medium still remains an open question. A large variety of physical experiments, in which transmutation reactions take place, suggests the existence of a characteristic object that is the same for all types of experiments. Therefore, it should be assumed that as a result of ionization of a weakly excited condensed matter, local, stable, electron-ion formations, so called "capsules" with a strong magnetic field inside appear in it [13, 14]. Experimental data show that the size of the "capsules" is estimated at $L = 10^{-8} \div 10^{-5}$ m. It is known that the transmutation process is accompanied by an unknown radiation, which leaves "strange" traces in photoemulsions, on metallographic sections and which, when interacting with a substance, changes its structure and chemical composition. It is possible that those "capsules", originating in condensed matter and moving inside and outside that matter, represent that "strange" radiation, which is recorded in many experiments. Since "capsules" are magnetic formations, an external magnetic field should

be used to produce them, to effectively connect them with each other and to arrange them into long structures. That technology was applied in experiments by A.V.Vachaev and N.I. Ivanov [3], V.A.Krivitsky [15], V.A.Pankov and B.P.Kuzmin [16]. Thus, it can be said that a magnetic "nesting Russian doll" is formed in transmutation reactions (**Table 1**). The magnetic moments of protons, neutrons and nuclei are approximately three orders of magnitude less than the magnetic moment of an electron. Therefore, the magnetic fields generated by their orthobosons will be approximately the same as those of spin electron condensate (μ_p = $1.41 \cdot 10^{-26}$ J/T = $8.79 \cdot 10^{-8}$ eV/T, μ_n = $-0.97 \cdot 10^{-26}$ J/T = $-6.02 \cdot 10^{-8}$ eV/T).

Separate attention should be paid to the chemical element helium, namely, orthohelium, which has a strong magnetic field. In orthohelium, the magnetic moments of electrons are parallel. The calculation (1) shows that the magnetic field at the center of the atom is ~ 410 T, and at the orthohelium radius R_2 = $8.76 \cdot 10^{-11}$ m, the magnetic field is ~ 70 T. As experiments have shown, the magnitude of such a field is sufficient to trigger transmutation reactions.

When two orthohelium atoms interact, they form a nuclear transmolecule of "beryllium-8" (**Fig. 4**a). Two transhelium nuclei form a nuclear orthoboson in that transmolecule. The "Be-8" transmolecule is stable, because the two transhelium nuclei cannot merge at reaction energy Q < 0. The radius of transmolecule "^{8}Be" will be R_{Be} = $4.4 \cdot 10^{-12}$ m, and the magnetic fields will be: in the center B_s^0 (Be) = $5.4 \cdot 10^5$ and at a distance of $1.2 \cdot R_{Be}$ from the center B_s^R (Be) = $1.1 \cdot 10^5$ T. The transmolecule "Be-8" attaches another atom of orthohelium to itself, forming the transmolecule "carbon-12". The transmolecule "^{12}C" is also stable because it consists of three ^{4}He nuclei: two paired transhelium nuclei and one unpaired ^{4}He (Fig. 4b). The radius of the transmolecule "^{12}C" is R_C = $3.0 \cdot 10^{-12}$ m, and the magnetic fields are: in the center B_s^0 (C) = $2.6 \cdot 10^6$ T and at a distance of $1.2 \cdot R_C$ from the center B_s^R (C) = $5.2 \cdot 10^5$ T. Subsequently, the transmolecules "^{8}Be" and "^{12}C" due to their own ultrastrong magnetic fields, are attracted to each other and enter into exchange interaction with their electronic Bose condensates. As a result, multinuclear transmolecules $n \cdot {}_2^4He$ with a helium Bose condensate are formed. The creation of such transmolecules causes multinuclear reactions, with the emission of protons, neutrons, alpha-particles and heavy fragments [17]:

$$n \cdot {}_2^4He \rightarrow {}_{2n-1}^{4n-1}A + p + Q,$$

$$n \cdot {}_2^4He \rightarrow {}_{2n}^{4n-1}B + n + Q,$$

$$n \cdot {}_2^4He \rightarrow {}_{2(n-1)}^{4(n-1)}C + {}_2^4He + Q,$$

$$n \cdot {}_2^4He \rightarrow A + B + C + ... + Q,$$

where Q is the energy released by the reaction.

Atoms of other chemical elements in ultrastrong fields of the "^{8}Be", "^{12}C" transmolecules can also transform into transatoms and enter into low-energy transmutation reactions. So the hydrogen atom in a strong and ultrastrong magnetic fields, due to electron oscillation, is converted into the hydrogen transatom "H". In this case, a photon with an energy of 2·13.6 = 27.2 eV [13] is emitted. Energy 13.6 eV is the

Table 1

Magnetic "nesting Russian dolls"

"Nesting Russian dolls"	Size, m	Magnetic field, T
External field	0.01 ÷ 0.1	0.1 ÷ 10
"Capsules"	$10^{-9} \div 10^{-5}$	> 20
Electron orthobosons	~10^{-12}	$10^5 \div 10^{10}$
Nuclear orthobosons	<10^{-13}	>10^7
Proton and neutron orthobosons	<10^{-14}	>10^{10}

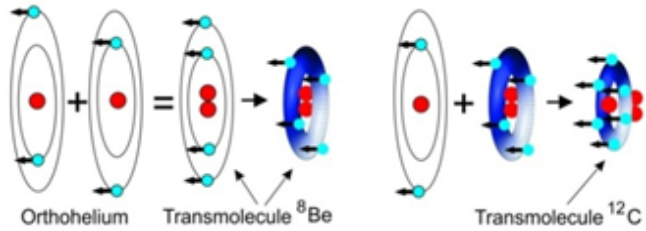

Fig. 4. *Formation of transmolecules ^{8}Be and ^{12}C.*

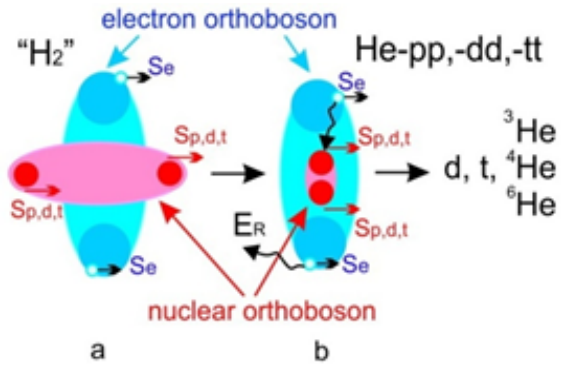

Fig. 5. *Transformation of hydrogen transmolecule into "helium" transmolecule.*

ionization energy of the hydrogen atom. In the case of recombination of an electron with the H^+ ion, a photon with an energy of 3·13.6 = 40.8 eV is emitted, and when the electron recombines with a molecular hydrogen ion H_2^+ with formation of two hydrogen transatoms 2"*H*", two photons with energies of 32.7 eV are emitted. In a strong magnetic field, the hydrogen molecule H_2, two hydrogen atoms 2*H*, and two hydrogen transatoms 2"*H*" form a hydrogen transmolecule "H_2"with an energy level of 102.7 eV (**Fig. 5**a, **Fig. 6**). This transmolecule transforms into a helium-*pp* transmolecule with an electron energy level of $3E_a$ = 163.2 eV (Fig. 5b, Fig. 6). The hydrogen molecule H_2 and two hydrogen atoms 2*H* can turn into a helium-*pp* transmolecule directly, bypassing the "H_2" stage. In an ultrastrong magnetic field, the electron levels in the hydrogen atom and in the molecular ion of

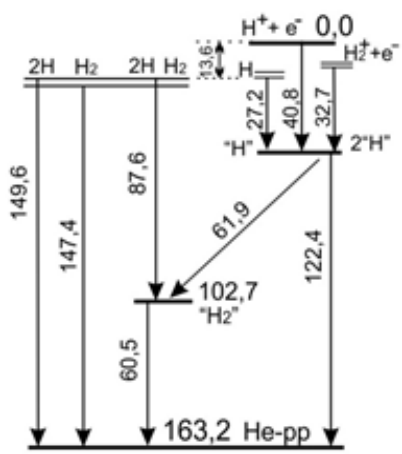

Fig. 6. *Scheme of electron transitions in the hydrogen-helium transmolecule in He + H_2 plasma.*

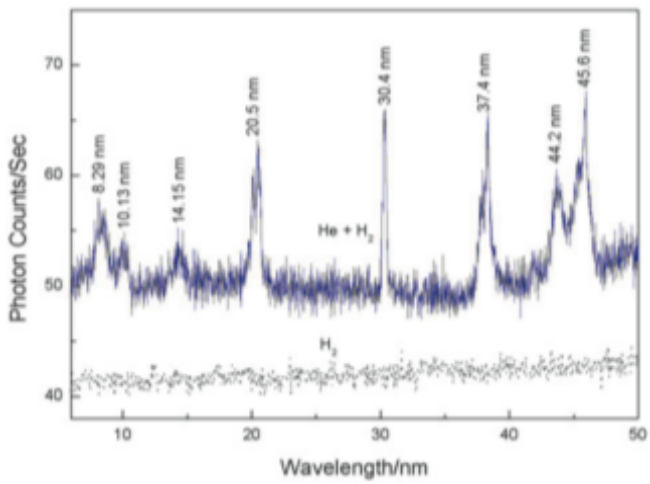

Fig. 7. *Short-wave spectrum in He + H_2 and H_2 plasmas* **[18].**

Table 2

Wave lengths and energy of lines in spectrum He + H_2.

λ, nm	8.29	10.13	14.15	20.5	30.4	37.4	44.2	45.6
E, eV	149.6	122.4	87.6	60.5	40.8	33.16	28.05	27.2

hydrogen H_2^+ are split, so lines with energies of 28.05 eV and 33.16 eV appear in the spectrum (**Table 2**). Fig. 6 shows a supposed transition scheme. The same transitions and transformations will occur with deuterium and with tritium in a strong magnetic field. Helium-*dd* and helium-*tt* transmolecules are formed in those cases. In the work of R.Mills and P.Ray on extreme ultraviolet spectroscopy of helium-hydrogen plasma [18], these emission lines were observed (**Fig. 7**, Table 2). Those lines were registered at microwave discharge in a helium mixture with 2% of hydrogen at room temperature and at pressures from 20 to 1 torr. They appear in a mixture of helium and hydrogen only, but are absent in pure helium or hydrogen and in mixtures of hydrogen with other noble gases.

6. NUCLEAR ORTHOBOSONS. TRANSMUTATION REACTIONS

The helium-*pp*, helium-*dd*, and helium-*tt* transmolecules are nuclear orthobosons. They enter non-Coulomb nuclear transmutation reactions with the formation of protons, neutrons, deuterons, tritons, ^{3}He, ^{4}He, ^{6}He nuclei (Fig. 5) [13]. Transmutation reactions can occur with the participation of electron orthobosons $+2e^-$:

$p + p + 2e^- \rightarrow d + \nu_e + e^- + 1.44$ MeV
$d + d \rightarrow t + p + 4.03$ MeV
$d + d \rightarrow {}^3He + n + 3.26$ MeV
$d + d + 2e^- \rightarrow {}^4He + 2e^- + 23.85$ MeV
$t + t \rightarrow {}^4He + 2n + 11.3$ MeV
$t + t + 2e^- \rightarrow 2e^- + 12.3$ MeV + ${}^6He$ (β-, $T_{1/2}$ = 0.8c) $\rightarrow {}^6Li + e^- + \tilde{\nu}_e + 3.5$ MeV.

Thus, orthohelium with its own strong magnetic field is a catalytic element that creates, in a mixture with hydrogen, conditions for formation of hydrogen-"helium" transmolecule and for realization of nuclear fusion reaction of two protons and an electron orthoboson. Other inert gases do not create strong magnetic fields.

Nuclear levels, in a strong magnetic field due to its interaction with magnetic moments of protons and neutrons, split $\Delta E(p, n) = \pm \mu(p, n) \cdot B_s^0$. That is why all even-even nuclei with a spin equal to zero ($I = 0$) obtain a mechanical moment $I \neq 0$ [13]. For example, the spin of the nucleus ${}_6^{12}C$ is $I = 0$, but the mechanical moment of the transatom "${}_6^{12}C$" is $I \neq 0$. The identical transnuclei will also enter into non-Coulomb transmutation reactions [$I({}_3^6Li) = 1$]:

${}^6Li + {}^6Li + 2e^- \rightarrow 2e^- + {}^{12}C + 28.17$ МэВ,
${}^{12}C + {}^{12}C + 2e^- \rightarrow 2e^- + {}^{24}Mg + 13.93$ МэВ.

In a strong magnetic field, an atom, from an "amorphous state", is transformed into an ordered, magnetic "crystal". The same happens with the nucleus, but already in the ultrastrong magnetic field of the spin electron condensate. A transnucleus is an ordered, nuclear magnetic "crystal". Nucleons in the nucleus, as well as electrons in an atom, can form nucleon orthobosons: proton-proton and neutron-neutron orthobosons (Table 1). Apparently, intra-nuclear nucleon magnetic resonance is also possible in the nucleus. Apparently, intra-nuclear reactions with two neutrons can occur in neutron-rich transnuclei: $n + n + A_1 \rightarrow d + e^- + \tilde{\nu}_e + A_2 + Q$ (3.04 MeV) with subsequent reactions $d + d + B \rightarrow {}^4He + B + Q$ (23.85 MeV), where $A_{1,2}$ and B are parts of the nucleus in which intra-nuclear reactions occur. The energy Q released in the intra-nuclear reaction must take into account the changed energy balance in the entire nucleus. The energy released in the reaction, if it proceeded outside the nucleus, is given in brackets The assumption of such types of reactions follows from experiments on electron explosion of metallic targets [19]. In these experiments with targets made of Cu, Ag, Ta and Pb, the appearance of multiple track clusters with a well-pronounced expansion center and with a number of tracks > 100 is noted. The clusters include α-particles, lithium nuclei, and probably heavier nuclei with energies of the order of several MeV/nucleon, i.e. nuclei, in which the number of neutrons is approximately equal to the number of protons. In target nuclei, the number of neutrons is 1.3÷1.5 times more than the number of protons.

Nuclear transformations of radioactive isotopes into stable isotopes and heavy nuclei dissotiations, like fission, but with the formation of stable fragments occur in transnuclei. Such dissociations are discussed by V.A.Krivitsky. in the book [15]. Obviously, it should be assumed that as a result of fusion of transatoms into a general formation, but with non-identical transnuclei, the latter also enter into transmutation reactions

7. TECHNOLOGIES

Not all atomic electrons, but only a part of them can, in the process of forced transitions, be transformed into orthobosons. Thus, each atomic nucleus Z can have $Z/2$ "chemical" transelements or "transatomic chimeras". A part of "transatomic chimera" will be represented by electrons in a paired boson state, the other part will be represented by electrons, which fill the "chimera" orbitals. Here, "chimera" orbitals should be understood as "traditional" orbitals with corrections due to magnetic and electric field influence created by transatomic paired electrons of the transatom on its unpaired electrons. Thus, many other transelements

are added to the existing chemical elements in Mendeleev Periodic Table.

Since not all atomic electrons can pass into the orthoboson state, there are three possibilities for the existence of chimeric transatoms.

The first case. When converting an atom into transatom, a situation may arise in which the number of orthobosons will be Ob = 1 or Ob = 2. In this case, the energy of magnetic attraction between Chemical TransAtoms (ChTA) is less than the energy of thermal motion [5]. Then the ChTA cannot connect between each other due to their magnetic attraction. However, for such transatoms, the formation of chemical molecules with both ChTA and ordinary atoms on the basis of chemical bonds is not excluded..

The second case. The energy of the interacting Magnetic TransAtoms (MTA) is enough to form a complex of transatoms based on their magnetic attraction, but it is not enough to overcome the Coulomb barrier of repulsive, atomic electrons, i.e. to form a nuclear transmolecule.

And the third case. There is a formation of nuclear transmolecule from the Nuclide TransAtoms (NTA) followed by the launch of transmutation reaction.

For MTA and NTA transatoms, the formation of chemical molecules with ordinary atoms on the basis of chemical bonds is also not excluded.

Based on the properties of transatoms and transmolecules discussed above, it is possible to implement the following obvious technologies:

- The release of nuclear energy in the process of transmutation allows to create new type energy generators: powerful, compact, non-radiative. Such generators can be used in home conditions.
- The possibility of transforming one element into another allows to obtain rare elements and their isotopes from cheap elements, including to obtain superheavy elements and, possibly, supercharged nuclei.
- A method to eliminate radioactive waste by converting radioactive isotopes into stable isotopes has appeared.
- Spin and magnetic transatoms can be used in computing technology, for example, in quantum computer technologies as qudites with $D = 3$ and $D = 5$ [20]. Since ChTA with Ob = 1 has S = 1, and therefore, it has three states -1, 0, +1, and ChTA with Ob = 2, S = 2 already has five states -2, -1, 0, +1, +2.
- It is possible to create various devices based on materials with low density, but with huge magnetic, both constant and variable, fields.
- It is possible to create materials with record strength characteristics, with magnetic transatoms in their composition, since the binding energy between them is much greater than the energy of any chemical bonds.
- To the chemical elements present in the Periodic Mendeleev table, a great lot of other "chemical" trans-elements are added. So, if one confines himself to nuclei with Z charge from 2 to 100, then the number of transelements without Lorentz sub-shells, will be ~ 2500. This opens up huge prospects in chemistry, materials science, industry, etc.

8. SPIN MATTER

Let us briefly consider possible and non-trivial technologies that use the "spin" matter - spin electron condensate as basis.

- After experimental confirmation of the Einstein-Podolsky-Rosen (EPR) paradox, it became obvious that entangled pairs could be used for information communication between objects. If two matrices are created on the basis of spin electron orthobosons, the orthobosons of which are pairwise entangled, then when the orthoboson state changes in one of the matrices, the orthoboson states in the other matrix will also change. Thus, information will be transmitted almost instantaneously and at any distance, since the EPR paradox

does not depend on speed or distance. In the EPR paradox, the wave functions of the partners in an entangled pair overlap maximally, but they themselves can be maximally far from each other. – "Spooky action at a distance".

- Experiments on cold nuclear fusion (cold fusion - *CF*) conducted by I.S. Filimonenko in the sixties of the last century, led to the creation of a research program, one item of which reads - the implementation of "thrust without mass removal". Apparently, this point did not appear by chance, and it is associated with the *CF* phenomenon and the low-energy transmutation phenomenon.

  In the 30s of the last century, the French mathematician E.Cartan hypothesized that the proper rotation of material objects creates a torsion of space around them, just as the gravitational mass of material objects creates a curvature of space around them.

  In the theory of physical vacuum by G.I.Shipov [21], "all particles are field microgyroscopes consisting of Riemann curvature and Ricci torsion, which generate their spins. Therefore, permanent magnets, which magnetic field is generated by electron spin, detect right and left static Ricci torsion fields around themselves. Apparently, under certain conditions and properties of a material object, the torsion of space caused by it can compensate for the inherent curvature of space. Thus, the rotation will extinguish gravity - "Waves extinguish the Wind". As a result, it can be assumed that the rotating inertial mass reduces or fully compensates for the gravitational mass, and it either decreases or disappears. In addition, the torsion field or, in other words, the field of inertia can cause the body to move without a mass drop. The English scientist John Searl created, from rotating, self-moving magnets, generators, which not only convert the energy of their rotation into electrical energy, but also lose weight. The loss in weight was expressed in the fact that the rotating magnetic disks rose above the ground and were lost in the sky. In the end, John Searl learned to control the disks in flight.

  The experiments of J. Searl were repeated in Russia, the USA and Taiwan. In Russia, a device similar to the Searl generator was created by V.V. Roshchin. and S.M.Godin [22]. That device allowed to generate electric power up to 7 kW and it would lose or gain in weight up to 50%, depending on the direction of rotation.

  Summarizing what has been said in this paragraph, it can be assumed that a solid body that has, in its composition, a macroscopic rotating ensemble of unidirectional electron orthobosons, "loses its weight", and moves without inertia and without mass dropping in the direction corresponding to direction of rotation and orientation of magnetic moments of orthobosons relative to that rotation. The impression appears that the magnetic field created by the magnetic moments of electrons increases the thrust of the whole body. The rotation of the ensemble of electron orthobosons along the circumference can be, obviously, self-moving, like in case of disks in experiments of J. Searl. But it is possible to organize the movement of orthobosons along the circumference in the form of electron current without resistance.
- Indeed, unlike electrons in superconductors, which are paired into a Cooper pair with $S = 0$, electrons in a transatom are paired into orthodoson with $S = 1$. It is possible to realize superconductivity using electron orthobosons. Superconductivity with the help of Cooper pairs is ensured by a low temperature. At present, a number of mercury-containing superconductors have the highest critical temperature ~–138°*C*. Orthoboson superconductivity is provided by a strong magnetic field. Thus, the orthobosons superconductivity does not depend on temperature (up to temperature

destruction of the conductor) and can be realized at room temperature and above it. The orthobosons themselves, which create a magnetic field, can provide a strong magnetic field in the conductor. It is possible that superconductivity at room temperature registered in palladium by dissolving deuterium in it with the concentration of atoms of the latter more than two per palladium atom in cold nuclear fusion reactions, is realized by orthobosons.

By and large, the requirement of magnetic field presence is not necessary, since for the existence of an orthoboson it is necessary that electrons in the orthoboson are in the same energy state and that their wave spatial function is antisymmetric. And since the trajectories of electrons in orthoboson represent double helix, the conductor through which the orthobosonic current flows should probably consist of two twisted micro-, and possibly nano-filaments. The double-filament structure of the conductor and exchange interaction between electrons make the motion of electrons strictly correlated, and their spatial wave function - antisymmetric. Organic molecules like DNA molecules must probably be used as conductors. In organic molecules, superconductivity can be organized on the basis of the hydrogen, namely the proton orthoboson.

- The proposal to use organic molecules as superconductors seems to be quite acceptable, as known are successful works [23-25] on low energy transmutation of elements in microbiological cultures, including the transmutation of radioactive isotopes into stable isotopes. Transmutation of isotopes in biocultures occurs in rapidly growing biological systems, in which RNA molecules and proteins are synthesized on DNA matrix. The DNA provides storage and transmission of information through a genetic program on the development and functioning of living organisms. In essence, biological systems are dynamic information systems that correct their activities as a result of data exchange both between the elements-structures that make up a biological system, and between the biological system itself and external surrounding systems. If we assume that the information exchange between DNA molecules, RNA and proteins involves electron and proton orthobosons, and if we project the properties of orthobosons formulated in this chapter onto biological systems, then a physical basis appears for explaining such fantastic phenomena as exchange of information between biological objects separated by large distances, telepathy, levitation.

9. CONCLUSION

The phenomenon of low energy nuclear reactions led to the creation of a theory of spin nuclide electron condensate. Thus, the taming and "domestication" of nuclear energy occurred. Thanks to the SNEC theory, spintronics is expanding its research not only on collective states of spin electron matter, but also on states of spin protons and spin nuclear matter. Spintronics of biological objects, animals and humans appears. A new front of scientific research, and associated creation of advanced technologies passes through such areas as: inertial field, low energy nuclear reactions, orthoboson superconductivity at high temperatures, inertia-free and non-gravitational motion of bodies without mass rejection, instantaneous transfer of information over any distances, creation of new materials, biospintronics.

REFERENCES

1. *Proceedings of the 1-25th Russian Conferences on Cold Transmutation of Nuclei of Chemical Elements.* 1993-2017, Sochi.
2. *Proceedings of the 1-21th International Conferences for Condensed Matter Nuclear Science.*
3. Balakirev VF, Krymsky VV, Bolotov BV, Vasilieva NV, Vachaev AV, Ivanov

NI, Kazbanov VI, Pavlova GA, Solin MI, Urutskoev LI. *Vzaimoprevrashcheniya khimicheskikh elementov* [Mutual transformation of chemical elements]. Ekaterinburg, Urals Branch of RAS Publ., 2003, 64 p. (in Russ.).

4. Mishinsky GV, Kuznetsov VD, Penkov FM. Nizkoenergeticheskaya transmutatsiay atomnykh yader khimicheskikh elementov. Raspredelenie po elementam v produktakh transmutatsii. Nukleosintez [Low energy transmutation of atomic nuclei of chemical elements. Element distribution in the products of low energy transmutation. Nucleosynthesis]. *Zhurnal formiruyushchikhsya napravleniy nauki* (*ZhFNN*), 2017, 17-18(5):61-81 (in Russ.). http://www.unconv-science.org/.
5. Mishinsky GV. Magnitnye polya transatomov. Spinovy-nuklidny-elektronny kondensat [Magnetic fields of transatoms. Spin-nuclide-electronic condensate]. *ZhFNN*, 2017, 15-16(5):6-25 (in Russ.).
6. Slichter ChP. *Principles of magnetic resonance*. New-York, Springer, 1963, 246 p.
7. Fock V.A. Bemerkung zur Quantelung des harmonischen Oszillators im Magnetfeld. *Z.Phys*., 1928, 47:446-448.
8. Heiss WD, Nazmitdinov RG. Orbital magnetism in small quantum dots with closed shells. Pis'ma v ZhETF, 1998, 68(12):870-875.
9. Landau LD, Lifshitz EM. *Teoriya polya* [Field theory]. Moscow, Nauka Publ., 1973, 138 p.
10. Mishinsky G.V. Atom v silnom magnitnom pole. Prevrashchenie atomov v transatomy [Atom in a strong magnetic field. Transformation of atoms to transatoms]. *Radioelectronics. Nanosystems. Information Technologies* (*RENSIT*), 2017, 9(2):147-160; DOI: 10.17725/rensit.2017.9.147.
11. Cooper LN. Bound electron pairs in a degenerate Fermi gas. *Phys.Rev*, 1956, 104:1189.
12. Heisenberg W. Über die Spektra von Atomsystemen mit zwei Elektronen. *Z. Phys*., 1926, 39(7):499-518.
13. Mishinsky GV. Bezkulonovskie yadernye reaktsii transatomov. Energiya zvezd i nukleosintez [Non-Coulomb nuclear reactions of transatoms. Stellar energy and nucleosynthesis]. *RENSIT,* 2018, 10(1):35-52; DOI: 10.17725/rensit.2018.10.35.
14. Mishinsky GV. Transatomy - transyadra i ikh svoystva [Transatoms – Transnuclei, and their properties]. *Materials of the 18th Russian conference on cold transmutation of nuclei of chemical elements*, 2012, Moscow, pp. 94-106 (in Russ.).
15. Krivitsky VA. *Paradoksy transmutatsii i razvitie Zemli* [Paradoxes of transmutation and the development of the Earth]. Moscow, NITs"Academica" Publ., 2016, 238 p.
16. Pankov VA, Kuzmin BP. Demonstratsionnaya metodika sinteza elementov iz vody v plazme elektricheskogo razryada [Demonstration technique for the synthesis of elements from water in an electric discharge plasma]. *Aktualnye problemy sovremennoy nauki* [Actual problems of modern science]. 2008, 44(5):112-116 (in Russ.).
17. Mishinsky GV. Mnogoyadernye reaktsii v kondensirovannom gelii [Multinuclear reactions in condensed helium]. *RENSIT*, 2017, 9(1):94-105; DOI: 10.17725/rensit.2018.9.94
18. Mills R, Ray P. Extreme ultraviolet spectroscopy of helium-hydrogen plasma. *J. Phys. D:Appl. Phys*., 2003, 36:1535-1542.
19. Adamenko SV, Selleri F, A. van der Merwe. *Controlled Nucleosynthesis. Breakthroughs in Experiment and Theory. Series: Fundamental theories in Physics*. Springer, 2007, v. 156, 780 p.
20. Kiktenko EO, Fedorov AK, Strakhov AA, Man'ko VI. Single qudit realization of the Deutsch algorithm using superconducting many-level quantum circuits. *Phys. Lett. A*, 2015, 379, 1409.
21. Shipov GI. *Teoriya fizicheskogo vakuuma, teoriya, eksperimenty, tekhnologii* [The theory of physical

vacuum, theory, experiments, technology]. Moscow, Nauka Publ., 1997, 450 p.
22. Roshchin VV, Godin SM. *Eksperimental'noye issledovaniye fizicheskikh effektov v dinamicheskoy magnitnoy sisteme* [Experimental study of physical effects in a dynamic magnetic system]. Pis'ma v ZhTF, 2000, 26(24):70-75.
23. Vysotskii VI, Kornilova AA. *Nuclear fusion and transmutation of isotopes in biological systems*. Moscow, Mir Publ., 2003, 302 p.
24. Kornilova AA, Vysotskii VI. Sintez i transmutatsiya stabilnykh i radioaktivnykh izotopov v biologicheskikh sistemakh [Synthesis and transmutation of stable and radioactive isotopes in biological systems. *RENSIT*, 2017, 9(1):52-64; DOI:10.17725/rensit.2017.9.52.
25. Kurashov V.M., Sakhno T.V. Mikrobiologicheskiy sposob transmutatsii khimicheskikh elementov i prevrashcheniya izotopov khimicheskikh elementov [Microbiological method of transmutation of chemical elements and conversion of isotopes of chemical elements. *Patent RU 2 563 511 C2* May 15, 2014.

SEMINAR "RESEARCH IN THE FIELD OF SPINTRONICS AND THE PROSPECTS FOR CREATING AN ELEMENT BASE ON ITS BASIS"

Gennady Ya. Krasnikov, Oleg A. Telminov

Joint-stock company Molecular Electronics Research Institute, http://niime.ru/
Moscow 124460, Russian Federation

gkrasnikov@niime.ru, otelminov@niime.ru

Abstract. **Information on the seminar of the Department of Nanotechnologies and Information Technologies of the Russian Academy of Sciences jointly with the Scientific Council of the Russian Academy of Sciences "Fundamental problems of the element base of information and computing systems and control systems and materials for its creation" and the consortium "Advanced materials and element base of information and computing systems" is presented, which was held on June 26 2018 at the Kotelnikov Institute of Radioengineering and Electronics RAS. The seminar was attended by 48 representatives from 22 leading specialized organizations and enterprises in Moscow and Moscow region, St. Petersburg and Nizhny Novgorod, Yekaterinburg, Novosibirsk and other research centers. 10 reports were heard and discussed. A decision was taken on measures to develop ongoing research in the field of spintronics and the prospects for creating domestic information-computing and control systems based on it, as well as to ensure the technological independence of Russia.**

Keywords: **spintronics, element base, materials and devices of spintronics**

PACS: 01.10 Fv

Received June 28, 2018, accepted 09 Juli 2018
RENSIT, 2018, 10(3):425-426 **DOI: 10.17725/rensit.2018.10.425**

The seminar was attended by:

members of the Council - Gribov B.G., Corr Memb RAS; Telminov O.A., Ph.D.; Akchurin R.Kh., Dr Sci Chem; Gorbatsevich A.A., Corr Memb RAS; Gornev E.S., Dr Sci Eng; Zlomanov V.P., Dr Sci Chem; Kobeleva S.P., Ph.D.; Levchenko A.A., Dr Sci Phys&Math; Nikitov SA, Corr Memb RAS; Salashchenko N.N., Corr Memb RAS;
from Kurnakov IGIC RAS - Ketsko V.A., Dr Sci Chem;
from IPTM RAS - Mikhailov G.M., Dr Sci Phys&Math; Egorov V.K., PhD;
from Kotelnikov IRE of RAS - Anciperov V.E., PhD; Barabanenkov Yu.N., Dr Sci Phys&Math; Grachev V.I., Research Fellow; Dyuzhinov I.N., Research Fellow; Logunov M.V., Dr Sci Phys&Math; Ovsyannikov G.A., head of lab.; Polzikova N.I., Dr Sci Phys&Math; Sharaevskaya A.Y., Junior Research Fellow;
from Mokerov ISVCH RAS - Gamkrelidze S.A., Dr Sci Eng;
from IPMT HPM RAS - Fraerman A.A., Dr Sci Phys&Math;
from IPM UB RAS - Milyaev M.A., Ph.D.; Ustinov V.V., acad. RAS;
from Rzhanov ISP SB RAS - Nenashev A.V., Ph.D.
from ISSP RAS - Devyatov E.V., Dr Sci Phys&Math, Ryazanov V.V., Dr Sci Phys&Math, Uspenskaya L.S., Dr Sci Phys&Math;
from IHBB RAS - Bulanov A.D., Dr Sci Chem; Churbanov M.F., acad. RAS;
from MIPT - Morozov A.I., Dr Sci Phys&Math;
from JSC MERI"NIIME" - Dianov A.M., Koldaev I.M., Ph.D.;
from NRU "MIET" - Kozlov A.V., Ph.D., Soloviev S.V., engineer;
from NPK "Technology Center" Amelichev V.V., Ph.D.; Vasiliev D.V., Research Fellow;
from the Russian Quantum Center - Kozhayev MA, Research Fellow;
from RTU-MIREA - Fedulov F.A., graduate student; Fetisov L.Yu., Ph.D., Fetisov Yu.K., Dr Sci Phys&Math;
from Kotelnikov FIRE of RAS - Vilkov EA, Dr Sci Phys&Math, Chigarev S.G., Ph.D., Chucheva G.V., prof. RAS;
from CKP "MST and EKB" MIET - Demin GD, PhD;
from CST FSB of Russia - Lopatin VV, PhD;
from YaF FTIAN RAS - Trushin O.S., PhD.

During the seminar 10 reports were heard:

1. Fetisov Yu.K., Sigov A.S. Spintronics: physical fundamentals and devices.
2. Ustinov V.V., Milyaev M.A. Metallic nanospintronics and the element base of magnetic sensors.
3. Nikitov S.A., Sadovnikov A.V. Streintronics - a new area of spintronics and magnonics.
4. Zinovyeva A.F., Nenashev A.V., Zarodnyuk T.S., Gornov A.Yu., Dvurechensky A.V. Quantum logical operations on spin states in a continuous microwave field.
5. Fraerman A.A. Magnetic states and transport properties of ferromagnetic nanostructures: the effect of tunneling magnetoresistance and its application.
6. Logunov M.V., Nikitov S.A. Prospects for the development of information recording and processing devices based on magnetic domains and domain boundaries.
7. Morozov A.I. Magnetoresistive memory recording electric field.
8. Ryazanov V.V. Hybrid Josephson structures for superconducting electronics and spintronics devices.
9. Uspenskaya L.S. Switching the spin-polarized current of hybrid structures based on permalloy.
10. Belotelov V.I., Kozhaev M.A., Chernov A.I., Savochkin I.V., Zvezdin A.K. Excitation of spin waves by femtosecond optical pulses.

The presentations of the speakers reflected the level of research conducted in the field of spintronics and the prospects for creating an element base on its basis in Russia, which will make it possible to draw up objective and scientifically based plans for the development of Russian microelectronics for the coming years.

Summing up, the chairman of the seminar, Corresponding Member of the RAS S.A. Nikitov noted the high scientific and technical level of the reports and expressed hope for strengthening cooperation between organizations and enterprises in the field of development of spintronics and the creation of an element base based on it.

Radioelectronics. Nanosystems. Information Technologies (abbr. RENSIT)
Certificate El. no. FS77-60275 on 19.12.2014 of the Ministry of Telecom and Mass Communications of Russian Federation, Moscow
ISSN: 2414-1267online. Http://www.rensit.ru. Publisher - Vladimir I. Grachev. 2018, 30 Dec.
Computer printing, page-proofs, graphics, photos of work - the editors RENSIT.